THE ASTROPHYSICAL JOURNAL, 470:1–37, 1996 October 10

THE *HUBBLE SPACE TELESCOPE* KEY PROJECT ON THE EXTRAGALACTIC DISTANCE SCALE. VI. THE CEPHEIDS IN NGC 925[1]

N. A. SILBERMANN
Infrared Processing and Analysis Center, Jet Propulsion Laboratory, California Institute of Technology, MS 100-22, Pasadena, CA 91125; nancys@ipac.caltech.edu

PAUL HARDING
Steward Observatory, University of Arizona, Tucson, AZ 85721; harding@as.arizona.edu

BARRY F. MADORE
NASA Extragalactic Database, Infrared Processing and Analysis Center, California Institute of Technology, MS 100-22, Pasadena, CA 91125; barry@ipac.caltech.edu

ROBERT C. KENNICUTT, JR.
Steward Observatory, University of Arizona, Tucson, AZ 85721; robk@as.arizona.edu

ABHIJIT SAHA
Space Telescope Science Institute, Baltimore, MD 21218; saha@stsci.edu

PETER B. STETSON
Dominion Astrophysical Observatory, Victoria, BC, Canada V8X 4M6; peter.stetson@hia.nrc.ca

WENDY L. FREEDMAN
Observatories of the Carnegie Institution of Washington, Pasadena, CA 91101; wendy@ociw.edu

JEREMY R. MOULD
Mount Stromlo and Siding Springs Observatories, Institute of Advanced Studies, Australian National University, ACT 2611 Australia; jrm@merlin.anu.edu.au

JOHN A. GRAHAM
Department of Terrestrial Magnetism, Carnegie Institution of Washington, Washington, DC 20015; graham@jag.ciw.edu

ROBERT J. HILL
Laboratory for Astronomy & Solar Physics, NASA Goddard Space Flight Center, Greenbelt, MD 20771; hill@noether.gsfc.nasa.gov

ANNE TURNER AND FABIO BRESOLIN
Steward Observatory, University of Arizona, Tucson, AZ 85721; aturner@as.arizona.edu and bresolin@as.arizona.edu

LAURA FERRARESE AND HOLLAND FORD
Johns Hopkins University and Space Telescope Science Institute, Baltimore, MD 21218; ferrarese@stsci.edu and ford@stsci.edu

JOHN G. HOESSEL AND MINGSHENG HAN
University of Wisconsin, Madison, WI 53706; hoessel@uwfpc.astro.wisc.edu and han@adcode.astro.wisc.edu

JOHN HUCHRA
Harvard Smithsonian Center for Astrophysics, Cambridge, MA 02138; huchra@cfa.harvard.edu

SHAUN M. G. HUGHES
Royal Greenwich Observatory, Cambridge CB3 0EZ, England, UK; hughes@ast.cam.ac.uk

GARTH D. ILLINGWORTH
Lick Observatory, University of California, Santa Cruz, CA 95064; gdi@ucolick.org

RANDY PHELPS
Observatories of the Carnegie Institution of Washington, Pasadena, CA 91101; phelps@ociw.edu

AND

SHOKO SAKAI
Infrared Processing and Analysis Center, Jet Propulsion Laboratory, California Institute of Technology, MS 100-22, Pasadena, CA 91125; shoko@ipac.caltech.edu

Received 1996 March 11; accepted 1996 April 30

ABSTRACT

We report the detection of Cepheid variable stars in the barred spiral galaxy NGC 925, using the *Hubble Space Telescope* (*HST*) Wide-Field and Planetary Camera 2 (WFPC2). Twelve V (F555W) and four I (F814W) epochs of cosmic-ray split observations were obtained. Eighty Cepheids were discovered, with periods from 6 to $\sim$80 days. Light curves of the Cepheids are presented, and their corresponding period-luminosity diagrams are discussed. Using a distance modulus for the Large Magellanic Cloud Cepheids of 18.50 mag and an extinction of $E(V-I) = 0.13$ mag, the measured distance modulus to NGC 925 is 29.84 ± 0.16 mag, corresponding to a distance of 9.29 ± 0.69 Mpc. A mean reddening of $E(V-I) = 0.17$ mag is found for the Cepheids in this region of NGC 925.

Subject headings: Cepheids — distance scale — galaxies: individual (NGC 925)

[1] Based on observations with the NASA/ESA *Hubble Space Telescope* obtained at the Space Telescope Science Institute, which is operated by AURA, Inc., under NASA contract NAS 5-26555.

1. INTRODUCTION

The observations presented in this paper are part of the *HST* Key Project on the extragalactic distance scale, whose main goal is to measure accurate distances to 18 nearby galaxies using Cepheid variables. This will provide the foundation for calibration of several secondary distance indicators such as the planetary nebula luminosity function, the Tully-Fisher relation, surface brightness fluctuations, and methods using supernovae (Kennicutt, Freedman, & Mould 1995). NGC 925 is the fourth galaxy to be searched for Cepheids as part of the *HST* Key Project. Previous galaxies were M81 (Freedman et al. 1994b; Hughes et al. 1994), M101 (Kelson et al. 1996; Stetson et al. 1996), and M100 (Freedman et al. 1994a; Ferrarese et al. 1996; Hill et al. 1996).

NGC 925 is classified as an SBcII-III galaxy by Sandage & Tammann (1981) and as an SBS3 galaxy by de Vaucouleurs et al. (1991). At $\alpha_{1950} = 2^h24^m$, $\delta_{1950} = 33°21'$ ($l = 144°.9$, $b = -25°.2$), it is a member of the NGC 1023 galaxy group (e.g., Tully 1980). The NGC 1023 group is a bound association of about 30 galaxies, at a distance of about 10 Mpc, with an estimated radius of about 0.8 Mpc. Distances to individual galaxies within the group have been measured using a variety of techniques, including spectral redshifts, isophotal diameters, planetary nebula luminosity functions, expanding photospheres of Type II supernovae, surface brightness fluctuations, and the Tully-Fisher relation (see § 7). In particular, the favorable inclination angle of NGC 925 (57°) has made it a popular target for Tully-Fisher application (see, for example, Table 9).

The *HST* observations and data reduction are described in §§ 2, 3, and 4. The properties of the Cepheid sample are discussed in § 5. In § 6, we present the derived distance to NGC 925, and we compare the results to previous distances determined to NGC 925 and the NGC 1023 group in § 7.

2. OBSERVATIONS

A description of the *Hubble Space Telescope* Wide-Field and Planetary Camera 2 (WFPC2) is given in the *HST* WFPC2 Instrument Handbook (Burrows et al. 1994). The instrument consists of four 800 × 800 pixel CCDs. Three of the CCDs make up the Wide-Field Camera (chips 2–4), each with 0".10 pixels and a 1'.3 × 1'.3 field of view; the fourth chip composes the Planetary Camera (chip 1) with 0".046 pixels and a 34" × 34" field of view. Each CCD has a readout noise of about $7e^-$ and can operate at either of two gain settings, 7 or $14e^-$ per ADU; the observations presented here were made with a gain setting of 7.

The observing window for NGC 925 was from 1994 August to October. The dates of observation were selected using a power-law time series in order to minimize period aliasing and maximize uniformity of phase coverage for the expected range of Cepheid periods, 10–60 days (Freedman et al. 1994b). Twelve epochs in *V* (F555W) and four in *I* (F814W) were obtained. Three observations in *B* (F439W) were also obtained, but because of the low signal-to-noise ratio of these data they were not used in the analysis presented here. One *V* and *I* epoch (1994 September 5) was lost due to guide star acquisition problems, and this observation was retaken on 1994 October 17. Observations for two other epochs were made with the telescope in coarse tracking mode, indicative of problems with the chosen guide star. New guide stars were used for epochs taken after September 5, and no further problems with tracking were reported. Two epochs (August 17 and October 17) were acquired at slightly different roll angles (with a difference of 0.5 degrees) compared to the other epochs. Each observation consisted of two cosmic-ray split exposures, with typical integration times of 1300 and 900 s. All observations were made with the camera at an operating temperature of −88°C. Table 1 lists the date, filter, and exposure time of each observation. The position of the *HST* field on NGC 925 is indicated in Figure 1 (Plate 1). The results presented in this paper are based entirely on the photometry in *V* and *I*.

TABLE 1

HST OBSERVATIONS OF NGC 925

UT Day (1994)	HJD 2449000.+	Filter	Exposure Time (s)
Aug 08	573.3690	F555W (V)	1300
Aug 08	573.4225	F555W (V)	900
Aug 08	573.4357	F814W (I)	1300
Aug 08	573.4899	F814W (I)	900
Aug 17	582.0039	F555W (V)	1100
Aug 17	582.0684	F555W (V)	1100
Aug 17	582.1351	F814W (I)	1100
Aug 17	582.1497	F814W (I)	1100
Aug 17	582.2025	F439W (B)	1100
Aug 17	582.2171	F439W (B)	1100
Aug 26	591.4571	F555W (V)	1300
Aug 26	591.4748	F555W (V)	900
Aug 29	594.4904	F555W (V)	1300
Aug 30	594.5577	F555W (V)	900
Sept 01	597.3079	F555W (V)	1300
Sept 01	597.3579	F555W (V)	900
Sept 06	601.1814	F439W (B)	1100
Sept 06	601.1959	F439W (B)	1100
Sept 08	604.3481	F555W (V)	1300
Sept 08	604.4037	F555W (V)	900
Sept 13	608.5700	F555W (V)	1300
Sept 13	608.6352	F555W (V)	900
Sept 17	613.3287	F555W (V)	1300
Sept 17	613.3828	F555W (V)	900
Sept 23	618.8916	F555W (V)	1300
Sept 23	618.9451	F555W (V)	900
Sept 29	625.3260	F555W (V)	1300
Sept 29	625.3788	F555W (V)	900
Sept 29	625.3920	F814W (I)	1300
Sept 29	625.4461	F814W (I)	900
Oct 07	633.3014	F555W (V)	1300
Oct 07	633.3556	F555W (V)	900
Oct 17	643.1546	F555W (V)	1300
Oct 17	643.2067	F555W (V)	900
Oct 17	643.2740	F814W (I)	1100
Oct 17	643.2886	F814W (I)	1100
Oct 17	643.3414	F439W (B)	1100
Oct 17	643.3560	F439W (B)	1100

3. PHOTOMETRIC REDUCTIONS

All observations were preprocessed through the standard Space Telescope Science Institute (STScI) pipeline, as described by Holtzman et al. (1995b). The images were calibrated with the most up-to-date version of the routine reference files provided by the Institute at the time the images were taken. The vignetted edges of the CCD chips were masked out using masks created by one of us (P. B. S.). Bad columns and pixels were also masked out using the data quality files produced by the pipeline.

The NGC 925 images were then multiplied by a pixel area map created by P. B. S. The cameras in WFPC2 produce significant geometric distortion in the images they generate. Because the flat fields employed in the standard

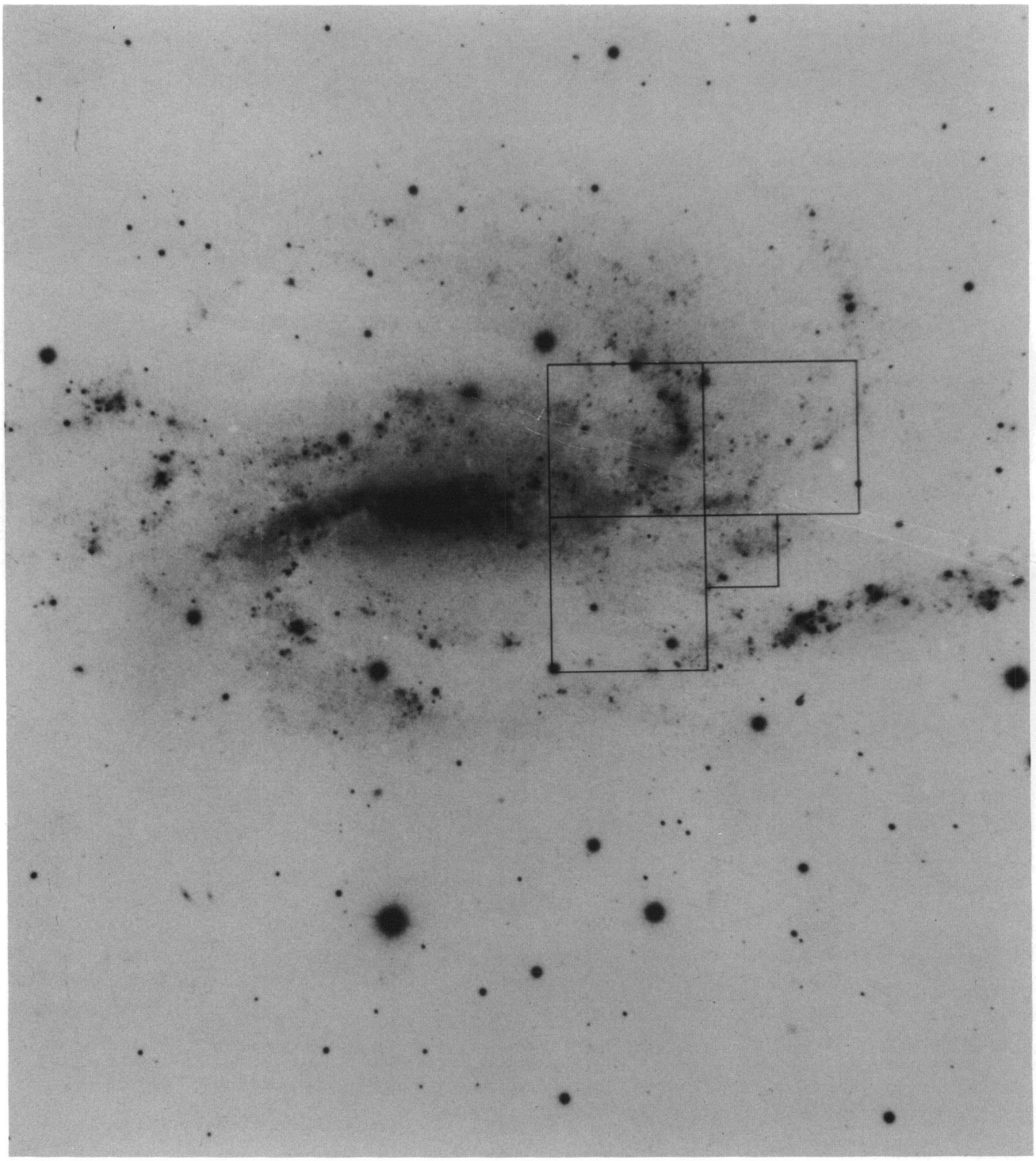

FIG. 1.—*HST* field is indicated in this picture from a photograph of NGC 925 in Sandage & Bedke (1988). North is toward the top, and east is to the left.

calibration procedure are normalized to preserve surface brightness, the variation in the areas of different pixels as projected onto the sky means that integrated fluxes are not conserved in pipeline-calibrated images. This is rectified by multiplying the recorded intensity in each pixel by that pixel's normalized relative area. Our pixel-area map differs slightly from that of Holtzman et al., in that they renormalize each datum to the area of the largest pixel in each image, whereas we renormalize each datum to the area of the median pixel in each image (which is approximately 1.6% smaller than the largest pixel), thereby preserving the average value of the readout noise and gain in the recalibrated data. In a final step, the images were multiplied by four and converted to short integers in order to reduce the disk space required and to allow the possibility of data compression (in floating-point data all bits appear significant); this leads to an effective readout noise of 4.0 ADU and a gain of $1.75e^-$ per ADU in the new units, so that the noise in the image is still well sampled.

As a double-blind check on our reduction procedures, two of us separately reduced the NGC 925 data, each using a different profile fitting photometry package. N. A. S. used DAOPHOT II/ALLFRAME (Stetson 1994), and P. H. used a variation of DoPHOT (Schechter, Mateo, & Saha 1993; Saha et al. 1996). For a detailed description of each photometry package, the reader is referred to those respective publications.

3.1. *DAOPHOT II/ALLFRAME Reductions*

The extraction of stellar photometry from CCD images using the ALLFRAME package first requires an accurate list of stars in the images. *HST* images contain a significant number of cosmic-ray hits giving rise to large numbers of spurious "stars," found using automated star-finding programs. In order to construct a star list for each *HST* chip that contained few, if any, cosmic-ray hits, all the images for each WFPC2 chip were median averaged to produce clean cosmic-ray free images; this was done with software (written by P. B. S.) that corrects for translations, rotations, differential distortion, and different exposure times among the input images before median-averaging to generate the output image. DAOPHOT and ALLSTAR (Stetson 1987) were iteratively used to locate all the stars in each "clean" image. Usually two or three iterations were enough to locate all the stars, with a few remaining stubborn ones having to be added by hand. One more run through ALLSTAR then finalized the star lists. These lists were then used by ALLFRAME to obtain profile-fitting photometry of the stars in the original *HST* images. The cosmic-ray split pairs were *not* combined to produce single epoch images; ALLFRAME was used on all 24 *V* and 8 *I* images. The point-spread functions were derived from public domain *HST* WFPC2 observations of the globular clusters Pal 4 and NGC 2419 (Hill et al. 1996). A family of aperture corrections was generated by applying the program DAOGROW (Stetson 1990) to the NGC 925 data in combination with WFPC2 observations of NGC 2419, Pal 3, Pal 4, M101, and NGC 4725; the appropriate member of this family was then determined for each *HST* observation of NGC 925. The individual aperture corrections were then averaged to obtain a mean aperture correction for each chip and filter combination.

The conversion of ALLFRAME instrumental magnitudes to final, standard system magnitudes (Johnson *V* and Kron-Cousins *I*) is the same as was used for M100 (Hill et al. 1996; Ferrarese et al. 1996). We present only a brief outline of the full procedure here. In essence, the instrumental magnitudes were converted to the system of Holtzman et al. (1995a), and then his equations were used to go to the standard system. The final form of the conversion equations for the ALLFRAME instrumental photometry is

$$M = m + 2.5 \log t + C1 + C2(V - I) + C3(V - I)^2 , \quad (1)$$

where M is the standard magnitude, m is the instrumental magnitude, t is the exposure time, and $C1$–$C3$ are constants. The coefficients $C2$ and $C3$ were taken directly from Holtzman et al. (1995a, their Appendices A2 and A3) and are the same for all four chips. The $C1$ term includes the long exposure WFPC2 magnitude zero point, the ALLFRAME magnitude zero point, a correction for our multiplying the image data by four before converting them to integers, a gain ratio term (since our data were taken with a gain setting of 7, whereas Holtzman et al. calibrate *HST* data using a gain setting of 14), a correction for the pixel area map normalized differently from Holtzman et al. (1995a), and an aperture correction to go from our point-spread function (PSF) magnitudes to 0".5 apertures, as adopted by Holtzman et al. Each one of these corrections is discussed in detail in Hill et al. (1996). Table 2 lists each contribution to the $C1$ term. Table 3 lists the aperture corrections (AC) and zero point (ZP), which contains the gain ratio term, used for each chip and the resulting $C1$ term; also listed are the $C2$ and $C3$ terms for each chip.

3.2. *DoPHOT Reductions*

The DoPHOT reductions followed the procedure described by Saha et al. (1996) and its application to the *HST* Key Project data by Ferrarese et al. (1996) and Hill et al. (1996). A few small improvements to the procedure were made, including more accurate coordinate transformations between epochs and an improved procedure for determining aperture corrections. Details of these improvements are given in § 1 of the Appendix.

Calibration of DoPHOT magnitudes follows the procedure in Hill et al. (1996). The DoPHOT fit magnitudes

TABLE 2

CONTRIBUTIONS TO THE $C1$ COEFFICIENT

ALLFRAME zero point	−25.00
Integer images.....	+2.5 log 4
Pixel Area Normalization.....	+0.016
Aperture Correction	AC
WFPC2 Zero Point	ZP

TABLE 3

TRANSFORMATION EQUATION COEFFICIENTS

Chip	Filter	AC	ZP	$C1$	$C2$	$C3$
1.....	*V*	−0.106	22.510	−1.075	−0.52	0.27
2.....	*V*	−0.042	22.522	−1.000	−0.52	0.27
3.....	*V*	−0.043	22.530	−0.992	−0.52	0.27
4.....	*V*	−0.006	22.506	−0.979	−0.52	0.27
1.....	*I*	−0.133	21.616	−1.996	−0.63	0.25
2.....	*I*	+0.017	21.657	−1.805	−0.63	0.25
3.....	*I*	+0.005	21.638	−1.836	−0.63	0.25
4.....	*I*	+0.024	21.609	−1.846	−0.63	0.25

were corrected to an aperture of radius 5 pixels and exposure time of 1 s, and a zero-point calibration was applied to bring them to the 0".5 system of Holtzman et al. (1995a). These zero-point corrections are as given in Holtzman et al., but with a small correction applied to account for differences in star and sky apertures (Stetson et al. 1996). The prescription of Holtzman et al. (1995a) was then used to convert the instrumental magnitudes to V and I.

TABLE 4

COMPARISON OF ALLFRAME/DoPHOT

Chip	No. of Stars	$\overline{\Delta V}$	$\overline{\Delta I}$
1.....	38	-0.138 ± 0.006	-0.089 ± 0.002
2.....	36	-0.076 ± 0.006	-0.019 ± 0.001
3.....	31	-0.017 ± 0.006	$+0.011 \pm 0.004$
4.....	40	-0.080 ± 0.004	-0.007 ± 0.006

3.3. *Comparison of DAOPHOT and DoPHOT Photometric Systems*

The independent data reductions using ALLFRAME and DoPHOT provide a robust external test for the accuracy of the PSF-fitting photometry of these crowded fields. A detailed discussion and comparison of these programs will be presented in a future paper (Stetson et al. 1996). Here we summarize the results of our comparisons for NGC 925.

First, we compared the photometry for several relatively isolated stars on each of the chips. The comparisons are shown in Figure 2, which plots the difference in magnitudes between the two data sets as a function of ALLFRAME magnitude for each chip and for V and I, separately. The scatter, which is evident in each comparison, is partly owing to photometric errors at faint magnitudes, but there is an additional scatter for bright stars that reflects differences in the subtleties of the PSF-fitting, background determination, and splitting of stars in these crowded and undersampled fields. In addition, there are offsets of up to 0.10 mag in the mean magnitudes. Table 4 lists the average differences between the two data sets, subdivided by chip and filter. A detailed comparison of the photometry for NGC 925 and other galaxies indicates that most of these differences reflect uncertainties in the aperture corrections determined for individual chips, combined with systematic differences in the way in which the two programs isolate stars from the crowded background (Stetson et al. 1996).

We performed the same comparison for the 80 Cepheids in our final sample (§ 4), and comparisons of those data are shown in Figure 3. The mean offsets are slightly different than for the other comparison sample, but, given the scatter, the differences are not statistically significant. In both comparisons, the largest differences in magnitude scales are for the PC chip. Fortunately, however, this chip contains only a few Cepheids. Most of the variables are located on chips 3 and 4, where the agreement in photometry is quite good, so it is not surprising that when the ALLFRAME and DoPHOT data sets are reduced independently they yield

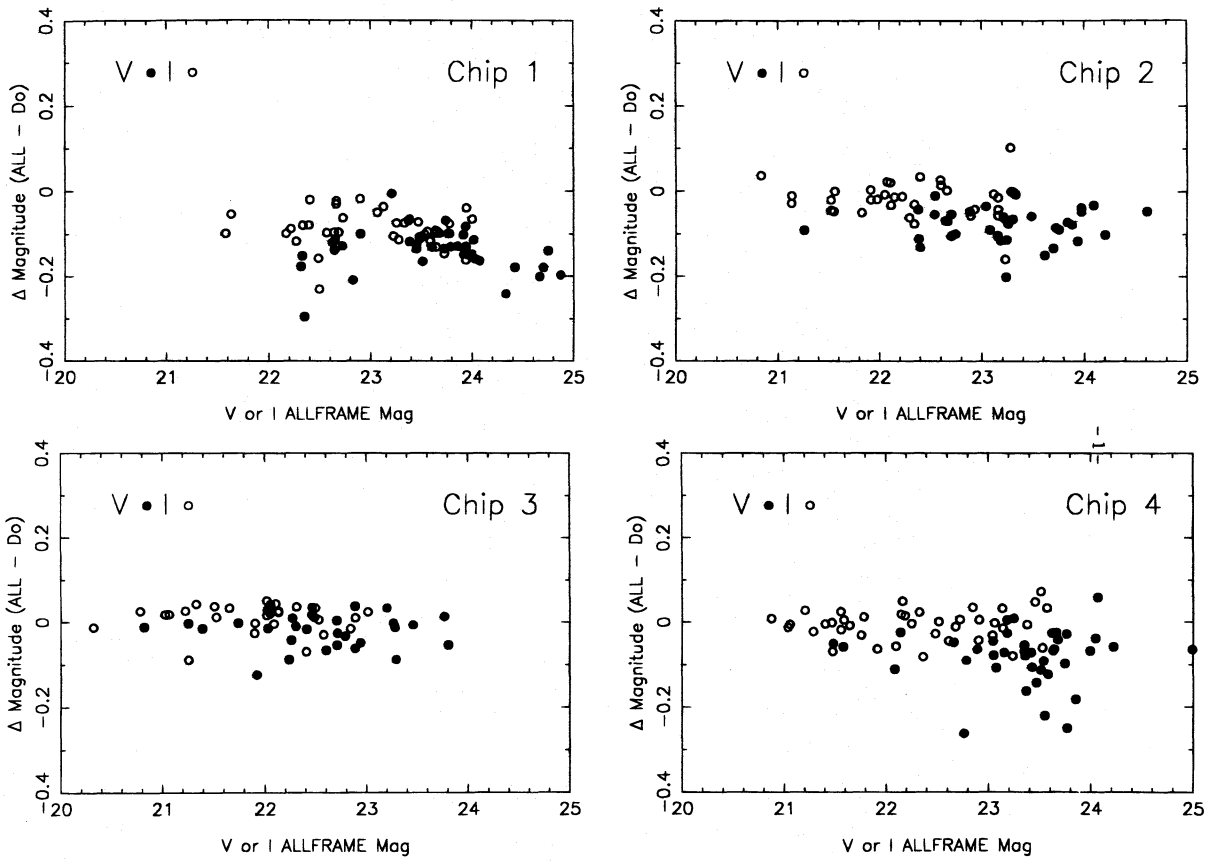

FIG. 2.—Comparison of the ALLFRAME and DoPHOT photometric systems. ALLFRAME and DoPHOT photometry for several fairly isolated stars in each chip is compared. V comparison is indicated by the filled circles. I comparison is indicated by the open circles. The best comparison is found in chip 3.

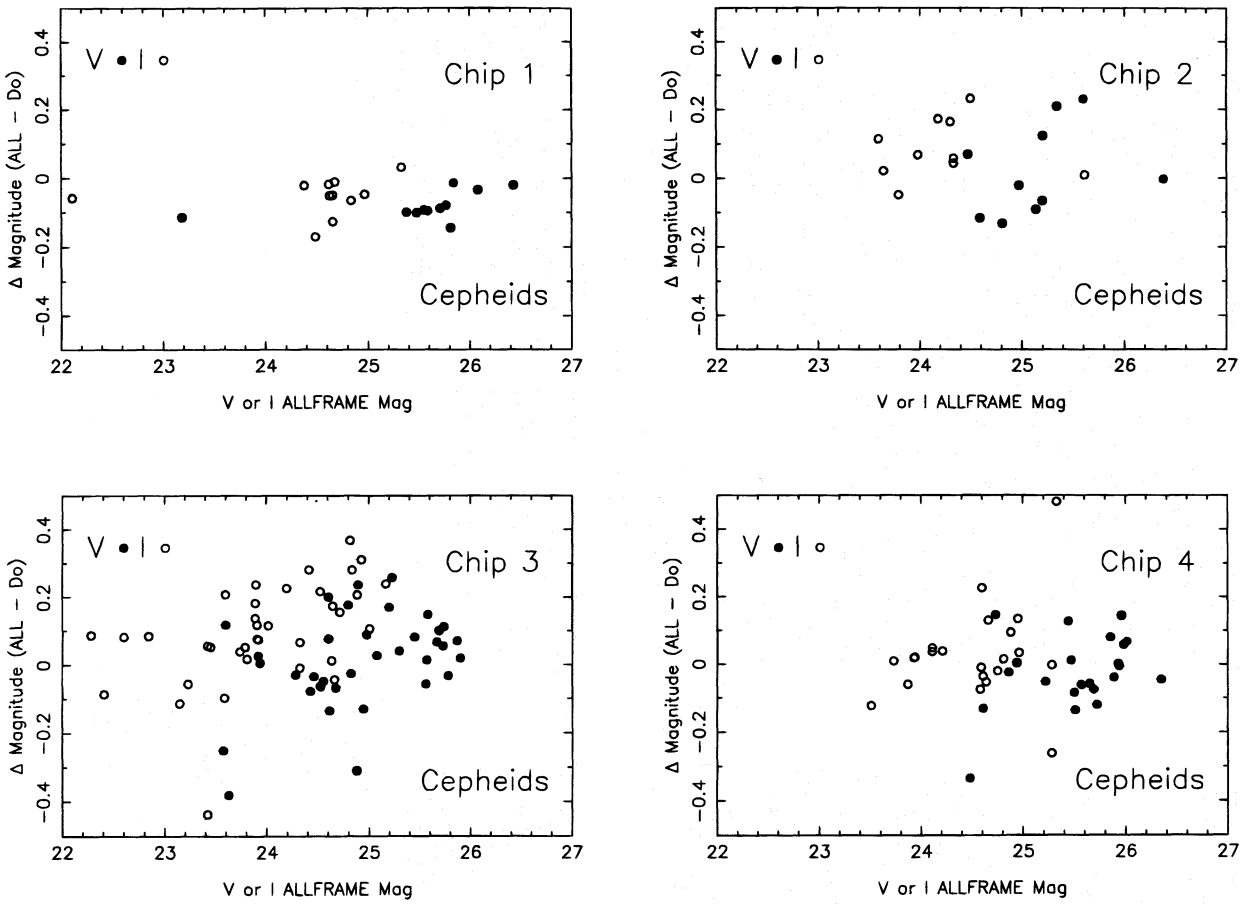

FIG. 3.—Comparison of the ALLFRAME and DoPHOT photometry for the Cepheids in NGC 925. The symbols are the same as for Fig. 2. As expected from the isolated star comparison, the Cepheid photometry in chip 3 has the best agreement.

nearly identical distance moduli to NGC 925 (§ 6). Nevertheless, we are continuing to explore the nature of the differences, and we shall present a more complete discussion in Stetson et al. (1996).

4. IDENTIFICATION OF VARIABLE STARS

Each of the two data sets described above was also analyzed independently for variable stars. Two methods were used to search for variable stars, using the ALLFRAME photometry. The first method was a search for stars with unusually high dispersion in their mean V magnitudes. The second method employed a variation on the correlated variability test, suggested by Welch & Stetson (1993). Periods for the candidate variables were found using a phase-dispersion minimization routine, as described by Stellingwerf (1978). The resulting light curves were checked by eye to verify the best period for each candidate. The search for variables in the DoPHOT reductions followed closely the procedure described in Saha & Hoessel (1990) and in Ferrarese et al. (1996). Candidates that were classed as having a $\geq 99\%$ confidence of being variables (based on a reduced chi-squared test) were then checked for periodicity using a variant of the method of Lafler & Kinman (1965). The number of spurious variables was minimized by requiring that the reduced chi-squared statistic be greater than 2.0 when the minimum and maximum values were removed from the calculation. The light curves of each variable candidate were then inspected individually, and any alternate minima in the phase dispersion relation were checked to see which produced the best Cepheid light curve. Generally, the minimum in the phase dispersion plot produced the best light curve. The image of each Cepheid candidate was also inspected at a number of epochs. Those falling in severely crowded regions or in areas dominated by CCD defects were also excluded.

The two lists of candidate variables, one from the ALLFRAME photometry and one from the DoPHOT photometry, were then combined; those candidates that appeared to be real variables in *both* the ALLFRAME and DoPHOT datasets were retained. As an independent check on the completeness of our variable star search, P. B. S. applied a test version of an automated light-curve fitting program to our data (Stetson 1996). This program independently recovered all of our high-quality variables, and drew attention to 10 additional candidates. The final sample comprises 80 Cepheid variables in NGC 925. In defining this sample, we have adopted a conservative approach, rejecting questionable candidates in order to ensure a high-quality Cepheid sample that is as free as possible from selection biases or possible systematic errors in the periods or mean magnitudes, at the expense of some completeness.

Finder charts for the 80 selected Cepheids are shown in Figures 4 and 5. Figure 4 shows the four *HST* chips with the Cepheids indicated. Figure 5 shows small 51 × 51 pixel fields (5″.0 for the wide-field CCDs and a 2″.5 for the planetary camera CCD) centered on each Cepheid.

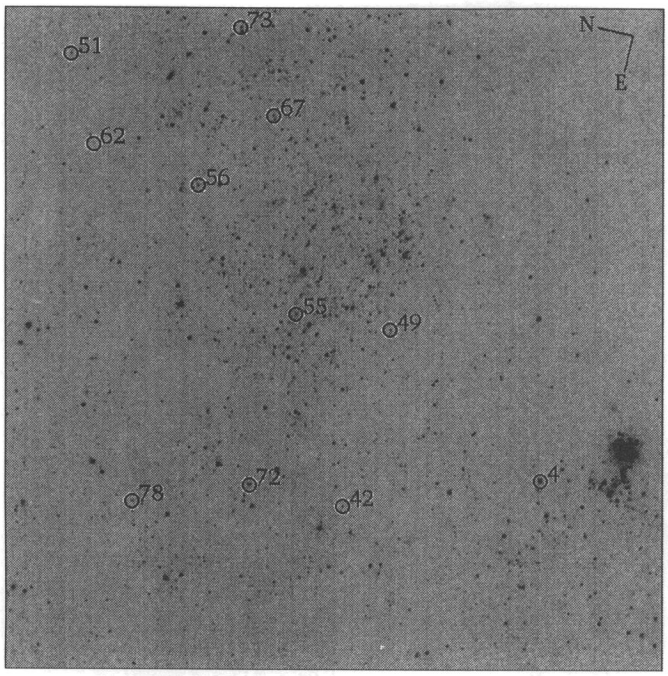

FIG. 4*a*

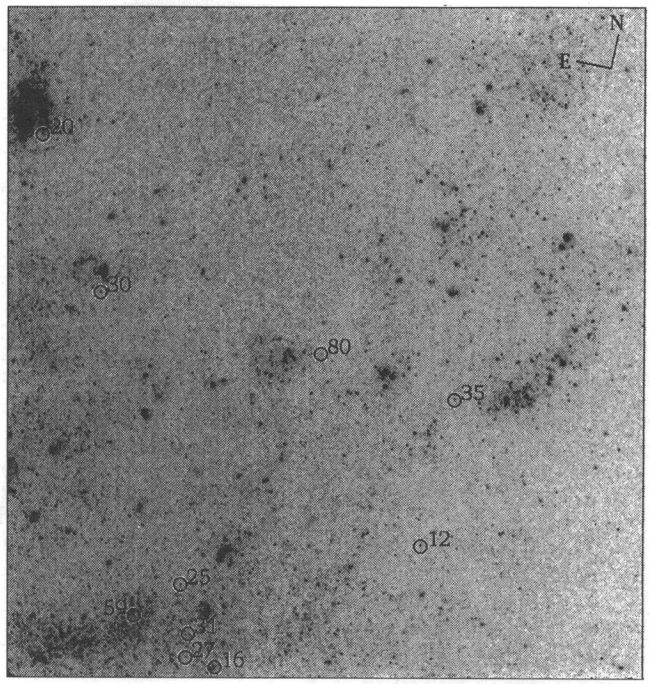

FIG. 4*b*

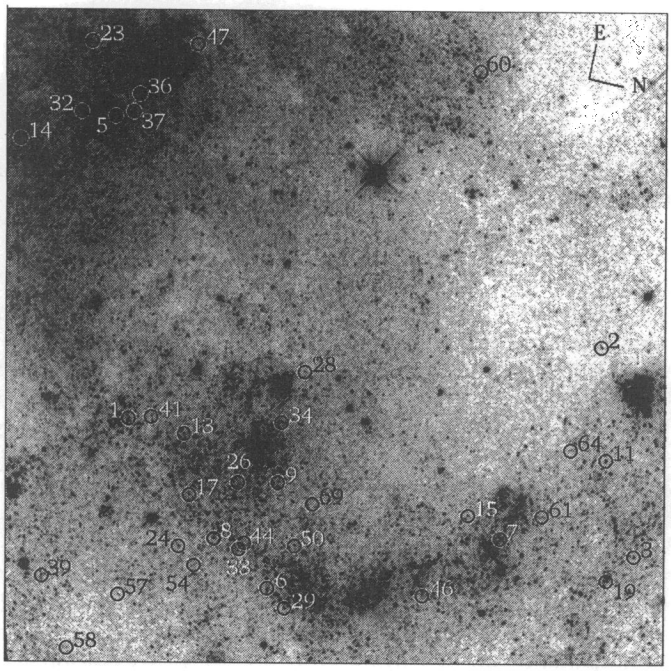

FIG. 4*c*

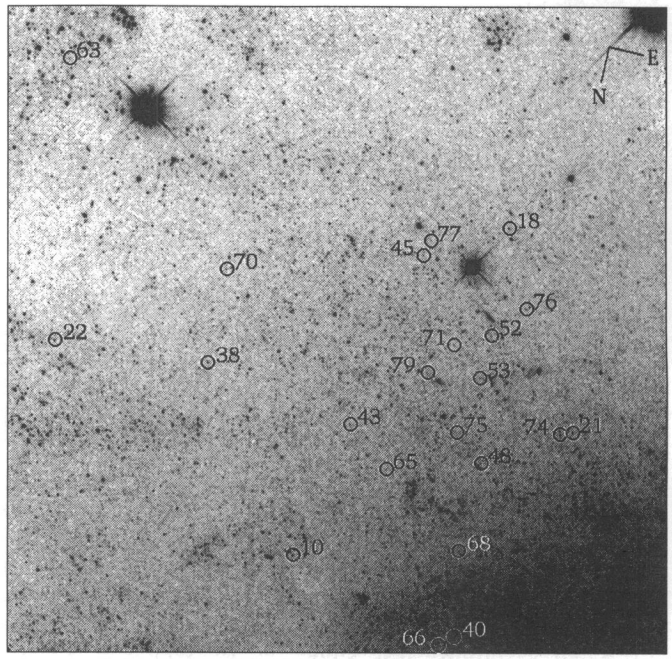

FIG. 4*d*

FIG. 4.—(*a*) Finder chart for the NGC 925 Cepheids located in chip 1 (the Planetary Camera) of the WFPC2 instrument. Field is 34″ × 34″. Cepheids are circled and labeled with their identification numbers, as listed in Table 7. North and east directions are indicated in the top right-hand corner. (*b*) Finder chart for the NGC 925 Cepheids located in chip 2 of the WFPC2 instrument. The field is 1.′3 × 1.′3. Cepheids are circles and labeled with their identification numbers, as listed in Table 7. North and east directions are indicated in the top right-hand corner. (*c*) Finder chart for the NGC 925 Cepheids located in chip 3 of the WFPC2 instrument. Field is 1.′3 × 13′. Cepheids are circles and are labeled with their identification numbers, as listed in Table 7. North and east directions are indicated in the top right-hand corner. (*d*) Finder chart for the NGC 925 Cepheids located in chip 4 of the WFPC2 instrument. Field is 1.′3 × 13′. Cepheids are circles and are labeled with their identification numbers, as listed in Table 7. North and east directions are indicated in the top right-hand corner.

There were a number of candidate variables that for one reason or another did not make our final cut as Cepheids. These are listed in § 3 of the Appendix as possible variables. In addition, a number of long-period ($P \gg 70$ days) variables were found. Since our 70 day observing window covers only a fraction of a cycle for these stars, we have not been able to determine accurate periods, but the stars are identified for future reference. A table in § 3 of the Appendix

1996ApJ...470....1S

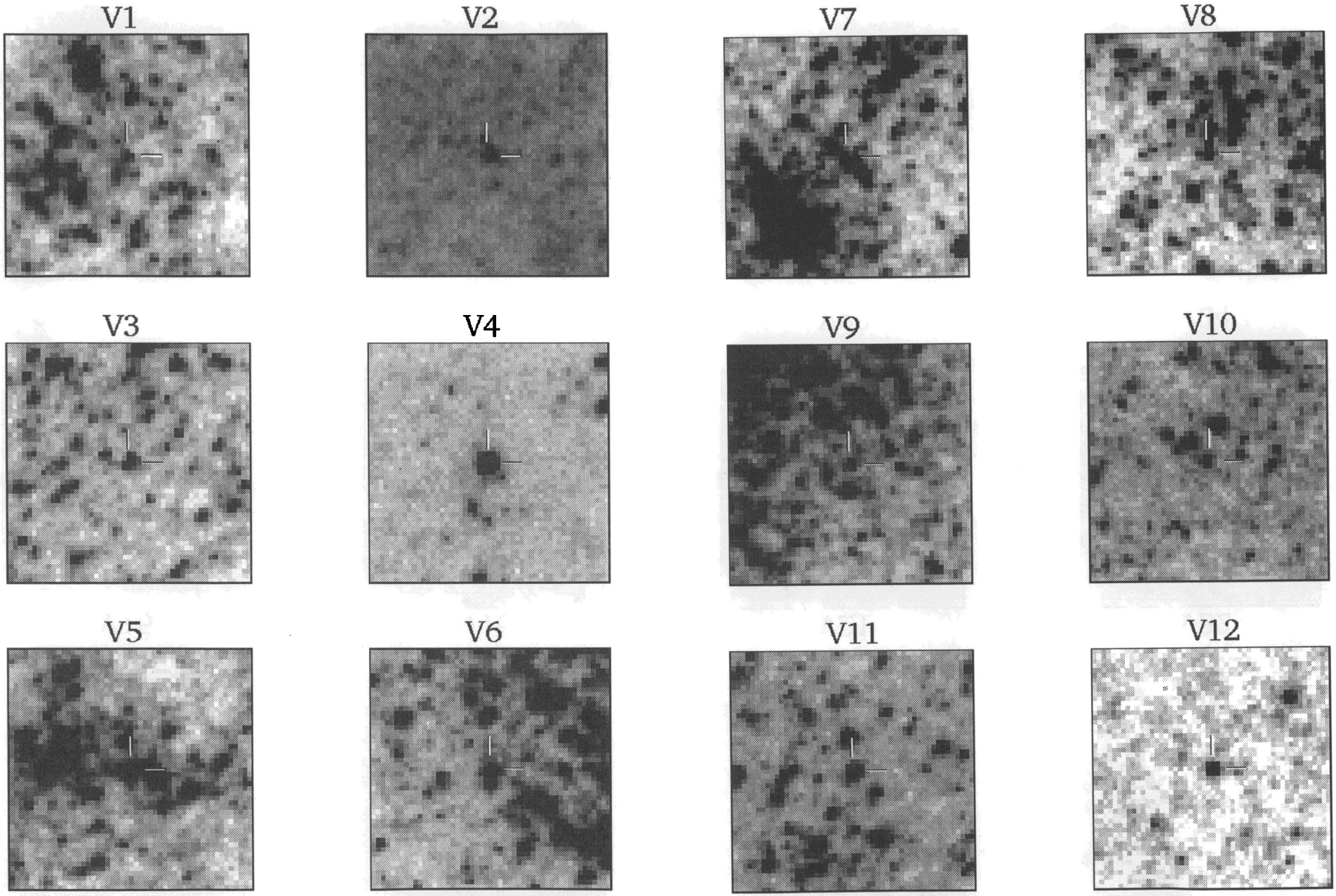

FIG. 5*a*

FIG. 5*b*

FIG. 5.—Finder charts for the NGC 925 Cepheids. Each panel is a 51 × 51 pixel field of view centered on the variable. Each panel has been independently scaled in intensity to clearly show the Cepheid.

1996ApJ...470....1S

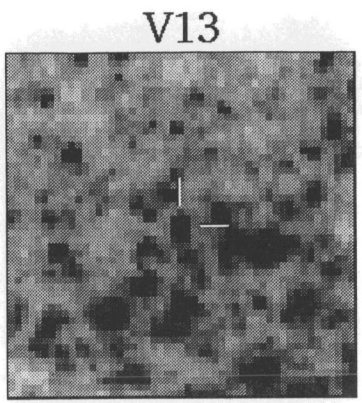

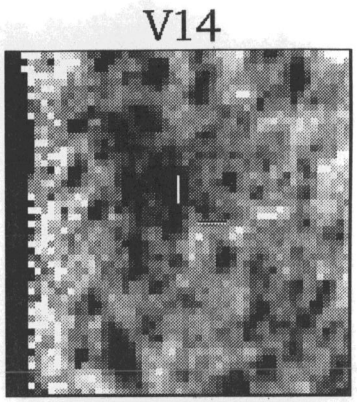

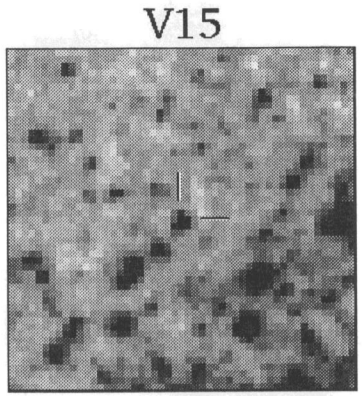

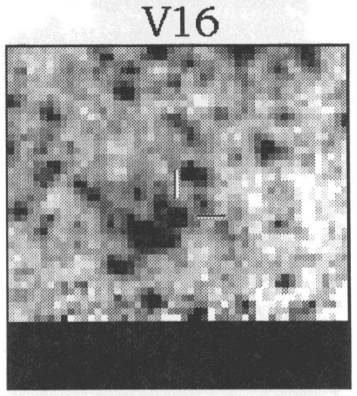

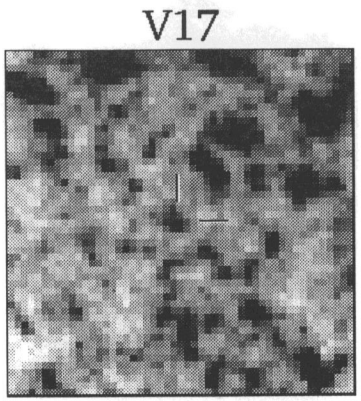

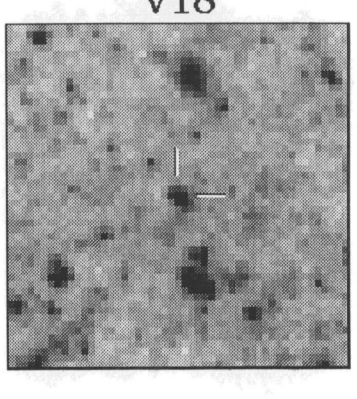

FIG. 5c

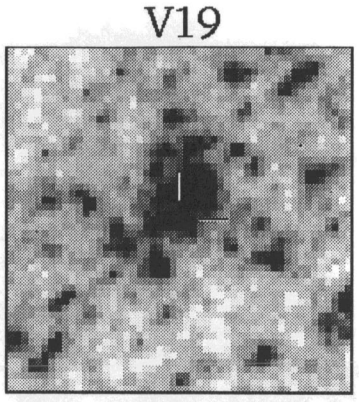

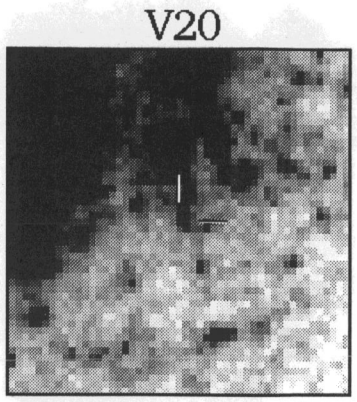

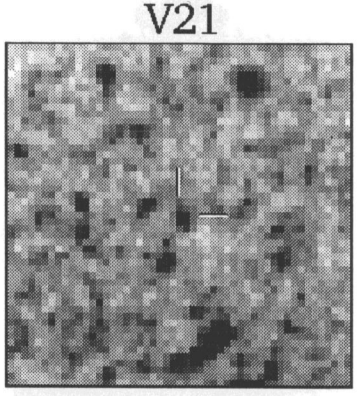

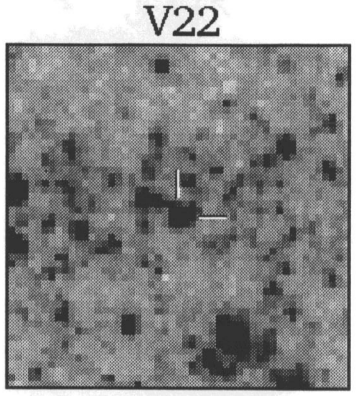

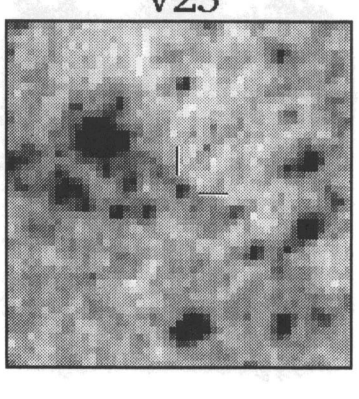

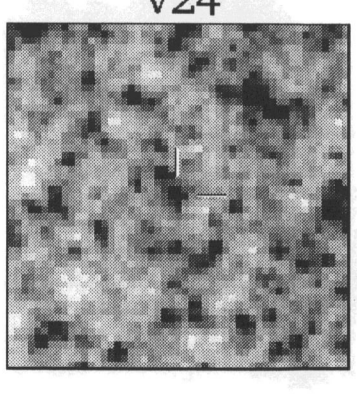

FIG. 5d

1996ApJ...470....1S

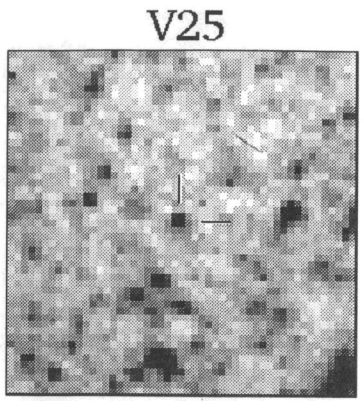

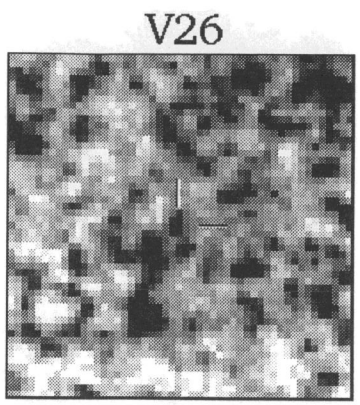

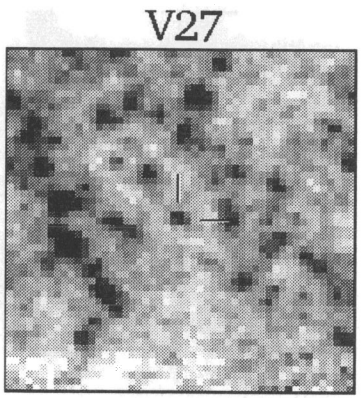

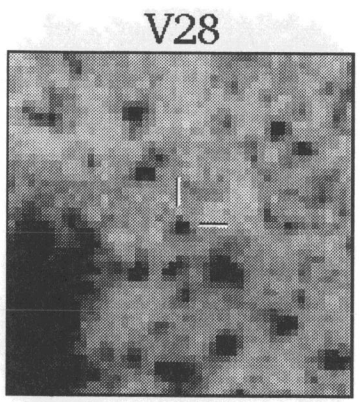

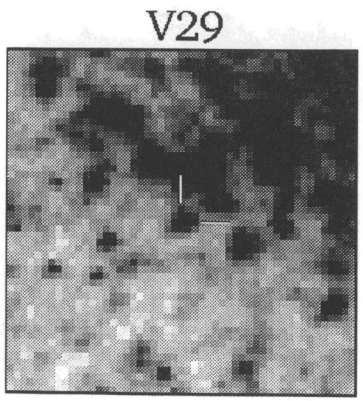

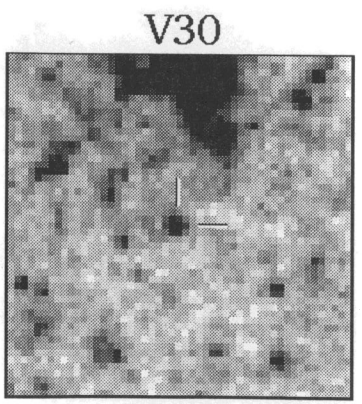

FIG. 5e

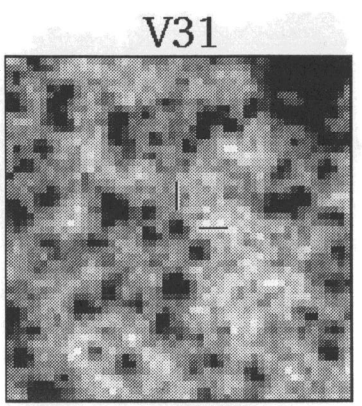

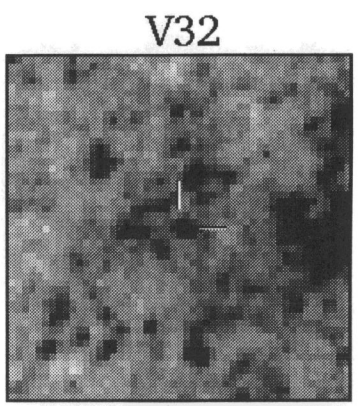

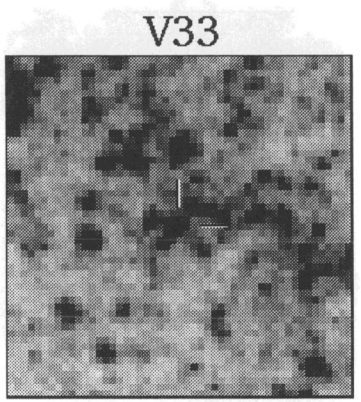

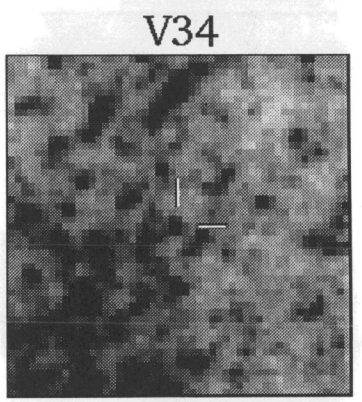

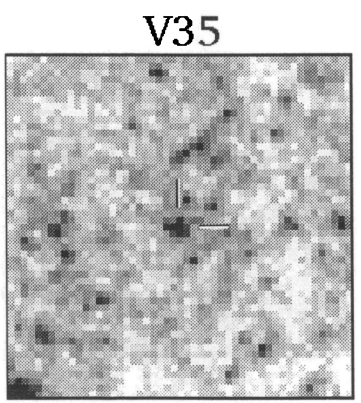

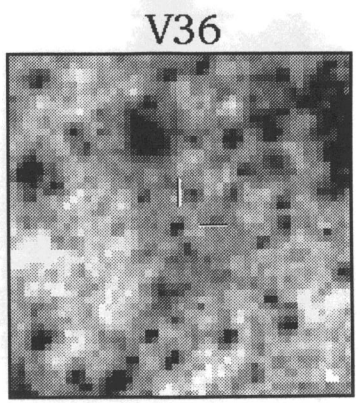

FIG. 5f

1996ApJ...470....1S

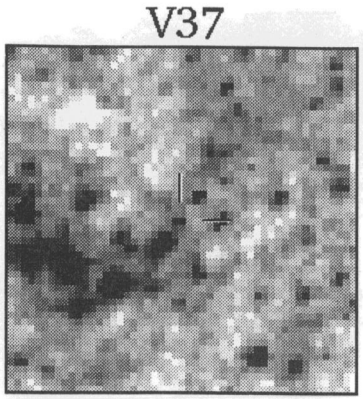

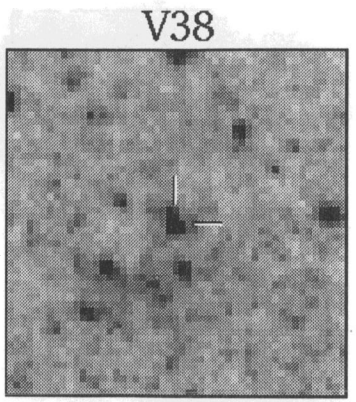

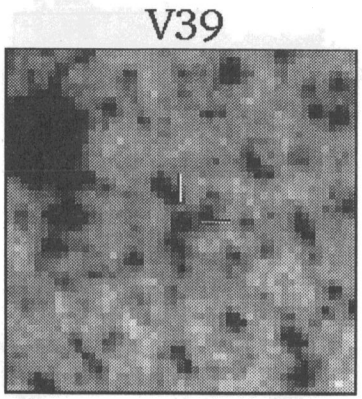

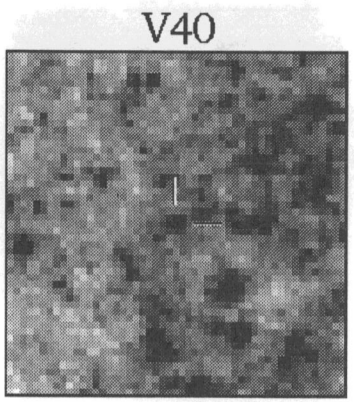

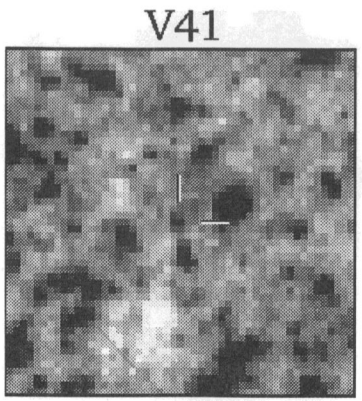

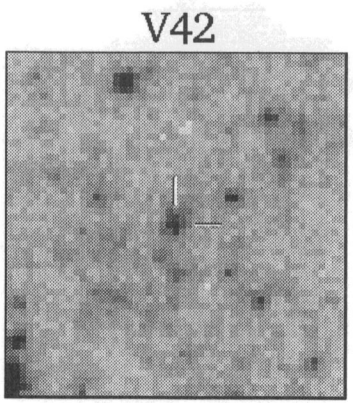

FIG. 5g

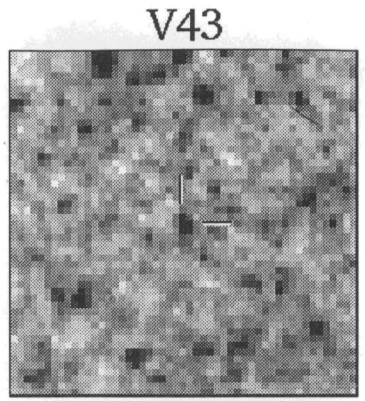

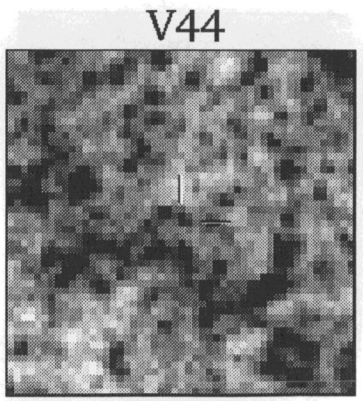

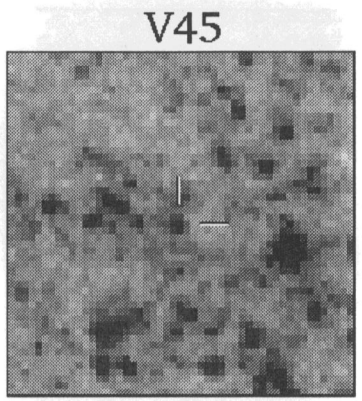

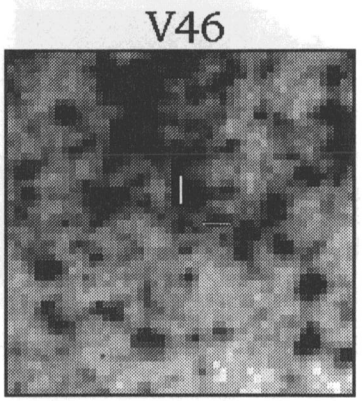

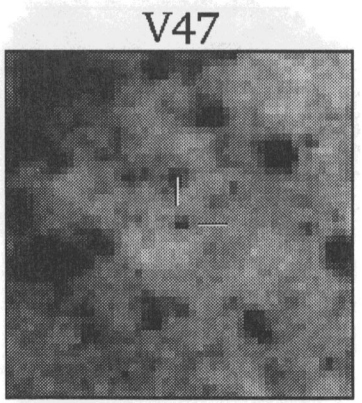

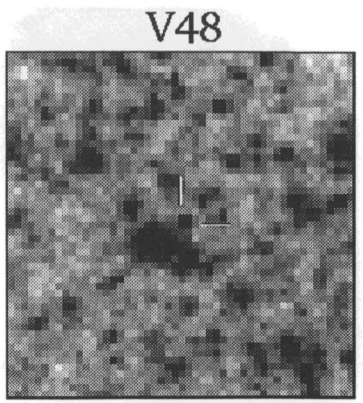

FIG. 5h

1996ApJ...470....1S

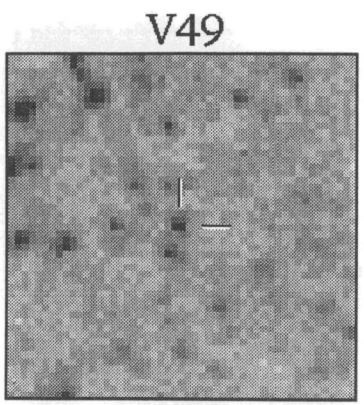

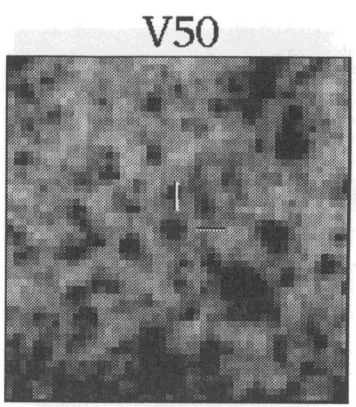

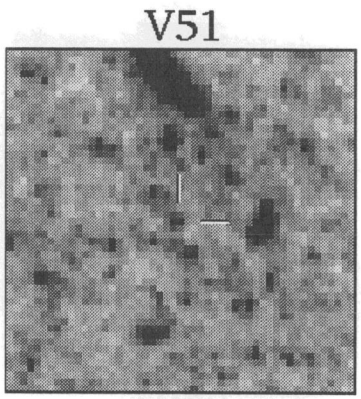

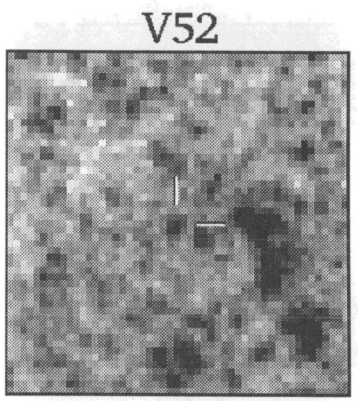

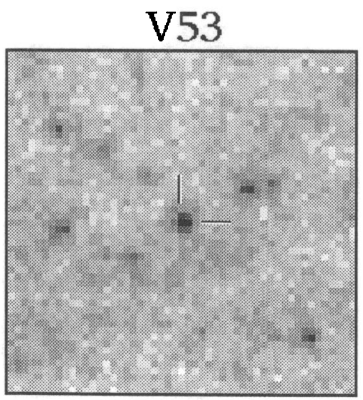

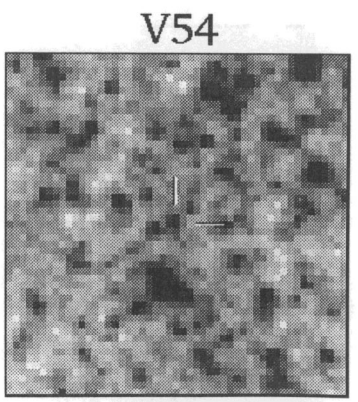

FIG. 5*i*

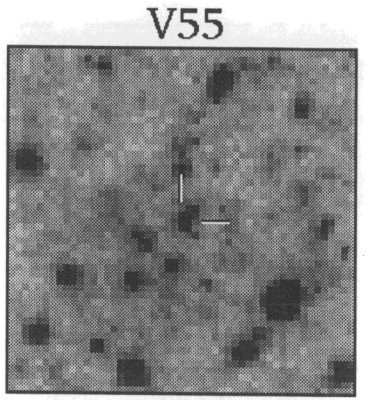

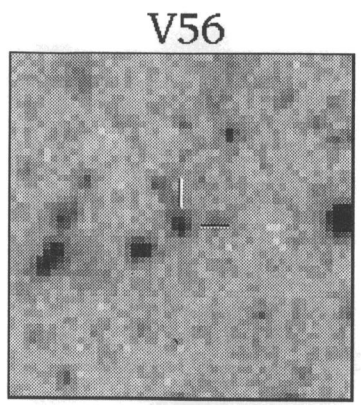

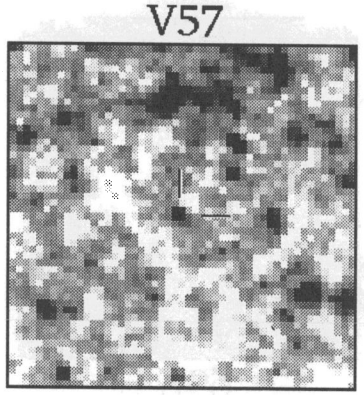

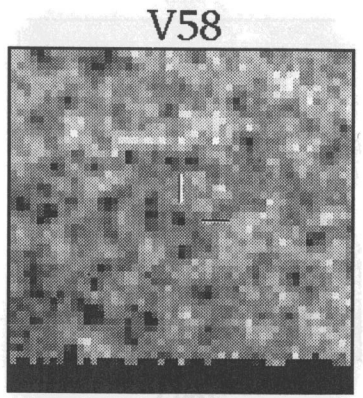

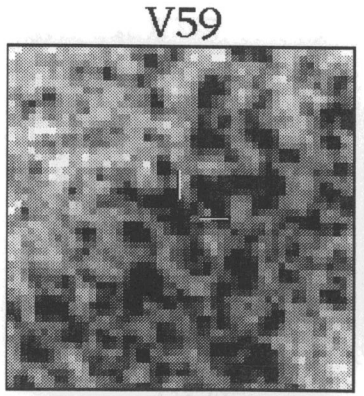

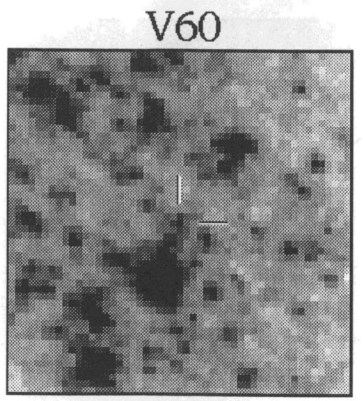

FIG. 5*j*

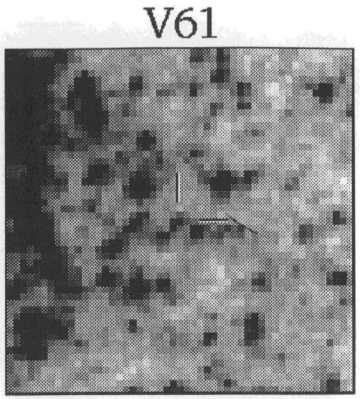

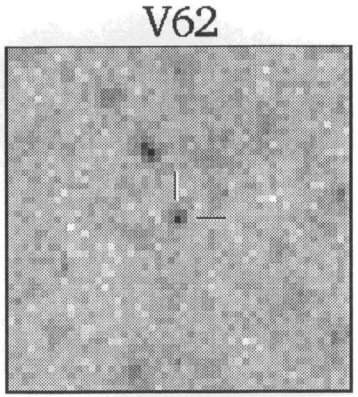

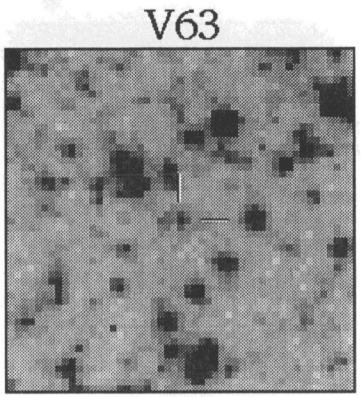

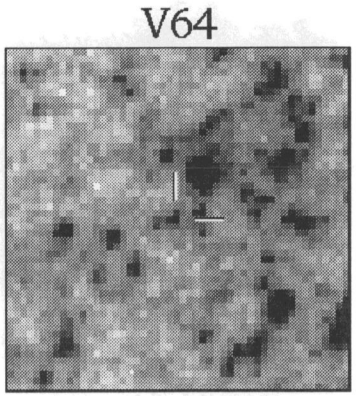

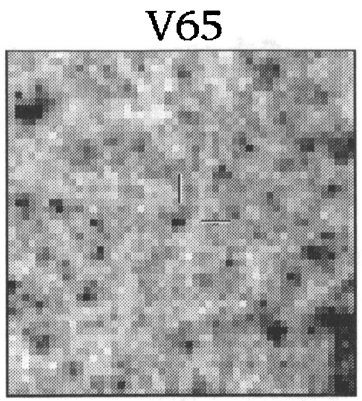

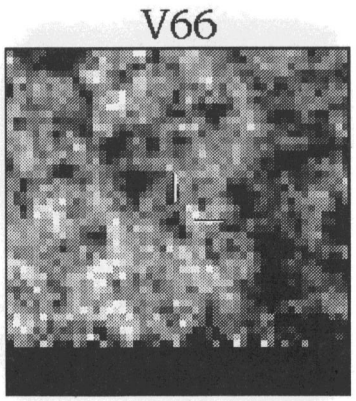

FIG. 5k

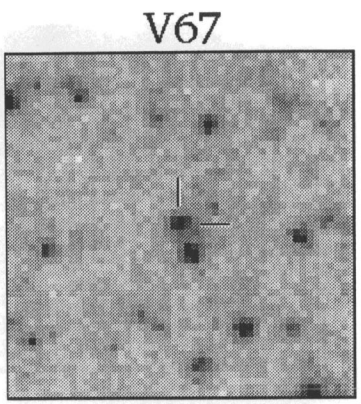

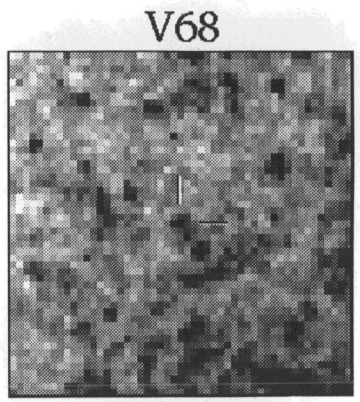

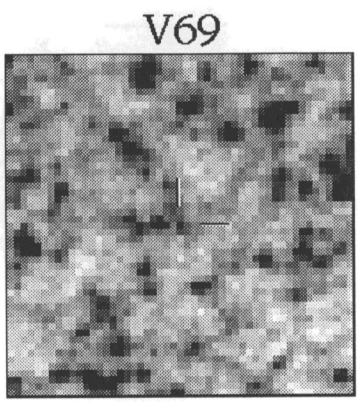

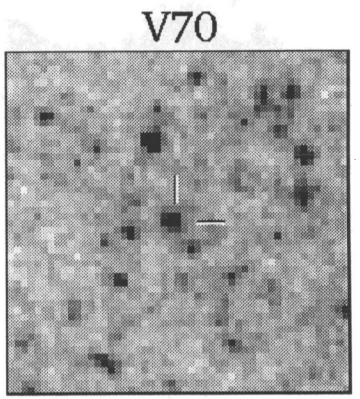

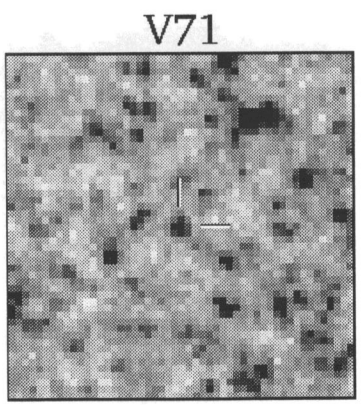

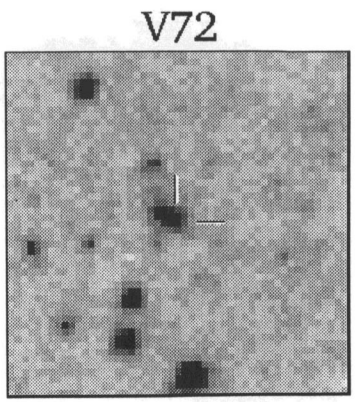

FIG. 5l

1996ApJ...470....1S

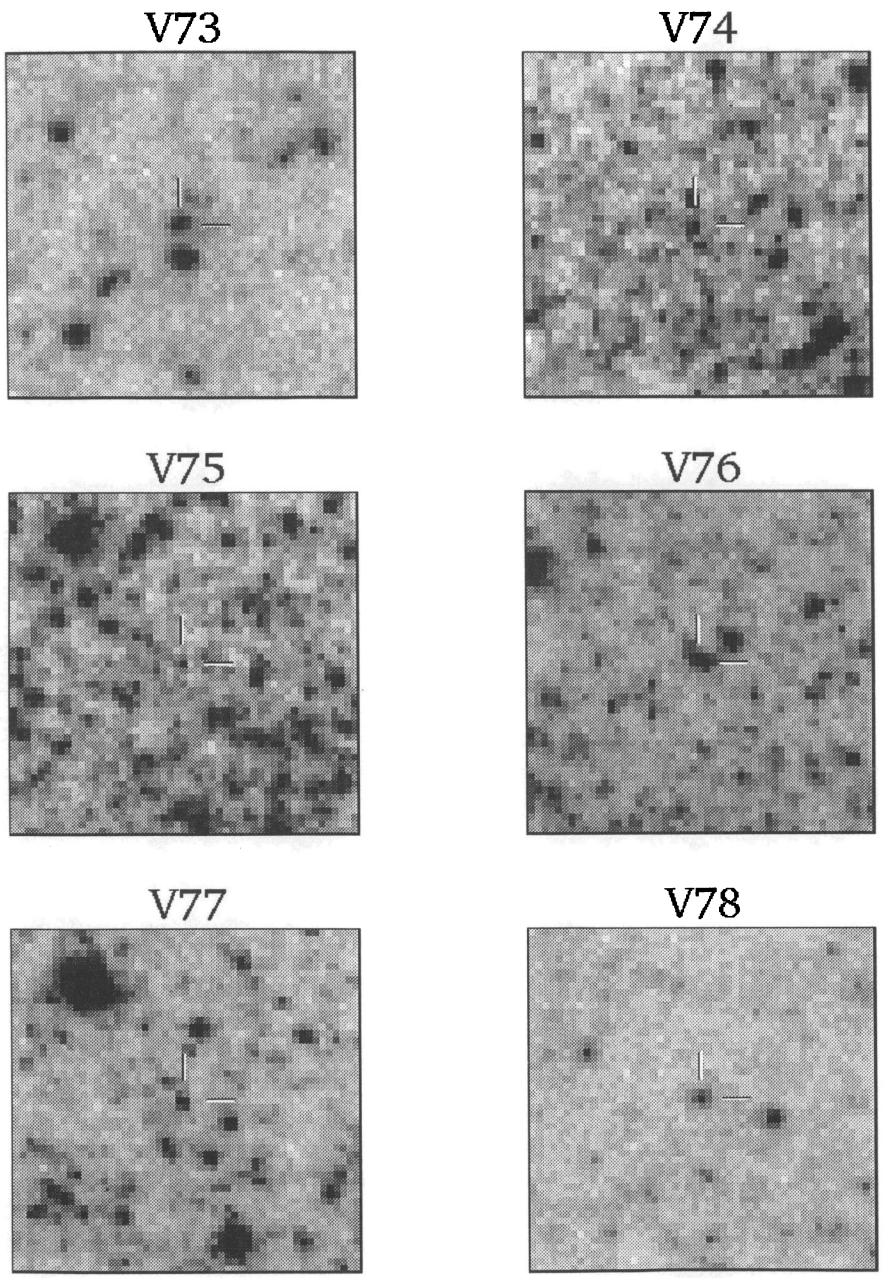

FIG. 5*m*

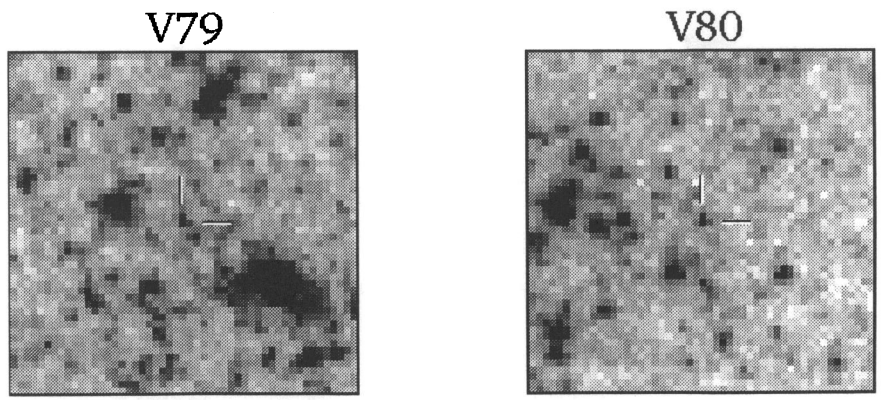

FIG. 5*n*

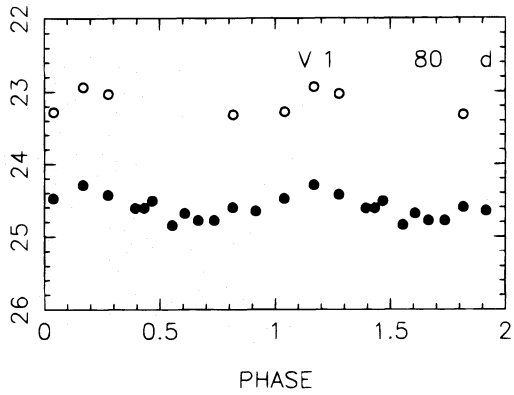

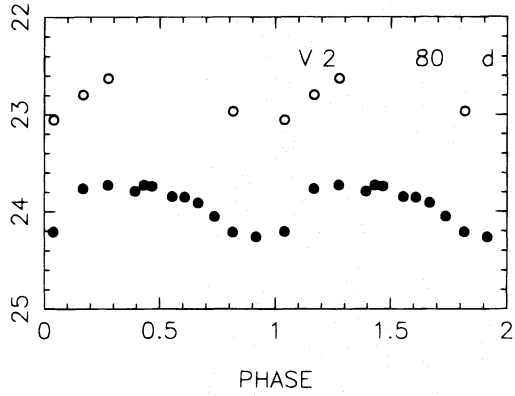

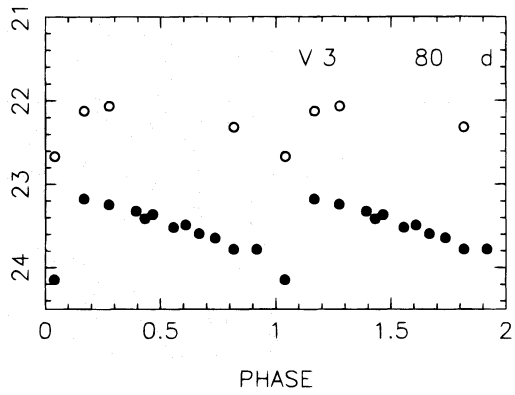

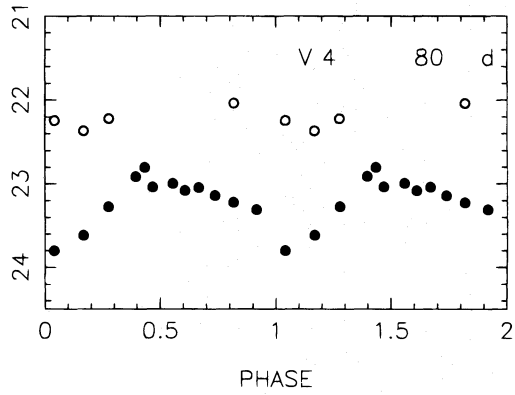

FIG. 6*a*

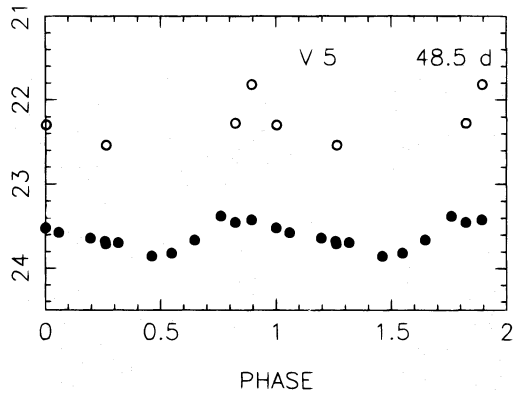

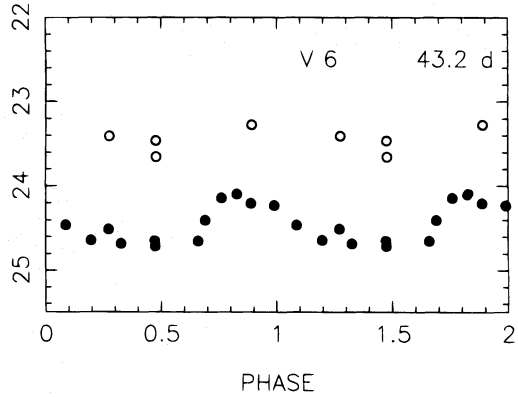

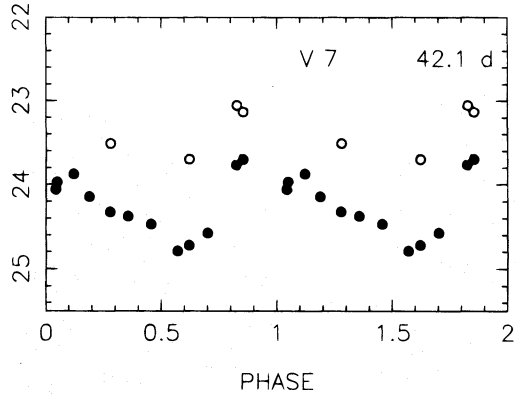

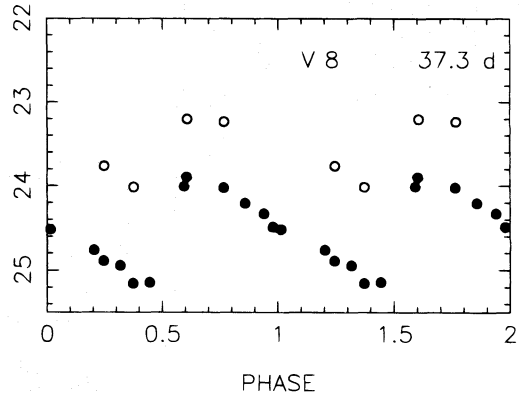

FIG. 6*b*

FIG. 6.—*V* and *I* light curves for the NGC 925 Cepheids. Magnitudes of cosmic-ray pairs of observations were averaged before being plotted. *V* observations are represented by the filled circles; the *I* observations are the open circles. Data are repeated over a second cycle for clarity.

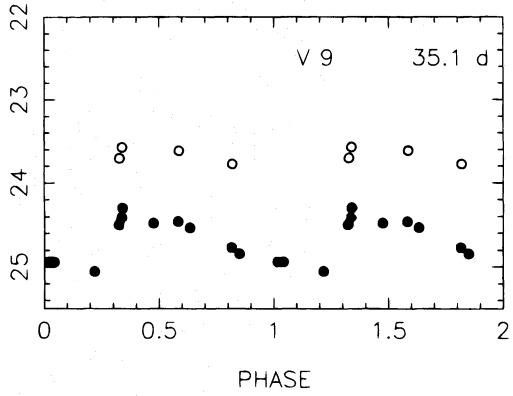

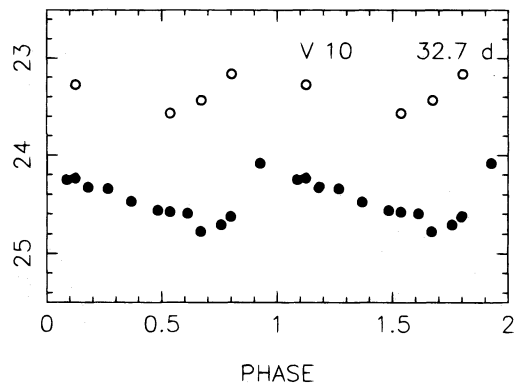

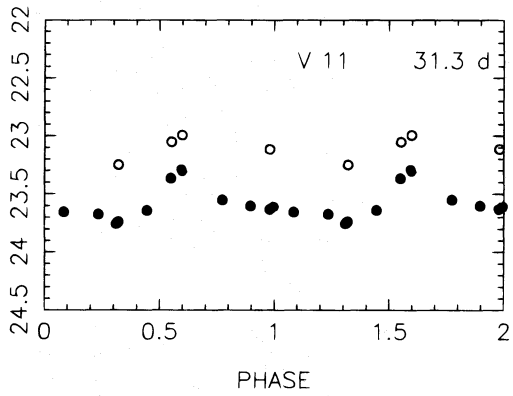

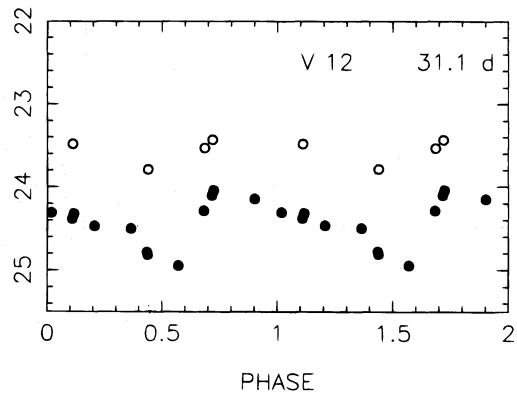

FIG. 6*c*

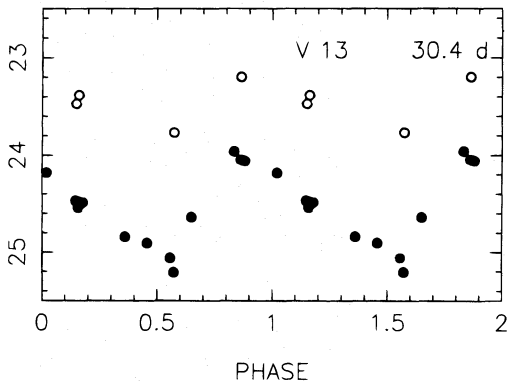

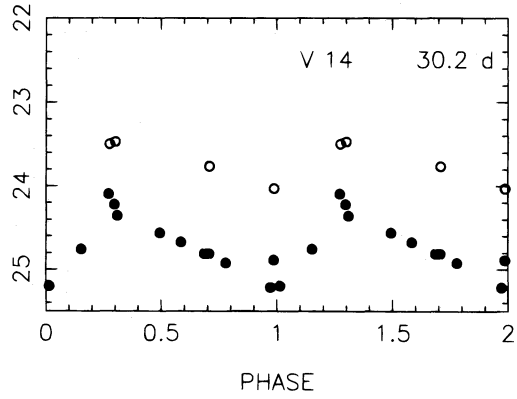

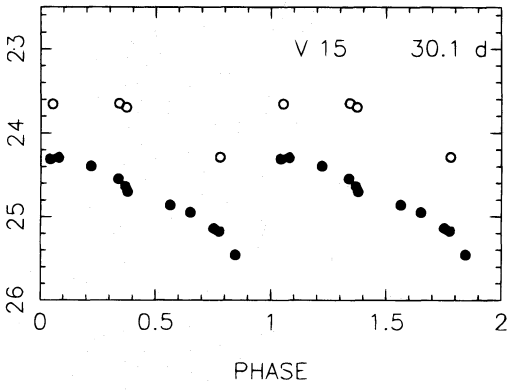

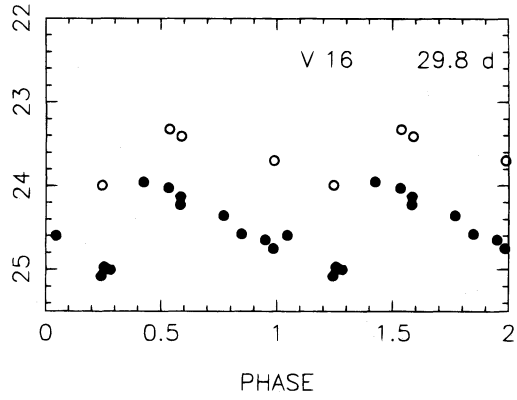

FIG. 6*d*

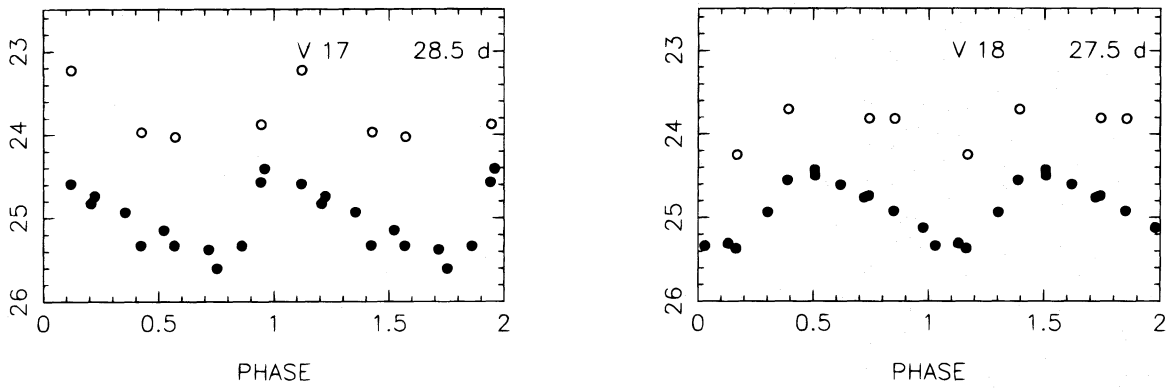

FIG. 6e

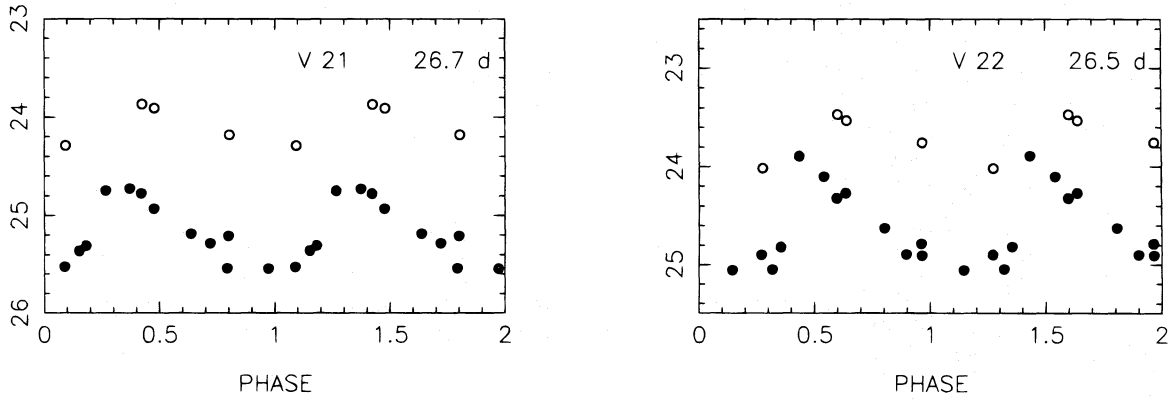

FIG. 6f

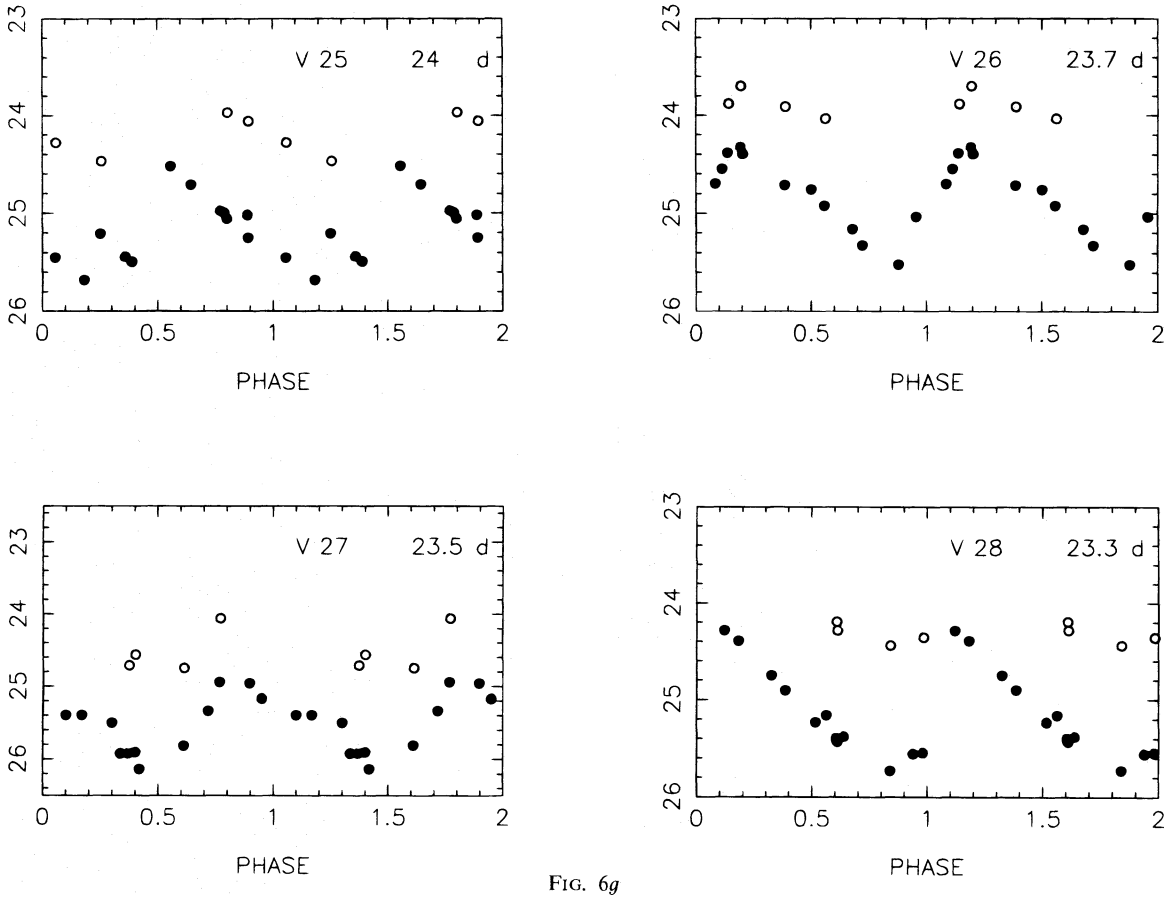

FIG. 6g

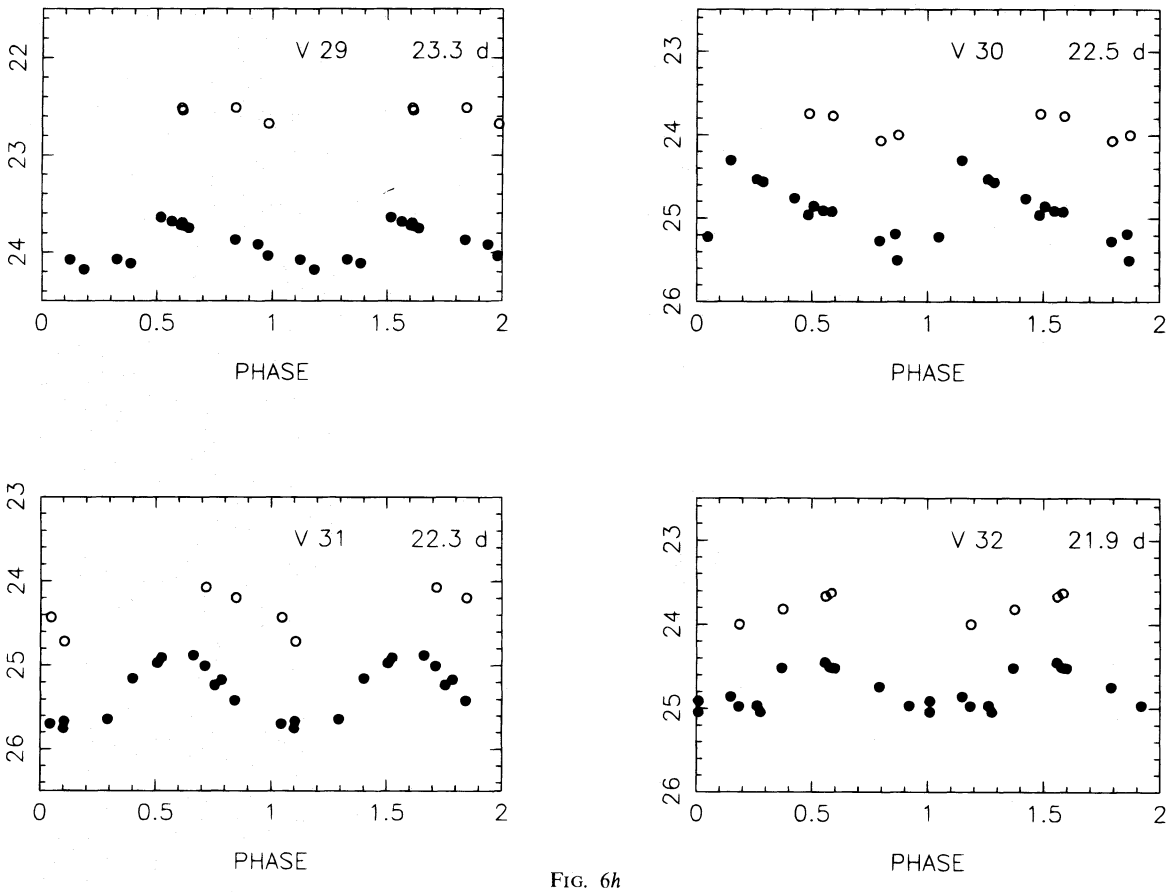

FIG. 6h

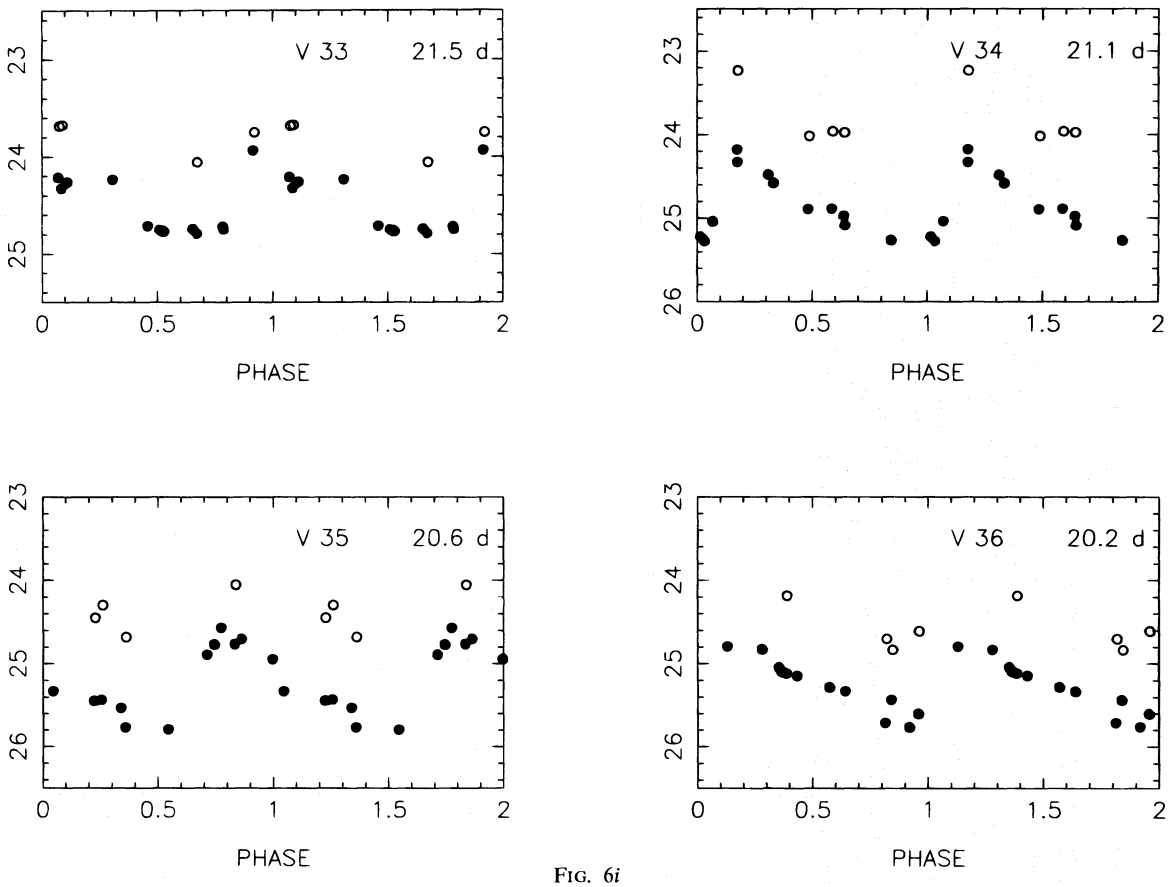

FIG. 6*i*

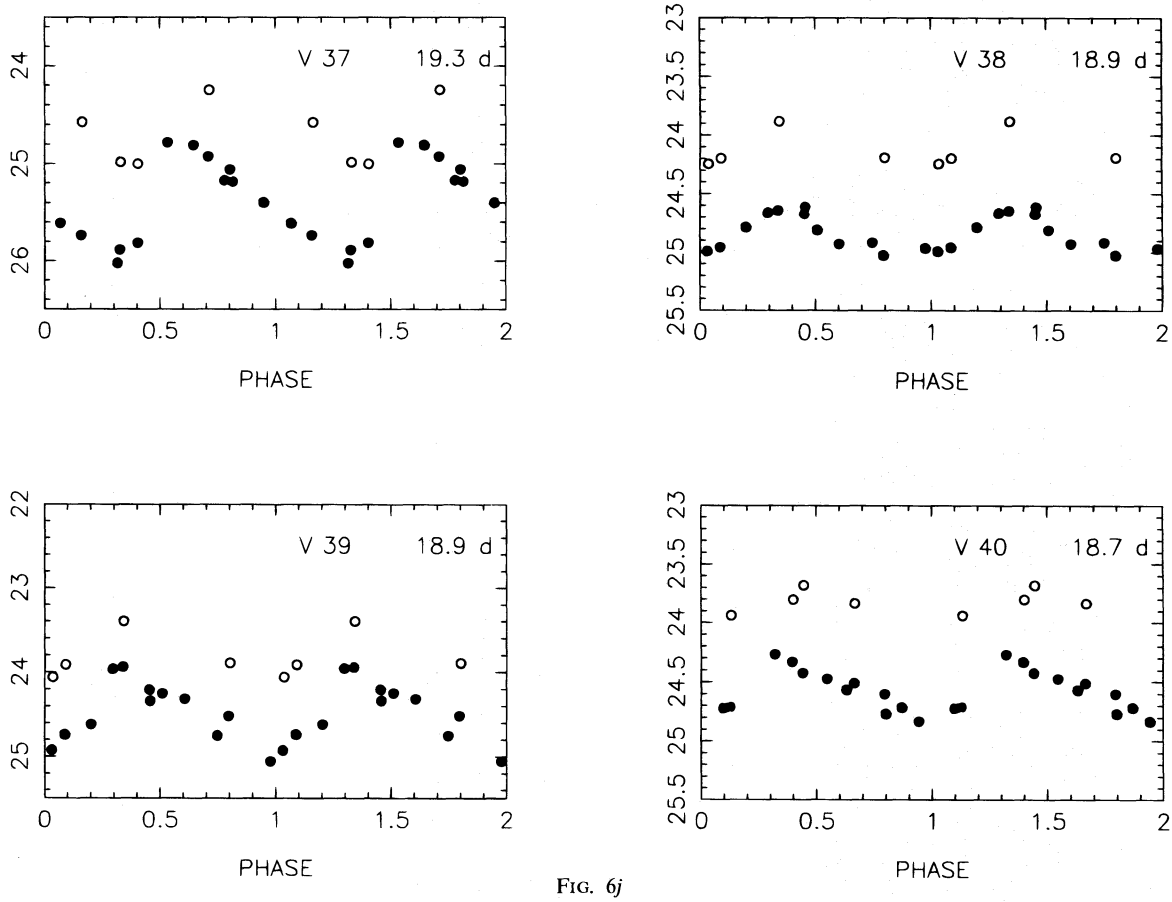

FIG. 6*j*

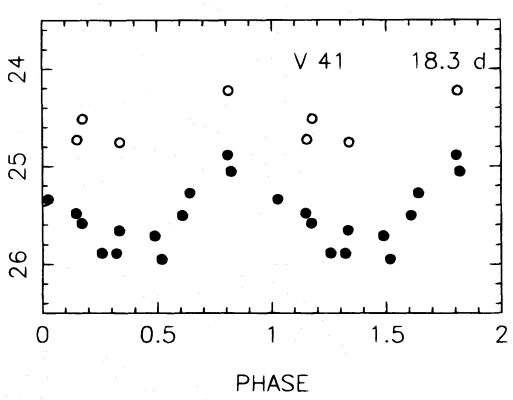

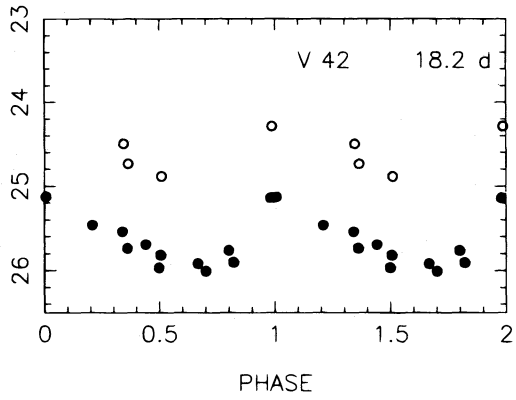

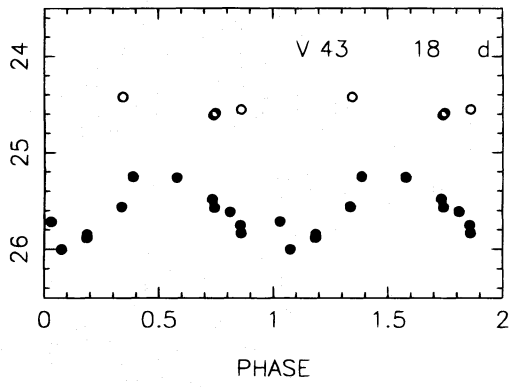

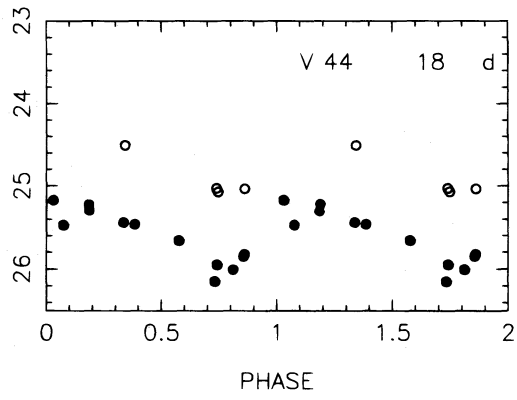

FIG. 6*k*

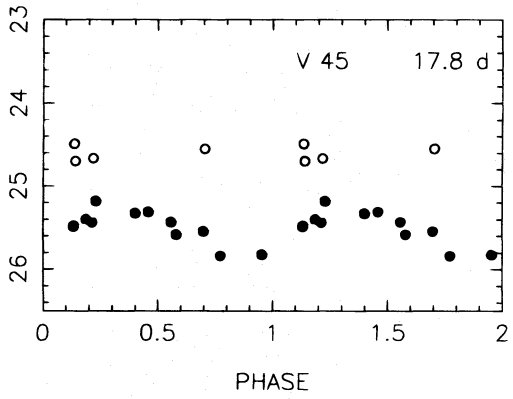

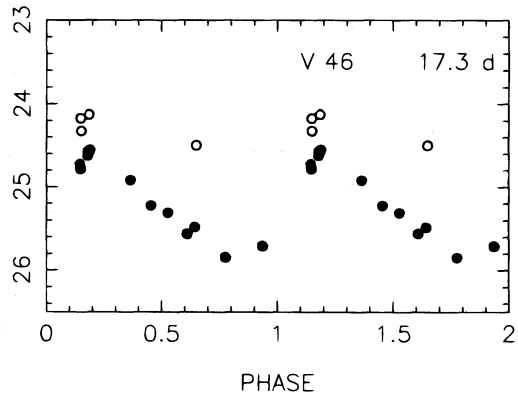

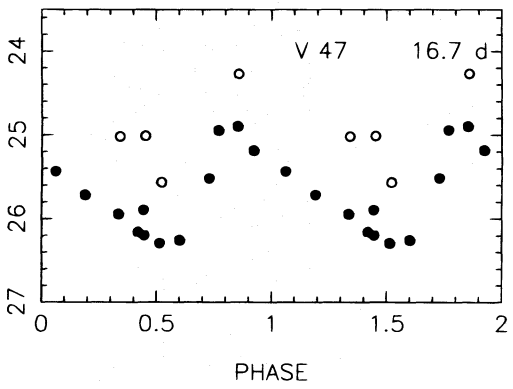

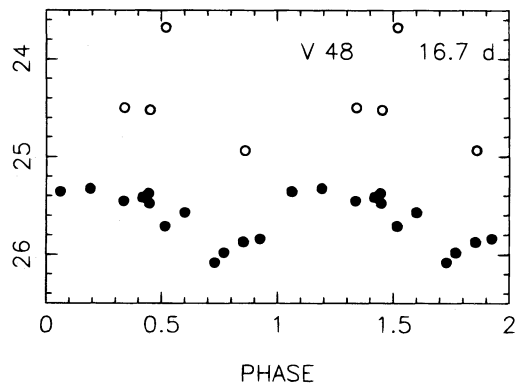

FIG. 6*l*

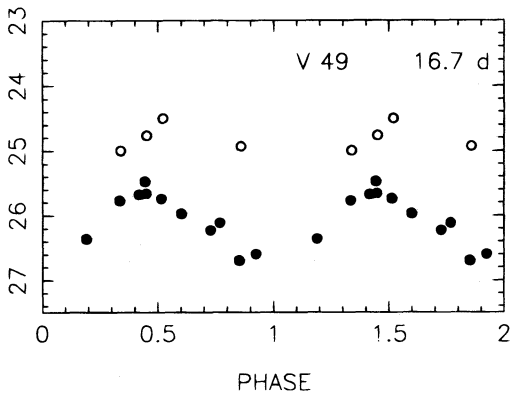

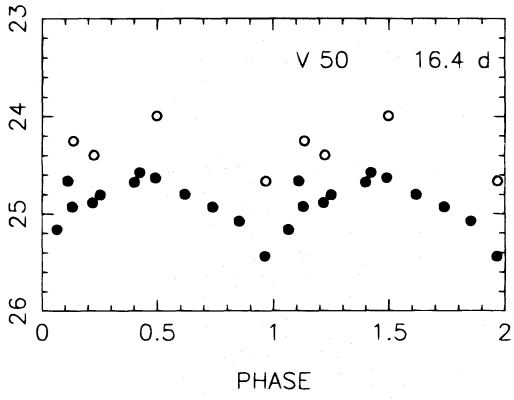

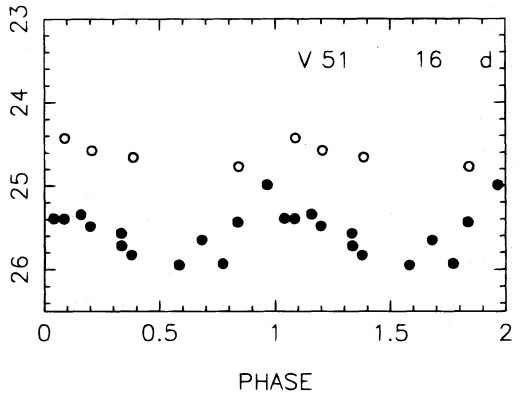

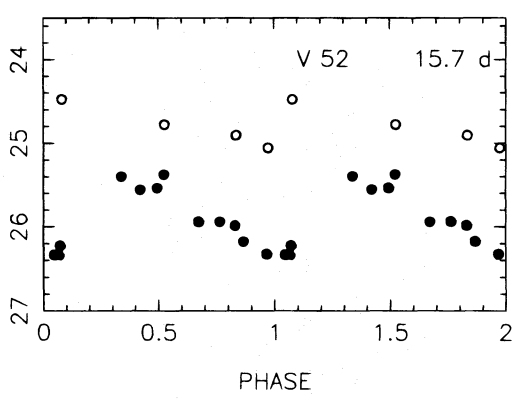

FIG. 6*m*

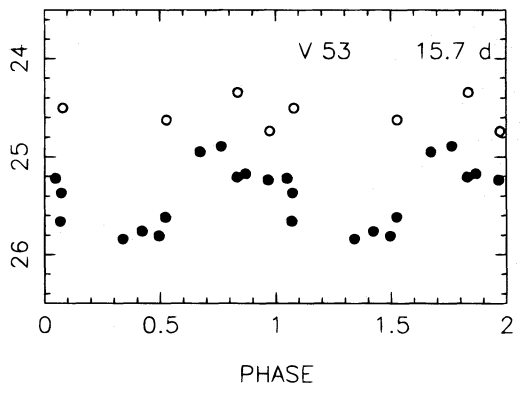

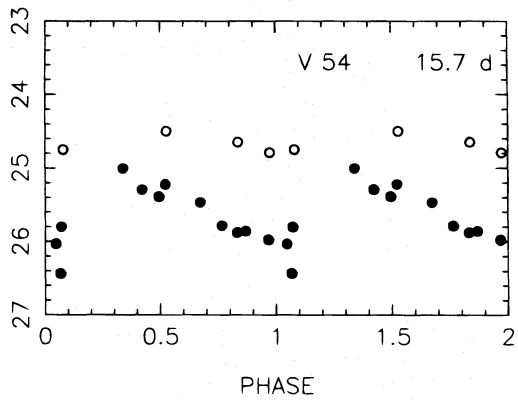

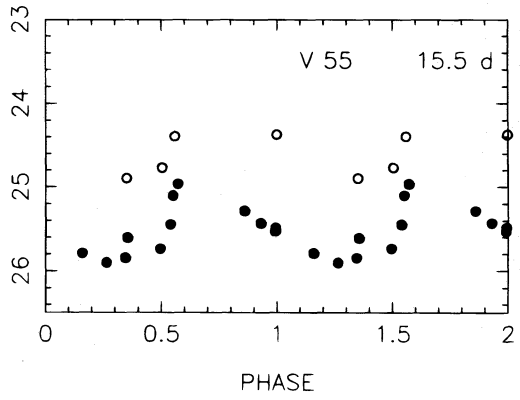

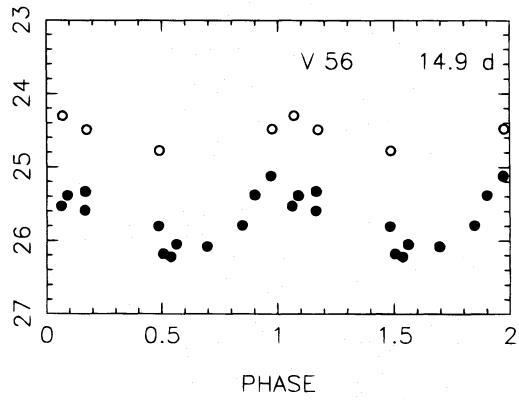

FIG. 6*n*

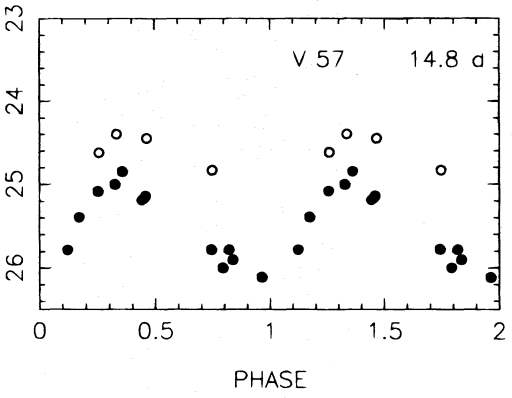

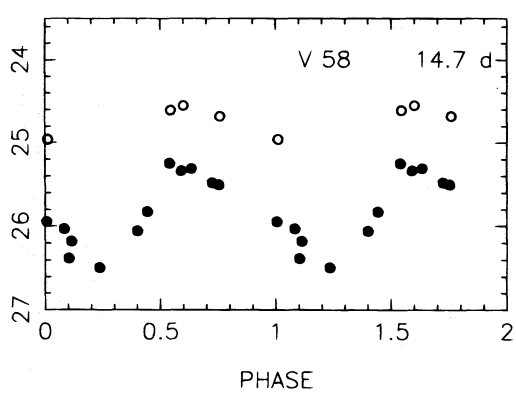

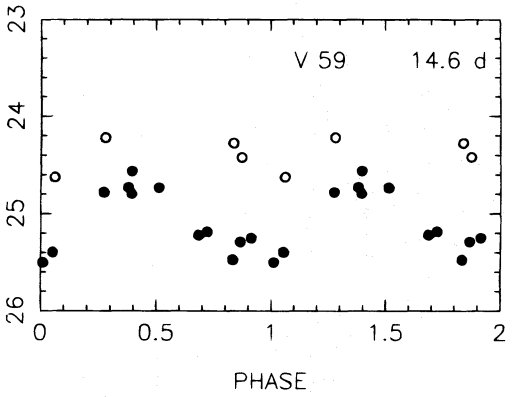

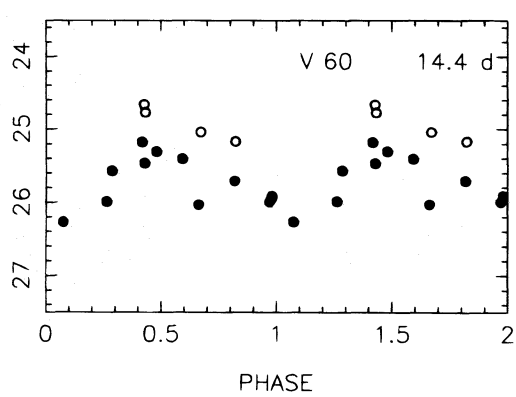

FIG. 6*o*

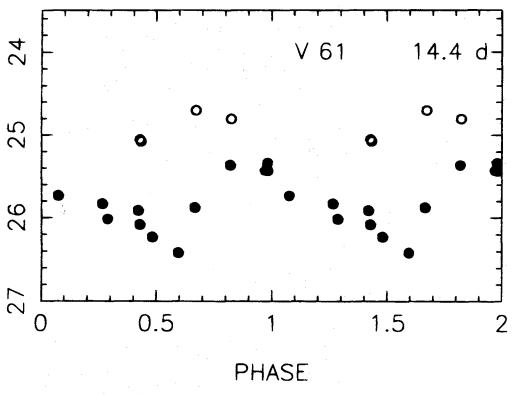

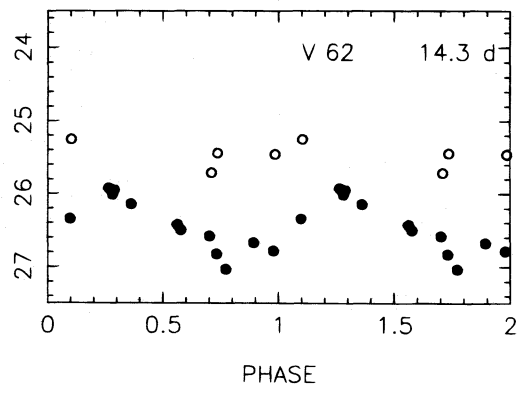

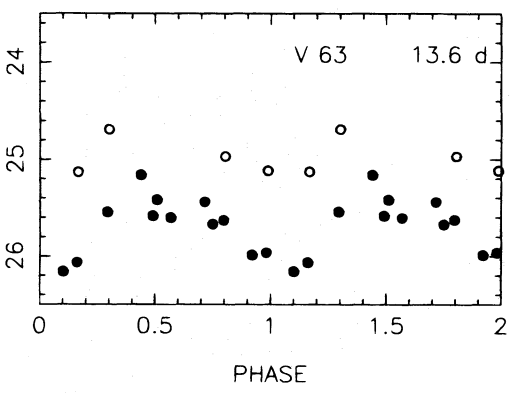

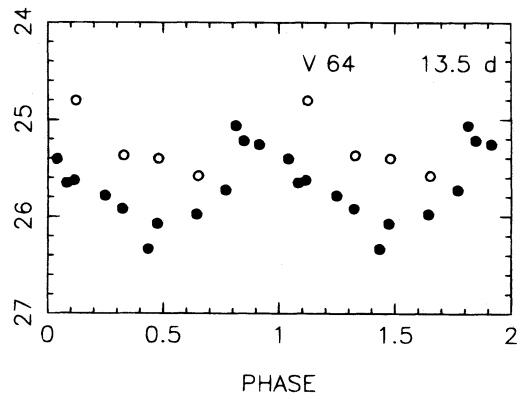

FIG. 6*p*

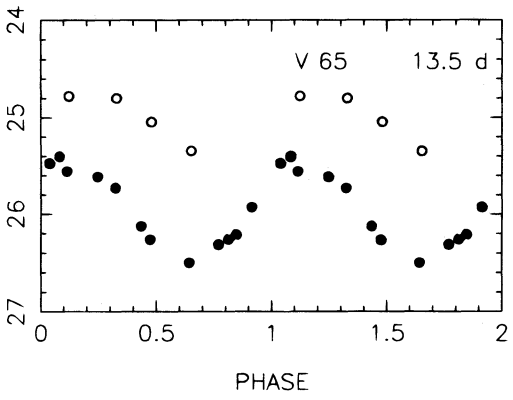

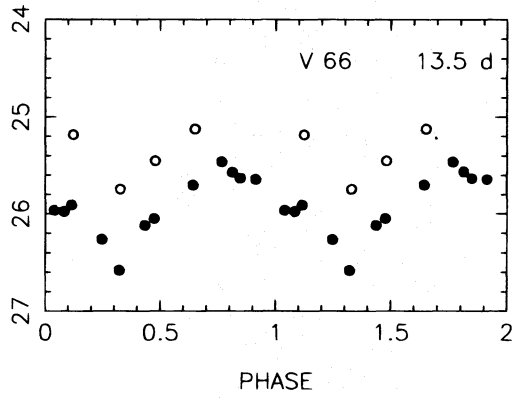

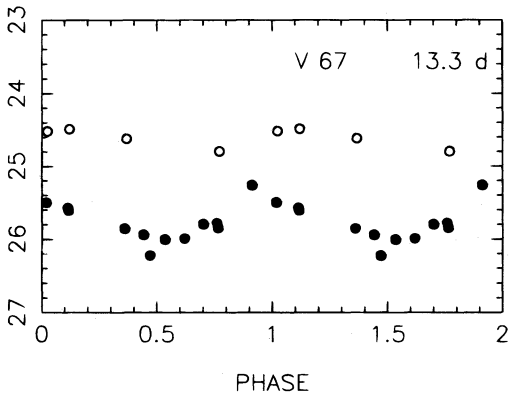

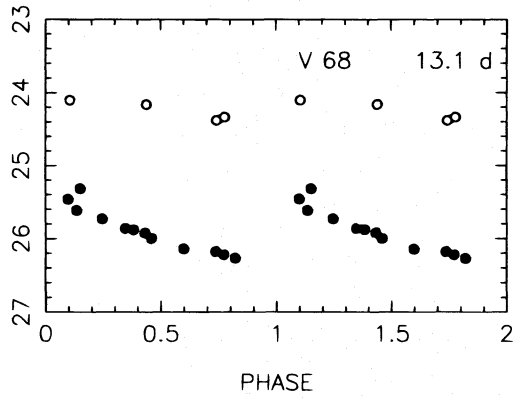

FIG. 6*q*

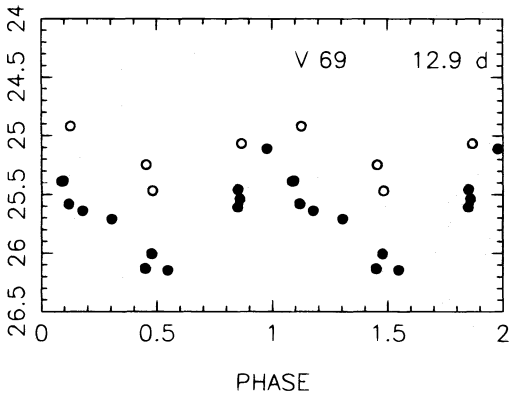

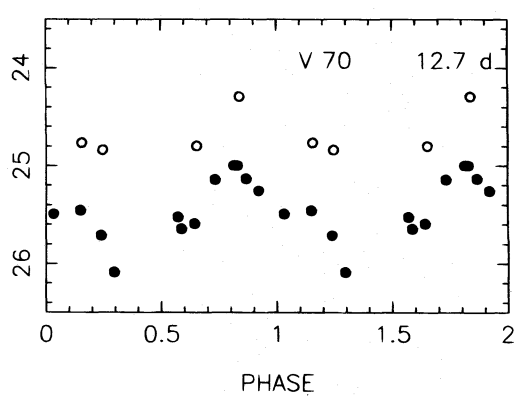

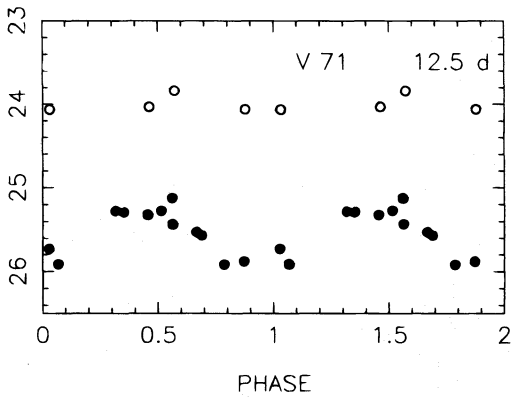

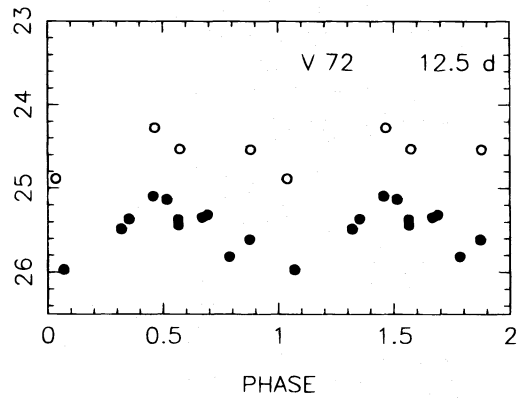

FIG. 6*r*

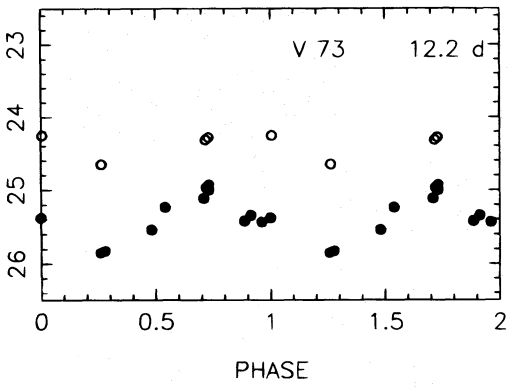

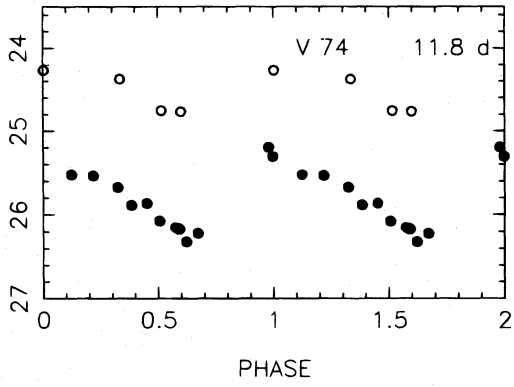

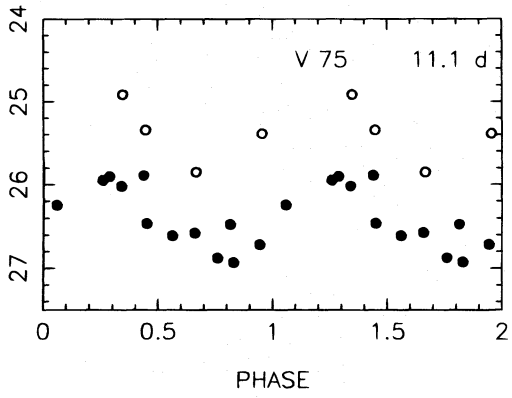

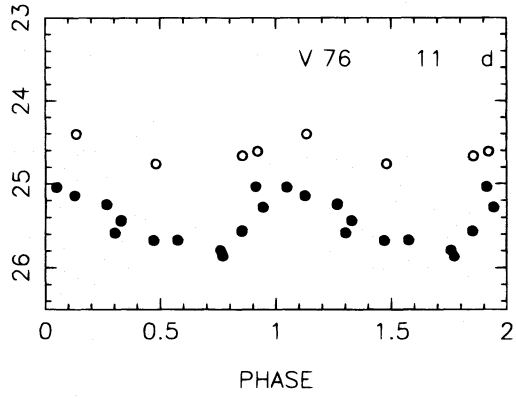

FIG. 6*s*

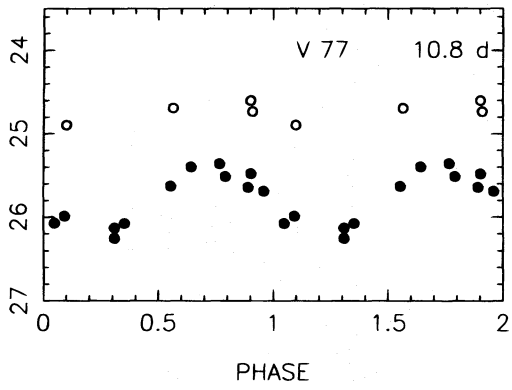

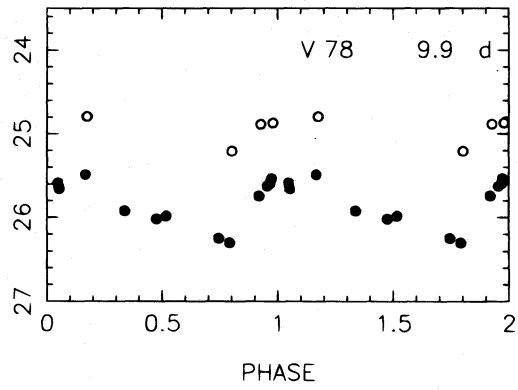

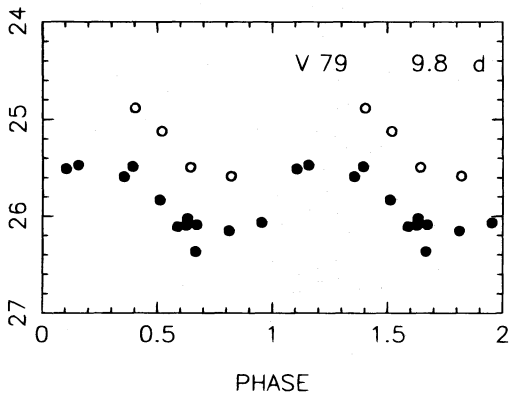

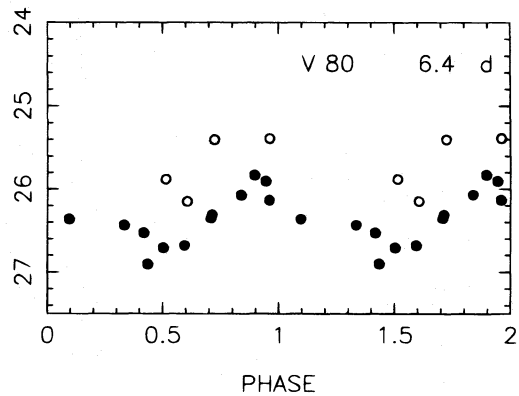

FIG. 6*t*

TABLE 5

V PHOTOMETRY FOR THE CEPHEIDS IN NGC 925

HJD	1		2		3		4		5		6		7		8		9		10	
2449000+	V	σ	V	σ	V	σ	V	σ	V	σ	V	σ	V	σ	V	σ	V	σ	V	σ
573.402	24.35	0.15	23.82	0.10	23.23	0.09	23.66	0.07	23.51	0.12	24.56	0.14	24.78	0.25	25.21	0.17	24.47	0.11	24.63	0.20
582.043	24.49	0.12	23.78	0.10	23.30	0.09	23.32	0.07	23.58	0.13	24.71	0.21	23.82	0.13	23.95	0.11	24.52	0.13	24.67	0.25
591.472	24.68	0.14	23.85	0.10	23.38	0.13	22.96	0.05	23.70	0.16	24.46	0.11	24.03	0.16	24.26	0.14	24.90	0.17	24.30	0.21
594.530	24.67	0.14	23.79	0.11	23.47	0.14	22.85	0.17	23.74	0.16	24.20	0.12	23.93	0.17	24.38	0.14	...	...	24.38	0.18
597.339	24.57	0.14	23.80	0.10	23.42	0.13	23.09	0.07	23.75	0.14	24.15	0.11	24.20	0.13	24.57	0.13	24.99	0.17	24.39	0.22
604.382	24.90	0.17	23.90	0.11	23.58	0.12	23.04	0.07	23.91	0.16	24.28	0.17	24.43	0.19	24.82	0.16	25.11	0.19	24.61	0.19
608.609	24.74	0.17	23.91	0.10	23.55	0.26	23.13	0.07	23.88	0.18	24.52	0.12	24.53	0.13	25.00	0.19	24.35	0.14	24.64	0.20
613.362	24.84	0.25	23.97	0.11	23.65	0.09	23.09	0.10	23.72	0.18	24.70	0.15	24.84	0.17	25.20	0.18	24.53	0.15	24.76	0.23
618.925	24.84	0.18	24.11	0.11	23.70	0.11	23.19	0.05	23.43	0.23	24.74	0.17	24.63	0.15	24.06	0.15	24.59	0.15	24.13	0.18
625.359	24.69	0.15	24.27	0.15	23.84	0.11	23.27	0.06	23.48	0.13	24.77	0.16	23.76	0.10	24.08	0.12	24.83	0.14	24.29	0.16
633.335	24.71	0.16	24.32	0.13	24.03	0.14	23.36	0.06	23.63	0.14	24.71	0.18	24.11	0.17	24.54	0.10	25.00	0.20	24.52	0.16
643.187	24.54	0.17	24.27	0.13	24.21	0.10	23.54	0.07	23.77	0.13	24.26	0.12	24.38	0.18	24.95	0.17	24.55	0.13	24.83	0.23

HJD	11		12		13		14		15		16		17		18		19		20	
2449000+	V	σ	V	σ	V	σ	V	σ	V	σ	V	σ	V	σ	V	σ	V	σ	V	σ
573.402	23.80	0.13	24.86	0.14	24.10	0.12	24.99	0.35	24.36	0.13	25.13	0.22	24.65	0.21	24.98	0.17	24.84	0.15	24.63	0.24
582.043	23.36	0.12	24.15	0.15	24.53	0.18	24.15	0.10	24.60	0.22	24.07	0.16	25.39	0.28	25.42	0.26	24.09	0.13	24.96	0.29
591.472	23.66	0.11	24.36	0.12	24.96	0.19	24.73	0.20	25.00	0.17	24.62	0.17	25.66	0.27	24.55	0.14	24.41	0.13	25.14	0.29
594.530	23.67	0.13	24.37	0.14	25.12	0.19	24.87	0.25	25.20	0.16	24.70	0.16	25.39	0.21	24.66	0.14	24.57	0.12	24.31	0.18
597.339	23.72	0.12	24.52	0.14	24.70	0.13	24.98	0.21	25.52	0.16	24.64	0.23	24.47	0.18	24.81	0.15	24.75	0.13	24.42	0.17
604.382	23.82	0.12	24.83	0.15	24.12	0.14	25.26	0.24	24.35	0.14	25.05	0.23	24.88	0.15	25.17	0.17	24.62	0.17	24.71	0.23
608.609	23.70	0.14	24.99	0.20	24.24	0.15	24.81	0.20	24.45	0.11	24.00	0.25	24.99	0.15	25.36	0.15	24.05	0.11	24.91	0.21
613.362	23.37	0.15	24.09	0.15	24.54	0.14	24.41	0.15	24.75	0.14	24.28	0.15	25.20	0.16	25.13	0.13	24.27	0.11	25.19	0.25
618.925	23.61	0.11	24.19	0.12	24.90	0.19	24.62	0.16	24.91	0.16	24.40	0.22	25.43	0.21	24.48	0.12	24.60	0.12	24.81	0.20
625.359	23.69	0.12	24.43	0.12	25.26	0.23	24.87	0.21	25.23	0.17	24.80	0.16	24.63	0.14	24.79	0.16	24.67	0.13	24.63	0.17
633.335	23.74	0.12	24.67	0.14	24.02	0.11	25.27	0.22	24.36	0.12	25.02	0.21	24.80	0.11	25.39	0.21	24.39	0.11	24.78	0.27
643.187	23.43	0.12	24.34	0.17	24.60	0.14	24.28	0.16	24.69	0.14	24.18	0.13	25.39	0.23	24.60	0.14	24.20	0.21	25.34	0.33

HJD	21		22		23		24		25		26		27		28		29		30	
2449000+	V	σ	V	σ	V	σ	V	σ	V	σ	V	σ	V	σ	V	σ	V	σ	V	σ
573.402	24.98	0.15	24.32	0.13	25.17	0.18	24.87	0.14	25.30	0.16	24.39	0.22	25.95	0.30	25.49	0.25	23.75	0.10	25.01	0.24
582.043	25.26	0.17	24.84	0.17	25.73	0.25	25.26	0.19	25.26	0.23	24.98	0.25	24.99	0.18	25.60	0.29	24.09	0.12	25.55	0.25
591.472	25.41	0.20	25.10	0.14	25.72	0.23	24.52	0.13	24.76	0.16	25.09	0.25	25.44	0.20	24.96	0.19	24.17	0.14	24.61	0.20
594.530	24.80	0.12	23.94	0.27	25.17	0.22	24.69	0.14	25.02	0.19	24.76	0.20	25.55	0.20	25.29	0.23	23.70	0.10	24.81	0.22
597.339	24.78	0.15	24.16	0.10	25.11	0.21	24.83	0.25	25.07	0.18	24.45	0.15	26.19	0.28	25.44	0.30	23.81	0.12	24.96	0.21
604.382	25.24	0.18	24.68	0.13	25.47	0.25	25.23	0.24	25.73	0.26	24.81	0.21	25.38	0.19	25.61	0.23	23.98	0.12	25.24	0.25
608.609	25.59	0.24	24.96	0.12	25.82	0.26	25.41	0.21	25.49	0.18	25.22	0.27	25.01	0.19	24.34	0.11	24.14	0.13	25.27	0.26
613.362	25.60	0.23	25.11	0.18	26.18	0.39	25.49	0.17	24.57	0.17	25.58	0.36	25.44	0.22	24.81	0.16	24.13	0.13	24.58	0.17
618.925	25.36	0.19	24.87	0.15	25.64	0.22	24.60	0.13	25.04	0.20	24.61	0.16	25.97	0.29	25.22	0.18	23.74	0.12	24.91	0.20
625.359	24.83	0.18	24.37	0.09	25.34	0.19	24.96	0.18	25.52	0.37	24.77	0.17	25.86	0.28	25.79	0.28	23.93	0.12	25.32	0.22
633.335	25.34	0.21	24.95	0.20	25.73	0.23	25.42	0.21	25.54	0.22	25.38	0.25	25.22	0.19	24.45	0.14	24.24	0.13	24.35	0.17
643.187	25.58	0.21	25.23	0.16	25.85	0.33	24.39	0.11	25.10	0.17	24.44	0.19	25.97	0.23	25.45	0.28	23.78	0.11	24.97	0.21

HJD	31		32		33		34		35		36		37		38		39		40	
2449000+	V	σ	V	σ	V	σ	V	σ	V	σ	V	σ	V	σ	V	σ	V	σ	V	σ
573.402	25.05	0.17	25.03	0.20	24.85	0.18	24.38	0.17	24.81	0.21	25.17	0.23	24.98	0.21	24.70	0.18	24.02	0.19	24.56	0.20
582.043	25.80	0.25	24.56	0.14	24.27	0.14	24.94	0.18	25.48	0.20	25.77	0.35	25.79	0.30	25.08	0.14	24.58	0.16	24.77	0.20
591.472	24.95	0.18	25.17	0.17	24.81	0.16	25.33	0.21	24.94	0.14	24.89	0.17	24.87	0.14	24.72	0.17	24.01	0.13	24.77	0.17
594.530	25.01	0.16	24.91	0.19	24.80	0.17	24.23	0.17	24.75	0.21	25.20	0.21	25.12	0.18	24.67	0.11	24.40	0.15	24.65	0.20
597.339	25.21	0.20	25.10	0.19	24.78	0.16	24.53	0.17	24.99	0.20	25.34	0.19	25.46	0.34	24.98	0.17	24.38	0.22	24.89	0.33
604.382	25.70	0.25	24.58	0.14	24.32	0.14	25.14	0.19	25.58	0.30	25.82	0.26	26.08	0.29	25.17	0.16	25.11	0.24	24.32	0.15
608.609	25.69	0.27	24.80	0.18	24.30	0.27	25.32	0.18	25.78	0.35	24.85	0.14	24.84	0.15	24.84	0.14	24.67	0.15	24.53	0.15
613.362	25.02	0.18	25.10	0.19	24.83	0.23	25.09	0.15	24.62	0.18	25.15	0.20	25.23	0.21	24.73	0.15	24.27	0.32	24.82	0.19
618.925	25.28	0.21	25.02	0.18	24.80	0.20	24.64	0.21	25.38	0.25	25.39	0.20	25.67	0.28	24.97	0.17	24.81	0.20	24.78	0.18
625.359	25.74	0.26	24.51	0.17	24.38	0.15	25.03	0.25	25.58	0.23	25.66	0.19	25.87	0.26	25.01	0.13	24.80	0.12	24.48	0.18
633.335	25.20	0.19	25.02	0.18	24.77	0.21	25.28	0.19	24.82	0.25	25.10	0.19	25.24	0.17	24.86	0.14	24.31	0.16	24.77	0.23
643.187	25.46	0.27	24.57	0.15	23.99	0.13	24.95	0.18	25.49	0.24	25.38	0.21	25.94	0.25	25.05	0.14	24.98	0.22	24.39	0.20

HJD	41		42		43		44		45		46		47		48		49		50	
2449000+	V	σ	V	σ	V	σ	V	σ	V	σ	V	σ	V	σ	V	σ	V	σ	V	σ
573.402	25.71	0.31	25.86	0.18	25.81	0.28	25.91	0.29	25.49	0.15	24.78	0.13	26.00	0.38	25.51	0.17	25.82	0.22	25.50	0.27
582.043	24.94	0.18	25.19	0.15	25.61	0.26	25.50	0.23	25.60	0.23	25.54	0.20	24.96	0.22	25.92	0.24	26.74	0.35	24.69	0.21
591.472	25.94	0.28	26.01	0.22	25.89	0.24	25.88	0.22	25.24	0.19	24.61	0.13	26.21	0.45	25.47	0.33	25.72	0.17	25.22	0.26
594.530	25.77	0.23	25.96	0.17	25.91	0.25	25.23	0.24	25.38	0.23	24.98	0.14	...	...	25.65	0.27	26.02	0.21	24.86	0.20
597.339	25.33	0.24	25.95	0.21	25.90	0.28	25.28	0.20	25.48	0.21	25.37	0.19	25.00	0.28	26.03	0.30	26.16	0.27	24.63	0.17
604.382	25.40	0.22	25.51	0.13	25.31	0.17	25.72	0.28	25.88	0.22	25.76	0.22	25.77	0.27	25.38	0.16	26.41	0.34	25.14	0.27
608.609	25.94	0.24	25.74	0.29	25.67	0.24	26.07	0.40	25.45	0.18	24.63	0.15	26.32	0.46	25.43	0.17	25.52	0.16	25.18	0.21
613.362	26.00	0.29	26.05	0.20	26.06	0.24	25.53	0.19	25.36	0.27	25.28	0.21	25.57	0.28	26.13	0.32	26.13	0.28	24.73	0.20
618.925	25.11	0.18	25.18	0.12	25.37	0.15	25.52	0.22	25.89	0.32	25.90	0.27	25.49	0.26	25.41	0.20	...	...	24.99	0.27
625.359	25.64	0.22	25.78	0.17	25.62	0.22	26.01	0.26	25.54	0.21	24.84	0.19	26.26	0.41	25.53	0.16	25.72	0.18	24.98	0.22
633.335	25.56	0.23	25.81	0.18	25.94	0.26	25.36	0.17	25.63	0.20	25.61	0.23	25.24	0.26	25.89	0.28	26.65	0.31	24.86	0.21
643.187	25.54	0.23	25.59	0.18	25.54	0.28	26.21	0.29	25.53	0.23	24.68	0.15	26.36	0.36	25.76	0.24	25.79	0.18	24.95	0.24

TABLE 5—*Continued*

HJD	51		52		53		54		55		56		57		58		59		60	
2449000+	V	σ	V	σ	V	σ	V	σ	V	σ	V	σ	V	σ	V	σ	V	σ	V	σ
573.402	25.48	0.18	25.43	0.16	25.67	0.19	25.28	0.17	25.53	0.14	25.85	0.18	25.84	0.21	26.00	0.30	24.83	0.24	25.73	0.21
582.043	25.88	0.33	26.28	0.28	25.42	0.22	25.86	0.24	25.15	0.13	25.58	0.15	25.06	0.18	25.39	0.21	25.34	0.27	25.23	0.25
591.472	25.04	0.13	25.99	0.22	25.00	0.14	25.53	0.26	25.84	0.19	26.13	0.20	26.17	0.34	26.55	0.34	24.78	0.18	26.33	0.37
594.530	25.39	0.17	26.23	0.28	25.23	0.15	25.92	0.23	25.66	0.14	25.43	0.16	25.45	0.19	25.88	0.24	25.36	0.21	25.63	0.24
597.339	25.62	0.18	26.39	0.30	25.27	0.18	26.09	0.32	25.50	0.16	25.44	0.15	24.90	0.17	25.37	0.21	25.38	0.24	25.36	0.22
604.382	25.98	0.19	25.59	0.23	25.86	0.20	25.45	0.17	25.58	0.17	26.10	0.22	25.96	0.31	26.24	0.30	24.61	0.26	26.05	0.32
608.609	25.44	0.21	25.99	0.25	24.95	0.14	25.85	0.30	25.95	0.25	25.84	0.18	25.84	0.20	26.11	0.30	25.27	0.25	26.05	0.38
613.362	25.77	0.20	26.39	0.27	25.71	0.17	26.41	0.30	25.01	0.15	25.64	0.18	25.25	0.19	25.54	0.23	25.55	0.31	25.46	0.25
618.925	25.70	0.18	25.61	0.21	25.82	0.21	25.35	0.22	25.48	0.20	26.27	0.20	25.84	0.22	26.44	0.30	24.84	0.18	26.00	0.30
625.359	25.44	0.15	26.04	0.26	25.26	0.19	25.94	0.28	25.89	0.16	25.17	0.11	25.14	0.20	25.31	0.23	25.52	0.24	25.52	0.28
633.335	26.00	0.17	25.45	0.20	25.89	0.29	25.06	0.20	25.34	0.16	26.23	0.21	26.06	0.29	26.09	0.45	24.78	0.24	25.97	0.31
643.187	25.57	0.22	26.38	0.31	25.29	0.14	26.03	0.22	25.78	0.20	25.47	0.12	25.20	0.22	25.56	0.25	25.44	0.37	26.09	0.33

HJD	61		62		63		64		65		66		67		68		69		70	
2449000+	V	σ	V	σ	V	σ	V	σ	V	σ	V	σ	V	σ	V	σ	V	σ	V	σ
573.402	25.42	0.19	26.40	0.33	26.12	0.30	26.13	0.33	26.32	0.25	26.10	0.32	25.62	0.21	26.29	0.34	26.19	0.30	25.51	0.24
582.043	25.97	0.29	26.63	0.28	25.68	0.26	25.69	0.21	25.61	0.20	25.96	0.26	25.90	0.14	26.03	0.32	25.64	0.31	25.05	0.14
591.472	25.79	0.25	26.20	0.26	25.64	0.24	25.12	0.17	26.31	0.28	25.62	0.22	26.27	0.20	25.39	0.27	25.67	0.24	25.58	0.23
594.530	26.07	0.37	26.55	0.43	25.49	0.18	25.46	0.18	25.53	0.22	26.02	0.29	25.85	0.19	25.95	0.26	25.45	0.20	25.05	0.15
597.339	26.29	0.27	...	...	26.04	0.32	25.80	0.26	25.67	0.23	26.32	0.30	25.31	0.13	26.21	0.38	25.77	0.25	25.55	0.15
604.382	25.48	0.26	25.98	0.17	25.21	0.18	25.79	0.25	26.36	0.37	25.52	0.19	25.99	0.24	25.69	0.25	25.52	0.16	25.71	0.18
608.609	25.89	0.25	26.48	0.41	25.73	0.30	25.72	0.22	25.45	0.13	26.03	0.36	25.83	0.19	26.07	0.27	25.70	0.28	25.31	0.21
613.362	26.48	0.45	26.72	0.43	26.21	0.26	26.39	0.38	26.18	0.30	26.17	0.33	25.66	0.19	26.34	0.42	26.21	0.28	26.14	0.19
618.925	25.51	0.25	26.06	0.22	25.47	0.27	25.28	0.21	26.12	0.18	25.69	0.24	26.05	0.20	25.80	0.32	25.17	0.16	25.20	0.17
625.359	26.14	0.26	26.88	0.37	26.02	0.31	25.98	0.30	25.78	0.35	26.63	0.38	25.55	0.17	26.25	0.27	26.07	0.36	25.77	0.23
633.335	25.49	0.20	26.00	0.22	25.66	0.27	25.32	0.18	25.98	0.30	25.79	0.21	26.04	0.24	25.80	0.26	25.45	0.19	25.19	0.13
643.187	25.93	0.32	26.83	0.36	25.60	0.21	26.04	0.23	26.67	0.25	25.76	0.26	25.91	0.25	25.53	0.25	25.60	0.18	25.64	0.22

HJD	71		72		73		74		75		76		77		78		79		80	
2449000+	V	σ	V	σ	V	σ	V	σ	V	σ	V	σ	V	σ	V	σ	V	σ	V	σ
573.402	25.94	0.24	25.66	0.15	25.42	0.14	26.22	0.30	26.63	0.40	25.20	0.19	26.04	0.19	25.79	0.16	25.89	0.28	26.58	0.29
582.043	25.50	0.22	25.49	0.16	25.16	0.15	25.73	0.25	25.94	0.23	25.52	0.21	25.70	0.26	26.35	0.27	25.54	0.22	25.95	0.23
591.472	25.35	0.19	25.53	0.13	25.59	0.19	25.58	0.18	25.95	0.25	25.91	0.29	25.54	0.15	26.27	0.19	25.65	0.18	26.58	0.35
594.530	25.19	0.33	25.42	0.17	24.98	0.15	25.94	0.18	26.71	0.39	25.13	0.19	26.13	0.27	25.71	0.17	26.42	0.34	25.88	0.22
597.339	25.80	0.48	25.86	0.21	25.48	0.16	26.38	0.32	26.53	0.42	25.64	0.22	26.18	0.28	25.97	0.20	26.08	0.25	26.48	0.30
604.382	25.35	0.25	25.41	0.17	25.28	0.14	25.59	0.19	26.52	0.39	25.33	0.17	25.74	0.24	25.64	0.15	26.14	0.22	26.95	0.42
608.609	25.63	0.20	25.36	0.14	25.47	0.17	26.21	0.27	...	...	25.49	0.16	26.13	0.36	26.07	0.23	25.56	0.17	26.41	0.25
613.362	25.98	0.27	26.02	0.18	25.87	0.17	25.25	0.17	26.00	0.34	25.85	0.31	25.57	0.19	25.67	0.17	26.16	0.27	26.12	0.28
618.925	25.34	0.19	25.18	0.16	25.04	0.14	25.92	0.24	26.52	0.34	25.30	0.33	26.51	0.37	26.03	0.20	25.53	0.16	26.40	0.29
625.359	26.01	0.24	...	...	25.90	0.20	25.36	0.16	26.07	0.31	25.61	0.24	25.53	0.16	25.54	0.12	26.21	0.31	26.36	0.29
633.335	25.60	0.23	25.39	0.12	25.39	0.13	26.28	0.34	26.30	0.30	25.72	0.25	25.45	0.23	25.58	0.14	26.15	0.33	26.18	0.23
643.187	25.41	0.22	25.14	0.11	25.01	0.12	26.13	0.25	26.77	0.41	25.73	0.24	25.68	0.18	25.64	0.17	26.08	0.20	26.75	0.32

lists the location and approximate mean V and I magnitude for these variables.

5. VARIABLE LIGHT CURVES AND PARAMETERS

In this section, we discuss the derived periods and mean magnitudes of the 80 Cepheid variables in NGC 925. The periods and mean magnitudes are in good agreement between the ALLFRAME and DoPHOT samples of Cepheids, assuring that no significant systematic errors in the photometry are present. For this reason, in order to simplify and shorten this section, we present only the ALLFRAME photometry. We briefly summarize the results of the DoPHOT-based analysis in the next section, with details given in § 2 of the Appendix.

5.1. *The V and I Photometry*

Light curves for the Cepheids are shown in Figure 6. For these light curves, the magnitudes obtained for the cosmic-ray split images taken within a single epoch were averaged, then the resulting mean magnitude at each epoch was plotted. For clarity, the error bars are not shown. The V and I ALLFRAME photometry is listed in Tables 5 and 6, respectively. In these tables, the first column lists the mean Heliocentric Julian Date of each epoch at midexposure. The remaining columns list the V or I magnitude and error, as reported by ALLFRAME, for each epoch.

As in the case of M100 (Ferrarese et al. 1996) and M101 (Kelson et al. 1996), mean V magnitudes for the Cepheids were determined two different ways. First, since the observations were preselected to evenly sample a typical 10–60 day Cepheid light curve, unweighted intensity averaged mean magnitudes were calculated. Second, to determine whether there was any bias in our data, phase-weighted mean intensity magnitudes $\langle m \rangle$ were also calculated using

$$\langle m \rangle = -2.5 \log \left[\sum_{i}^{N} 0.5(\phi_{i+1} - \phi_{i-1}) 10^{-0.4 m_i} \right], \quad (2)$$

where ϕ is the phase, and the sum is over the entire light cycle. The average difference between the unweighted and phase-weighted intensity averaged mean V magnitudes is only -0.014 ± 0.023 mag for the 80 Cepheids. This difference is quite small, as expected, since most of the Cepheids have nearly uniformly sampled light curves. While we present both intensity-weighted and phase-weighted mean V and I magnitudes in Table 7, we employ only the phase-weighted mean ALLFRAME magnitudes to determine the distance to NGC 925.

With only four I observations, mean I magnitudes were calculated as follows. Using the V and I magnitudes at the

TABLE 6

I PHOTOMETRY FOR THE CEPHEIDS IN NGC 925

HJD	1		2		3		4		5		6		7		8		9		10	
2449000+	I	σ	I	σ	I	σ	I	σ	I	σ	I	σ	I	σ	I	σ	I	σ	I	σ
573.469	22.99	0.10	22.85	0.07	22.17	0.08	22.43	0.05	22.32	0.08	23.46	0.12	23.75	0.13	24.06	0.16	23.62	0.16	23.61	0.18
582.149	23.08	0.09	22.68	0.07	22.11	0.07	22.29	0.05	22.35	0.10	23.51	0.11	23.11	0.11	23.25	0.11	23.67	0.14	23.72	0.18
625.425	23.37	0.14	23.01	0.09	22.36	0.06	22.10	0.05	22.38	0.07	23.70	0.14	23.18	0.08	23.29	0.08	23.82	0.15	23.31	0.14
643.288	23.33	0.12	23.10	0.09	22.71	0.09	22.31	0.06	22.58	0.09	23.32	0.10	23.56	0.11	23.81	0.13	23.75	0.11	23.67	0.20

HJD	11		12		13		14		15		16		17		18		19		20	
2449000+	I	σ	I	σ	I	σ	I	σ	I	σ	I	σ	I	σ	I	σ	I	σ	I	σ
573.469	23.31	0.13	23.84	0.11	23.24	0.10	24.08	0.18	23.70	0.13	24.05	0.18	23.71	0.10	23.85	0.11	23.82	0.14	23.75	0.13
582.149	23.06	0.13	23.48	0.08	23.52	0.16	23.55	0.14	23.70	0.14	23.38	0.12	24.02	0.18	24.29	0.13	23.49	0.15	24.20	0.19
625.425	23.18	0.12	23.53	0.09	23.82	0.15	23.81	0.29	24.34	0.19	23.75	0.11	23.93	0.14	23.85	0.13	23.75	0.12	23.93	0.16
643.288	23.12	0.14	23.58	0.24	23.43	0.11	23.52	0.14	23.74	0.11	23.46	0.16	24.07	0.16	23.80	0.15	23.49	0.13	24.31	0.19

HJD	21		22		23		24		25		26		27		28		29		30	
2449000+	I	σ	I	σ	I	σ	I	σ	I	σ	I	σ	I	σ	I	σ	I	σ	I	σ
573.469	23.95	0.12	23.57	0.09	24.01	0.17	23.80	0.16	24.11	0.13	23.75	0.15	24.61	0.20	24.33	0.17	22.59	0.07	23.79	0.17
582.149	24.22	0.13	23.79	0.14	24.63	0.24	24.22	0.13	24.52	0.14	24.09	0.15	24.11	0.13	24.52	0.14	22.72	0.11	24.05	0.20
625.425	23.91	0.16	23.51	0.11	24.16	0.18	23.82	0.12	24.33	0.17	23.96	0.15	24.80	0.17	24.49	0.23	22.56	0.06	24.12	0.24
643.288	24.33	0.13	24.05	0.12	24.46	0.25	23.69	0.12	24.02	0.15	23.94	0.13	24.76	0.20	24.24	0.14	22.56	0.08	23.82	0.18

HJD	31		32		33		34		35		36		37		38		39		40	
2449000+	I	σ	I	σ	I	σ	I	σ	I	σ	I	σ	I	σ	I	σ	I	σ	I	σ
573.469	24.12	0.12	24.05	0.15	24.12	0.15	23.28	0.21	24.11	0.14	24.24	0.21	24.30	0.14	23.93	0.13	23.45	0.14	23.88	0.16
582.149	24.76	0.21	23.68	0.14	23.74	0.13	24.01	0.18	24.35	0.15	24.76	0.30	24.63	0.25	24.23	0.12	23.95	0.15	23.98	0.16
625.425	24.48	0.16	23.71	0.22	23.73	0.12	24.02	0.15	24.73	0.23	24.66	0.27	25.06	0.28	24.24	0.11	23.97	0.15	23.72	0.16
643.288	24.24	0.12	23.87	0.15	23.81	0.13	24.07	0.14	24.50	0.17	24.89	0.28	25.04	0.30	24.29	0.14	24.03	0.13	23.85	0.19

HJD	41		42		43		44		45		46		47		48		49		50	
2449000+	I	σ	I	σ	I	σ	I	σ	I	σ	I	σ	I	σ	I	σ	I	σ	I	σ
573.469	24.81	0.19	24.95	0.21	24.59	0.16	25.09	0.28	24.71	0.18	24.23	0.13	25.07	0.31	24.54	0.16	25.06	0.22	24.72	0.23
582.149	24.29	0.21	24.35	0.13	24.46	0.19	24.56	0.24	24.59	0.16	24.55	0.15	24.32	0.21	24.97	0.19	24.99	0.20	24.05	0.15
625.425	24.57	0.20	24.80	0.19	24.63	0.23	25.13	0.27	24.53	0.16	24.38	0.11	25.08	0.36	24.56	0.11	24.83	0.18	24.31	0.22
643.288	24.78	0.18	24.56	0.13	24.65	0.16	25.08	0.28	24.74	0.12	24.18	0.16	...	...	24.63	0.20	24.64	0.15	24.45	0.21

HJD	51		52		53		54		55		56		57		58		59		60	
2449000+	I	σ	I	σ	I	σ	I	σ	I	σ	I	σ	I	σ	I	σ	I	σ	I	σ
573.469	24.83	0.22	24.81	0.21	24.67	0.16	24.55	0.21	24.44	0.15	24.84	0.16	24.88	0.18	25.01	0.30	24.27	0.17	25.22	0.25
582.149	24.72	0.21	24.91	0.22	24.54	0.20	24.80	0.31	24.46	0.16	24.36	0.11	24.40	0.13	24.60	0.23	24.50	0.13	24.72	0.18
625.425	24.49	0.20	24.94	0.16	24.39	0.15	24.70	0.32	24.96	0.20	24.54	0.11	24.67	0.19	24.66	0.23	24.26	0.10	24.83	0.20
643.288	24.64	0.20	25.09	0.20	24.78	0.16	24.84	0.28	24.84	0.22	24.56	0.12	24.50	0.19	24.73	0.18	24.68	0.21	25.10	0.29

HJD	61		62		63		64		65		66		67		68		69		70	
2449000+	I	σ	I	σ	I	σ	I	σ	I	σ	I	σ	I	σ	I	σ	I	σ	I	σ
573.469	24.86	0.21	25.32	0.24	25.17	0.24	25.46	0.27	25.08	0.23	25.50	0.33	24.55	0.13	24.38	0.17	25.74	0.39	24.81	0.19
582.149	25.10	0.23	25.66	0.30	25.01	0.27	24.87	0.18	24.82	0.20	25.23	0.25	24.86	0.17	24.20	0.15	24.98	0.27	24.59	0.14
625.425	25.13	0.30	25.51	0.36	25.16	0.31	25.43	0.29	24.84	0.22	25.78	0.36	24.58	0.19	24.42	0.22	25.19	0.37	24.88	0.18
643.288	24.75	0.19	25.52	0.26	24.73	0.21	25.40	0.24	25.38	0.27	25.17	0.32	24.68	0.14	24.14	0.14	25.13	0.29	24.84	0.22

HJD	71		72		73		74		75		76		77		78		79		80	
2449000+	I	σ	I	σ	I	σ	I	σ	I	σ	I	σ	I	σ	I	σ	I	σ	I	σ
573.469	24.10	0.16	24.60	0.19	24.32	0.15	24.80	0.28	...	...	24.44	0.18	24.93	0.22	24.95	0.16	25.17	0.23	25.83	0.31
582.149	23.88	0.11	24.60	0.16	24.38	0.15	24.41	0.21	25.38	0.25	24.65	0.21	24.64	0.17	25.28	0.27	24.93	0.23	25.44	0.26
625.425	24.10	0.13	24.95	0.18	24.71	0.15	24.30	0.17	24.95	0.23	24.71	0.21	24.77	0.18	24.86	0.21	25.63	0.35	25.38	0.24
643.288	24.07	0.12	24.34	0.15	24.35	0.13	24.79	0.20	25.44	0.24	24.80	0.21	24.73	0.23	25.01	0.22	25.35	0.27	25.93	0.27

NOTES TO TABLE 7.—V1. Three stars ~0".5 away. V2. Another star ~0".3 away. V3. Another star ~0".5 away. V4. Another star ~0".5 away. V5. Within spiral arm, may be blend with two or more stars. V6. On edge of spiral arm, another star ~0".3 away. V7. In spiral arm, probable blend with other stars. V8. On edge of spiral arm, may have faint nearby neighbors. V9. In spiral arm, three other stars within ~0".3. V10. Two other stars ~0".5 away. V11. Isolated, very blue color. Blend with very blue companion? V12. Isolated. V13. In spiral arm. V14. Near shadowed edge of detector, in middle of spiral arm. V15. On edge of spiral arm, bright neighbor ~0".5 away. V16. Close to shadowed edge of detector. V17. In spiral arm, possible blend with other stars. V18. May be blend with a faint companion. V19. About 0".4 from a multiple star complex. V20. On edge of an H II region. V21. On edge of spiral arm, possible blend of two stars. V22. May be blend with one or more fainter stars. V23. In spiral arm, very crowded region. V24. On edge of spiral arm, another star ~0".3 away. V25. In spiral arm. V26. In spiral arm, crowded region. V27. Close to shadowed edge of detector. V28. H II region close by. V29. On edge of spiral arm, another star ~0".5 away. V30. On edge of spiral arm, may have a faint companion. V31. Two other stars with ~0".3, somewhat crowded region. V32. In spiral arm, very crowded region. V33. In spiral arm, very crowded region. V34. On edge of spiral arm, may be blend with faint neighbors. V35. A few faint neighbors more than 0".5 away. V36. In spiral arm, crowded region. V37. In spiral arm, very crowded region. V38. Possible blend of two or more stars, odd-shaped light curve. V39. Near shadowed edge of detector, three faint neighbors ~0".5 away. V40. In a very crowded region. V41. In spiral arm. V42. Faint neighbor ~0".5 away. V43. Isolated. V44. In spiral arm, crowded region, another star ~0".2 away. V45. Faint neighbor ~0".5 away. V46. On edge of spiral arm, brighter neighbor ~0".5 away. V47. In spiral arm. V48. About arcseconds from a multiple star complex. V49. On edge of spiral arm, crowded region. V50. In spiral arm. V51. Isolated. V52. Faint neighbor ~0".5 away. V53. Several faint stars nearby. V54. On edge of spiral arm, another star ~0".3 away. V55. In spiral arm, very crowded region. V56. Another star ~0".3 away. V57. Isolated. V58. Near shadowed edge of detector, another star ~0".5 away. V59. In spiral arm, crowded region. V60. Close to multiple star complex. V61. On edge of spiral arm, two stars within ~0".3. V62. Isolated. V63. May have a very faint neighbor. V64. Isolated. V65. On outer fringes of spiral arm. V66. Near shadowed edge of detector, in a very crowded region. V67. Another star ~0".5 away. V68. In a very crowded region. Very red color. Probable blend with a red star. V69. In spiral arm, brighter star ~0".3 away. V70. Isolated. V71. Isolated. Very red color. Blend with red companion? V72. Possible blend with another star. V73. Another star ~0".2 away. V74. On edge of spiral arm, in a crowded region. V75. In outer fringe of spiral arm. V76. Brighter neighbor ~0.4 arcseconds away. V77. Faint neighbor ~0.5 arcseconds away. V78. Isolated. V79. Faint star ~0".3 away. V80. Isolated.

TABLE 7

PARAMETERS FOR THE NGC 925 CEPHEIDS

Ceph	Chip	RA (2000.0)	Dec	Period	Log P	V	V_{ph}	I	I_{ph}	$V-I$	$(V-I)_{ph}$
1	3	2:27:09.20	33:35:14.8	long	...	24.68	24.65	23.28	23.23	1.40	1.42
2	3	2:27:10.78	33:36:05.6	80.0	1.90	24.00	24.03	22.89	22.91	1.11	1.12
3	3	2:27:09.00	33:36:14.4	80.0	1.90	23.65	23.69	22.33	22.34	1.32	1.35
4	1	2:27:05.56	33:34:42.8	80.0	1.90	23.23	23.30	22.17	22.24	1.06	1.06
5	3	2:27:11.82	33:35:05.9	48.5	1.69	23.68	23.69	22.46	22.45	1.22	1.24
6	3	2:27:07.97	33:35:34.5	43.2	1.64	24.53	24.55	23.47	23.47	1.05	1.08
7	3	2:27:08.88	33:35:59.1	42.1	1.62	24.34	24.35	23.47	23.50	0.87	0.85
8	3	2:27:08.31	33:35:27.3	37.3	1.57	24.67	24.65	23.65	23.63	1.01	1.02
9	3	2:27:08.94	33:35:32.9	35.1	1.55	24.74	24.79	23.79	23.74	0.95	1.05
10	4	2:27:09.10	33:34:48.6	32.7	1.51	24.53	24.51	23.54	23.55	0.99	0.96
11	3	2:27:09.79	33:36:08.9	31.3	1.50	23.64	23.65	23.20	23.19	0.44	0.46
12	2	2:27:03.36	33:35:32.2	31.1	1.49	24.52	24.53	23.64	23.63	0.88	0.90
13	3	2:27:09.17	33:35:21.3	30.4	1.48	24.66	24.64	23.50	23.55	1.16	1.09
14	3	2:27:11.43	33:34:56.1	30.2	1.48	24.82	24.84	23.86	23.81	0.96	1.03
15	3	2:27:09.03	33:35:54.9	30.1	1.48	24.85	24.89	23.95	23.97	0.91	0.92
16	2	2:27:04.98	33:35:13.9	29.8	1.47	24.64	24.60	23.69	23.73	0.94	0.87
17	3	2:27:08.65	33:35:23.4	28.5	1.45	25.13	25.14	23.97	23.94	1.16	1.20
18	4	2:27:10.36	33:34:06.6	27.5	1.44	24.99	25.01	23.97	23.97	1.03	1.03
19	3	2:27:08.73	33:36:11.9	27.3	1.44	24.48	24.49	23.64	23.63	0.84	0.86
20	2	2:27:07.54	33:36:08.5	26.7	1.43	24.86	24.87	24.03	24.12	0.83	0.75
21	4	2:27:11.34	33:34:27.7	26.7	1.43	25.27	25.27	24.15	24.15	1.12	1.12
22	4	2:27:06.52	33:34:31.0	26.5	1.42	24.78	24.78	23.76	23.80	1.02	0.98
23	3	2:27:12.42	33:35:01.6	25.5	1.41	25.62	25.66	24.38	24.43	1.25	1.24
24	3	2:27:08.17	33:35:23.6	25.3	1.40	25.03	25.11	23.96	23.94	1.07	1.17
25	2	2:27:05.44	33:35:22.1	24.0	1.38	25.25	25.27	24.23	24.29	1.01	0.98
26	3	2:27:08.82	33:35:28.6	23.7	1.37	24.94	25.02	24.07	23.98	0.86	1.04
27	2	2:27:05.26	33:35:14.3	23.5	1.37	25.65	25.60	24.55	24.55	1.10	1.05
28	3	2:27:09.96	33:35:33.2	23.3	1.37	25.29	25.28	24.25	24.41	1.04	0.87
29	3	2:27:07.83	33:35:36.9	23.3	1.37	23.97	24.01	22.65	22.63	1.32	1.38
30	2	2:27:06.73	33:35:52.5	22.5	1.35	25.01	25.04	23.84	23.94	1.17	1.10
31	2	2:27:05.28	33:35:16.9	22.3	1.35	25.39	25.43	24.35	24.44	1.04	0.99
32	3	2:27:11.79	33:35:02.1	21.9	1.34	24.89	24.85	23.94	23.88	0.95	0.97
33	3	2:27:08.27	33:35:30.4	21.5	1.33	24.61	24.54	23.96	23.92	0.65	0.61
34	3	2:27:09.47	33:35:31.9	21.1	1.32	24.96	25.00	23.94	23.78	1.02	1.22
35	2	2:27:03.33	33:35:49.2	20.6	1.31	25.25	25.36	24.38	24.42	0.87	0.93
36	3	2:27:12.06	33:35:08.1	20.2	1.31	25.35	25.34	24.58	24.55	0.77	0.79
37	3	2:27:11.90	33:35:07.9	19.3	1.29	25.50	25.53	24.70	24.68	0.81	0.84
38	4	2:27:07.94	33:34:29.5	18.9	1.28	24.91	24.94	24.15	24.14	0.76	0.80
39	3	2:27:07.64	33:35:09.2	18.9	1.28	24.58	24.62	23.84	23.81	0.74	0.80
40	4	2:27:10.70	33:34:53.5	18.7	1.27	24.66	24.65	23.91	23.89	0.75	0.75
41	3	2:27:09.26	33:35:17.2	18.3	1.26	25.62	25.55	24.69	24.59	0.93	0.96
42	1	2:27:05.84	33:34:52.2	18.2	1.26	25.75	25.70	24.75	24.64	1.01	1.06
43	4	2:27:09.33	33:34:32.6	18.0	1.26	25.74	25.69	24.63	24.55	1.11	1.14
44	3	2:27:08.35	33:35:31.7	18.0	1.26	25.73	25.68	24.89	24.89	0.84	0.79
45	4	2:27:09.64	33:34:11.9	17.8	1.25	25.56	25.61	24.65	24.62	0.90	1.00
46	3	2:27:08.22	33:35:51.9	17.3	1.24	25.26	25.42	24.47	24.39	0.79	1.03
47	3	2:27:12.61	33:35:13.3	16.7	1.22	25.85	25.79	24.87	24.80	0.98	0.99
48	4	2:27:10.58	33:34:33.4	16.7	1.22	25.71	25.70	24.70	24.76	1.01	0.94
49	1	2:27:05.11	33:34:51.8	16.7	1.22	26.13	26.26	24.90	24.94	1.23	1.33
50	3	2:27:08.40	33:35:36.4	16.4	1.21	25.01	25.01	24.38	24.41	0.63	0.61
51	1	2:27:04.32	33:35:10.4	16.0	1.20	25.64	25.67	24.70	24.71	0.94	0.96
52	4	2:27:10.42	33:34:19.0	15.7	1.20	26.04	25.97	24.92	24.91	1.12	1.07
53	4	2:27:10.40	33:34:24.0	15.7	1.20	25.49	25.50	24.64	24.59	0.85	0.91
54	3	2:27:08.03	33:35:25.8	15.7	1.20	25.79	25.67	24.72	24.69	1.08	0.97
55	1	2:27:05.13	33:34:56.6	15.5	1.19	25.59	25.58	24.68	24.64	0.91	0.93
56	1	2:27:04.72	33:35:02.9	14.9	1.17	25.82	25.81	24.73	24.66	1.09	1.14
57	3	2:27:07.62	33:35:18.1	14.8	1.17	25.64	25.68	24.77	24.71	0.87	0.97
58	3	2:27:07.05	33:35:13.8	14.7	1.17	25.95	25.97	24.94	24.82	1.01	1.15
59	2	2:27:05.81	33:35:17.6	14.6	1.16	25.19	25.18	24.38	24.39	0.81	0.79
60	3	2:27:12.95	33:35:45.3	14.4	1.16	25.83	25.87	25.06	25.02	0.78	0.86
61	3	2:27:09.17	33:36:03.2	14.4	1.16	25.92	25.92	24.98	24.95	0.94	0.96
62	1	2:27:04.65	33:35:08.3	14.3	1.16	26.47	26.52	25.40	25.50	1.08	1.02
63	4	2:27:06.08	33:33:59.6	13.6	1.13	25.78	25.79	24.98	24.99	0.79	0.80
64	3	2:27:09.81	33:36:04.7	13.5	1.13	25.79	25.84	25.22	25.26	0.57	0.58
65	4	2:27:09.75	33:34:36.6	13.5	1.13	26.06	26.12	25.00	25.08	1.07	1.04
66	4	2:27:10.58	33:34:54.8	13.5	1.13	26.01	26.03	25.37	25.38	0.64	0.66
67	1	2:27:04.38	33:34:59.9	13.3	1.12	25.86	25.82	24.73	24.71	1.13	1.11
68	4	2:27:10.57	33:34:43.9	13.1	1.12	25.98	26.02	24.25	24.26	1.73	1.76
69	3	2:27:08.86	33:35:37.2	12.9	1.11	25.75	25.82	25.22	25.24	0.52	0.58
70	4	2:27:07.91	33:34:18.6	12.7	1.10	25.52	25.62	24.78	24.79	0.74	0.83
71	4	2:27:10.11	33:34:21.0	12.5	1.10	25.63	25.69	23.98	24.05	1.64	1.64
72	1	2:27:05.84	33:34:57.1	12.5	1.10	25.53	25.64	24.56	24.66	0.97	0.99
73	1	2:27:04.06	33:35:02.5	12.2	1.09	25.42	25.52	24.45	24.49	0.97	1.03
74	4	2:27:11.23	33:34:28.2	11.8	1.07	25.94	25.87	24.61	24.54	1.33	1.33
75	4	2:27:10.31	33:34:30.7	11.1	1.05	26.40	26.44	25.32	25.32	1.08	1.12
76	4	2:27:10.68	33:34:15.1	11.0	1.04	25.56	25.56	24.67	24.67	0.89	0.89
77	4	2:27:09.68	33:34:10.0	10.8	1.03	25.90	25.88	24.85	24.79	1.05	1.09
78	1	2:27:06.01	33:35:02.6	9.9	1.00	25.89	25.96	25.04	25.06	0.85	0.90
79	4	2:27:09.92	33:34:24.8	9.8	0.99	25.99	25.92	25.31	25.33	0.67	0.59
80	2	2:27:04.62	33:35:51.0	6.4	0.81	26.43	26.43	25.66	25.66	0.77	0.77

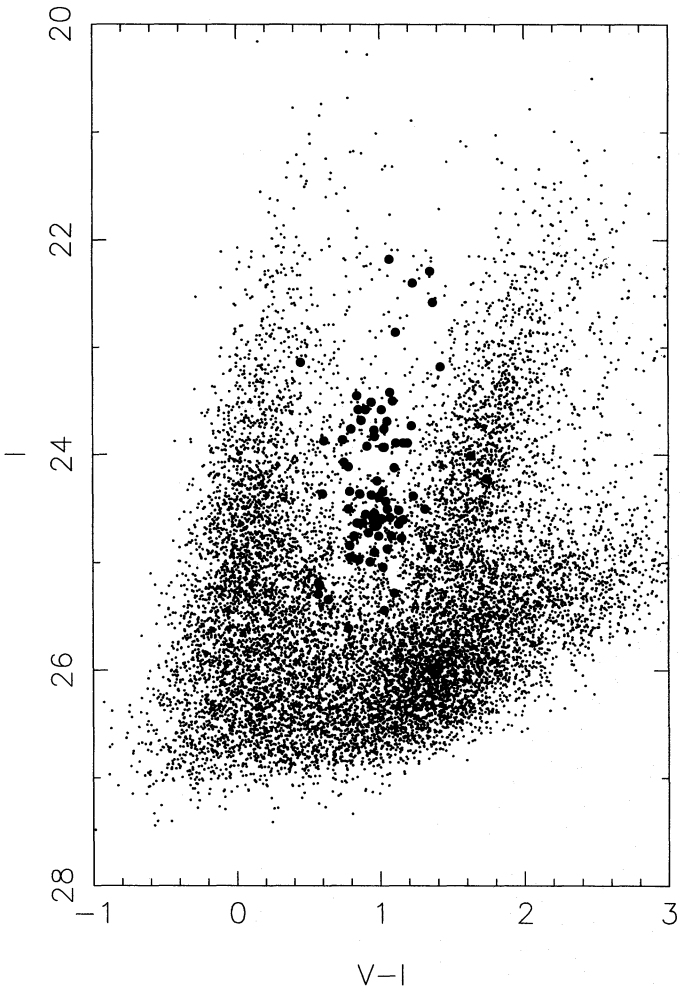

FIG. 7.—Color-magnitude diagram for the *HST* field of NGC 925. Cepheids are indicated by the large filled circles.

four I epochs, average V and average I magnitudes were calculated (again, magnitudes from cosmic-ray pairs were averaged first). Then the difference between the four epoch V average ($\langle V\rangle_4$) and 12 epoch V mean magnitude ($\langle V\rangle_{12}$) was calculated for each Cepheid. Since the amplitude of Cepheids in V is almost exactly twice the amplitude in I ($V{:}I = 1.00{:}0.51$; Freedman 1988), the four epoch I magnitude can be corrected to obtain the full 12 epoch I magnitude, as follows:

$$\langle I\rangle_{12} = \langle I\rangle_4 + 0.51(\langle V\rangle_{12} - \langle V\rangle_4)\,. \qquad (3)$$

Only photometry with errors less than 0.5 mag in V and 0.4 mag in I, as reported by ALLFRAME for each individual CCD image, were used in determining the average V or I magnitudes for the Cepheids. Cosmic-ray corrupted data were not used in determining mean magnitudes. The typical correction from the 4 to 12 epoch I magnitudes was 0.052 mag.

5.2. *Cepheid Parameters*

Table 7 lists derived parameters for the Cepheids. Column (1) gives the Cepheid identification number. Column (2) lists which chip the variable is on. Chip 1 is the Planetary Camera and chips 2–4 are the Wide-Field Cameras. Columns (3) and (4) list the right ascension and declination of each Cepheid. Columns (5) and (6) list the periods of the Cepheids, in days and log (days), respectively. Columns (7) and (8) list the mean V magnitudes, determined by an unweighted intensity average (col. [7]) and by a phase-weighted average (col. [8]). Columns (9) and (10) list the unweighted intensity average and phase-weighted average I magnitudes. Finally, columns (11) and (12) list the intensity-averaged and phase-weighted averaged $V-I$ colors for the Cepheids. Figure 7 shows an I versus $V-I$ color-magnitude diagram for the *HST* field of NGC 925, highlighting the 80 Cepheids. The Cepheids (*large filled circles*) lie between the blue and red plumes of nonvariable stars.

The Cepheid V1 has an uncertain period. The automated light-curve fitting program of P. B. S. indicates that it may have a period as long as 109 days. Cepheids V2, V3, and V4 all have periods close to 80 days (which is longer than our 70 day observing window), though it is unlikely that all three of them have exactly that same period. In Figure 4 and Table 7, we use a period of 80 days for the light curves and to calculate phase-weighted mean magnitudes for these four Cepheids, but we caution that the periods are uncertain.

6. PERIOD-LUMINOSITY RELATIONS AND THE DISTANCE TO NGC 925

The method used to determine the distance to NGC 925 is the same as in other papers in the Key Project series

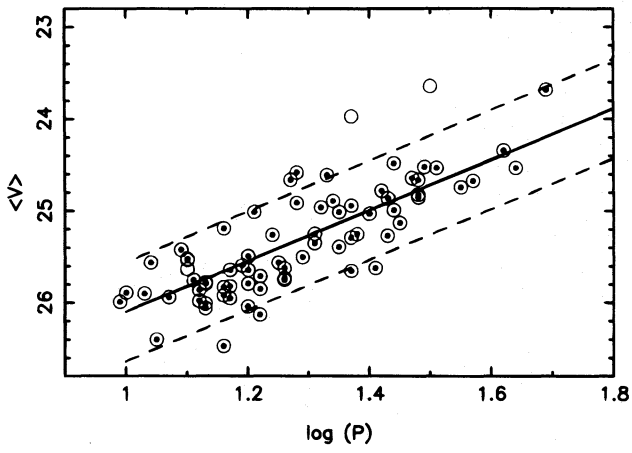

FIG. 8*a*

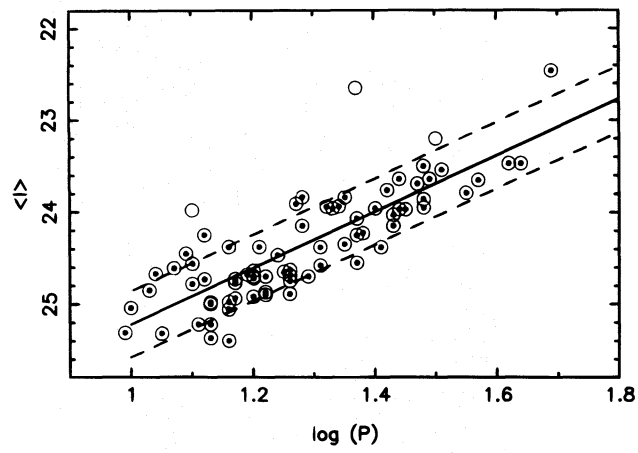

FIG. 8*b*

FIG. 8.—V and I period-luminosity relations for the Cepheids in NGC 925. Only those Cepheids with periods between 8 and 70 days are plotted. Solid line is the best fit to the NGC 925 data. Dotted lines indicate the scatter expected because of the intrinsic width of the Cepheid instability strip. Those Cepheids lying more than 4 σ from the mean relation are indicated by open circles.

TABLE 8

ERROR BUDGET IN THE DISTANCE TO NGC 925

Source	Error
WFPC2 V-band zero point	± 0.04
WFPC2 I-band zero point	± 0.04
Error in the $\langle V \rangle$ photometry	± 0.05
Error in the $\langle I \rangle$ photometry	± 0.04
Aperture correction uncertainty in V	± 0.04
Aperture correction uncertainty in I	± 0.05
Uncertainty in NGC 925 distance modulus (PL fitting)	± 0.06
Uncertainty in metallicity of NGC 925 Cepheids	± 0.08
Uncertainty in LMC distance modulus	± 0.10
Total uncertainty in true distance modulus	± 0.16

(Freedman et al. 1994b; Kelson et al. 1996; Ferrarese et al. 1996). Since this is the fourth paper to employ this method, only a brief discussion will be included here; for further information the interested reader is encouraged to read the detailed description by Ferrarese et al. (1996).

Standard period-luminosity (PL) relations for the LMC Cepheids are adopted from Madore & Freedman (1991). These relations assume a true LMC distance modulus of 18.50 mag and a total line-of-sight LMC Cepheid reddening of $E(B-V) = 0.10$ mag [$E(V-I) = 0.13$ mag]:

$$M_V = -2.76\ (\log P - 1.0) - 4.16\ , \quad (4)$$

$$M_I = -3.06\ (\log P - 1.0) - 4.87\ . \quad (5)$$

The PL relations for NGC 925 were determined from the 75 high-quality candidates with periods in the range 8–70 days. In order to avoid any incompleteness bias in fitting a slope to the NGC 925 data, only the zero point of the regression was solved for, with the slope of the fit fixed to the LMC values given above.

The V and I PL relations are shown in Figure 8. Again, the phase-weighted magnitudes have been used. The solid line in each figure represents the best fit to each dataset. The dashed lines drawn at ± 0.54 mag for the V PL relation and ± 0.36 mag for the I PL relation represent 2 σ deviations from the mean PL relations. In the absence of differential reddening, the intrinsic width of the Cepheid instability strip is expected to place the NGC 925 Cepheids within these limits. The open circles in Figure 8 represent Cepheids that fall more than 4 σ from the mean LMC PL relations.

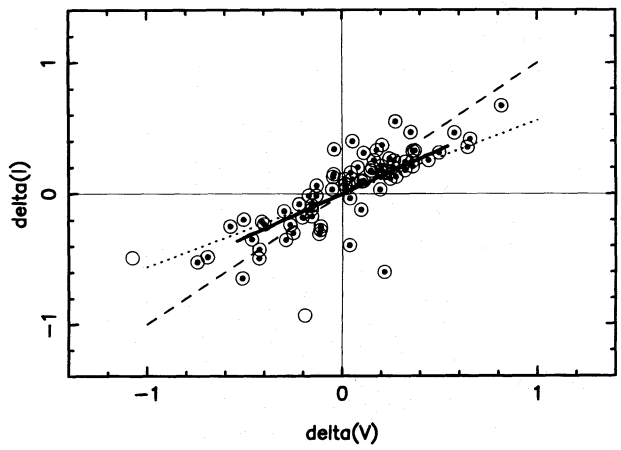

FIG. 9.—V versus I PL relation fitting residuals. Cepheids indicated by the open circles lie more than 4 σ from the expected ridge line. The scatter expected because of the intrinsic width of the Cepheid instability strip is indicated by the solid line. Dotted line indicates the reddening ridge line. Dashed line is the best fit to the NGC 925 data.

From these fits, the apparent distance moduli to NGC 925 are $\mu_V = 30.26 \pm 0.04$ mag and $\mu_I = 30.09 \pm 0.04$ mag. The quoted errors in the mean apparent distance moduli are calculated from the observed scatter in the NGC 925 PL data themselves.

To obtain the true distance modulus, the apparent reddening toward this particular sample of Cepheids in NGC 925 must be determined. In other words, the true distance is $\mu_0 \equiv \mu_V - A_V = \mu_I - A_I$, which, by definition, leads to

$$\mu_V - \mu_I = A_V - A_I = E(V-I)\ . \quad (6)$$

The observed difference in the apparent distance moduli for NGC 925 gives $E(V-I) = 0.17 \pm 0.03$ mag. Assuming a Cardelli, Clayton, & Mathis (1989) extinction law of $A_B{:}A_V{:}A_I = 3.3{:}1.0{:}0.6$, we obtain $A_V = 0.42$. The true distance modulus to NGC 925 is then $\mu_0 = 30.26 - 0.42 = 29.84 \pm 0.06$ mag, corresponding to a linear distance of 9.29 ± 0.26 Mpc (internal errors only).

The distance to NGC 925 was derived independently using the Cepheid parameters derived from the DoPHOT reductions. The procedures for determining mean magnitudes were identical to that described above, but a slightly different sample rejection criteria and PL fitting procedures were used (see § 1 of the Appendix). The resulting distance moduli are $\mu_V = 30.31 \pm 0.05$ mag, $\mu_I = 30.10 \pm 0.04$ mag, and true modulus $\mu_0 = 29.80 \pm 0.10$ mag. These differ from the ALLFRAME moduli by $+0.05$, $+0.01$, and -0.04 mag, respectively, consistent with the combined errors of the two determinations. (See § 2 of the Appendix for more details.)

Table 8 presents the error budget for this distance to NGC 925. These are systematic and random errors that may affect our distance estimate. Possible errors in our measured distance to NGC 925 owing to uncertainties in the WFPC2 zero points are ± 0.04 mag in both V and I (Hill et al. 1996). Estimated errors owing to uncertainty in the mean $\langle V \rangle$ and $\langle I \rangle$ ALLFRAME magnitudes are ± 0.05 mag and ± 0.04 mag, respectively. Possible errors in the aperture corrections are estimated to be ± 0.04 mag and ± 0.05 mag in V and I, respectively. Uncertainty in the PL fitting contributes an additional ± 0.06 mag, as discussed above.

Metallicity difference between the LMC and NGC 925 Cepheids is another possible source of error. An empirical test of the metallicity dependence of the Cepheid PL relations in M31 by Freedman & Madore (1990) found no statistically significant effect, within errors. Zaritsky, Kennicutt, & Huchra (1993) measured H II region oxygen abundances for all of the Key Project galaxies. They obtained log (O/H) = -3.37 for NGC 925. The models of Chiosi, Wood, & Capitanio (1993) then imply that the effect in distance modulus will be less than 0.1 mag in I. Therefore, we conservatively estimate the error owing to possible metallicity effects to be ± 0.08 mag in both V and I. Finally, we have adopted an LMC distance modulus error of ± 0.1 mag.

Adding the errors (for V or I) in quadrature gives us a total uncertainty of ± 0.16 mag (± 0.69 Mpc) in the distance to NGC 925. The dominant contribution to the error in the distance to NGC 925 is the uncertainty in distance to the LMC. Figure 9 shows the relation between the V and I band PL relation fitting residuals. The solid line shows the slope and full width of the expected correlation of data points caused by the intrinsic width of the instability strip.

TABLE 9

PREVIOUS DISTANCE DETERMINATIONS TO NGC 925

Method	Distance Modulus	Reference
Tully-Fisher (*B*-band)	28.99	Tully (1980)
Tully-Fisher (*B*-band)	28.68 ± 0.26	Bottinelli et al. (1985a)
Isophotal diameters	28.09 ± 0.43	Bottinelli et al. (1985a)
H I Index	28.48 ± 0.23	Bottinelli et al. (1985a)
Similar galaxies	28.60, 28.41	Bottinelli et al. (1985b)
Tully-Fisher (*H*-band)	28.69, 28.58	Bottinelli, Gouguenheim, & Teerikorpi (1988)
Tully-Fisher (*B*, *R*, *I*, & *H* bands)	28.8 ± 0.3	Pierce (1994)
Cepheids	29.84 ± 0.16	This paper

The dotted line shows the closely degenerate reddening trajectory. The Cepheids in the figure represented by the open circles lie 4 σ or more away from the expected ridge line. Excluding these outliers, there is very good agreement between the data and both the expected width and the slope of the residual correlations. Differential reddening would extend the correlation but it would not increase the vertical scatter. Uncorrelated photometric errors, of approximately 0.05 mag, shared between the *V* and *I* photometry are the most likely source of the remaining scatter seen in Figure 9.

7. COMPARISON TO PREVIOUS DISTANCE DETERMINATIONS

Most previous distance determinations to NGC 925 have been made using the Tully-Fisher relation or radial velocity measurements (which then require an adopted value of H_0 to obtain an estimated distance). The recent redshift studies of Strauss et al. (1992), Guthrie & Napier (1991), Tifft (1990), and Baiesi-Pillastrini & Palumbo (1986) have measured the heliocentric radial velocity of NGC 925 to be about 555 km s^{-1}. Some of the more recent direct distance measurements to NGC 925 are listed in Table 9. The recent Tully-Fisher distance measurements put NGC 925 within the distance range 5–6 Mpc.

Distances to several galaxies in the NGC 1023 group have been reported, including NGC 1023 itself, NGC 891, and NGC 1058 (Table 10). While NGC 925 is thought to be in this group, its membership has been questioned (Tully 1980; Pierce 1994). Our Cepheid distance for NGC 925 of 9.29 ± 0.69 Mpc is within 7% of estimated distances to NGC 891 (9.9 ± 0.8 Mpc) and NGC 1023 (9.9 ± 0.7 Mpc), as determined from planetary nebulae (Ciardullo, Jacoby, & Harris 1991), and a distance to NGC 1023 of 9.5 Mpc, as measured using surface brightness fluctuations (Tonry 1996). Application of the expanding photosphere method to the Type II supernova 1969L in NGC 1058 gives a distance of 11.2 ± 1.7 Mpc (Schmidt, Kirshner, & Eastman 1992). All of these distances tend to be slightly higher than our Cepheid distance to NGC 925, but, being a member of the NGC 1023 group, they are still consistent with NGC 925. Our distance is also consistent with Tully-Fisher distances, determined by Pierce (1994) for several other spiral members of the NGC 1023 group (NGC 891, NGC 949, and NGC 1003).

Figure 10 builds upon the Tully-Fisher relation for the

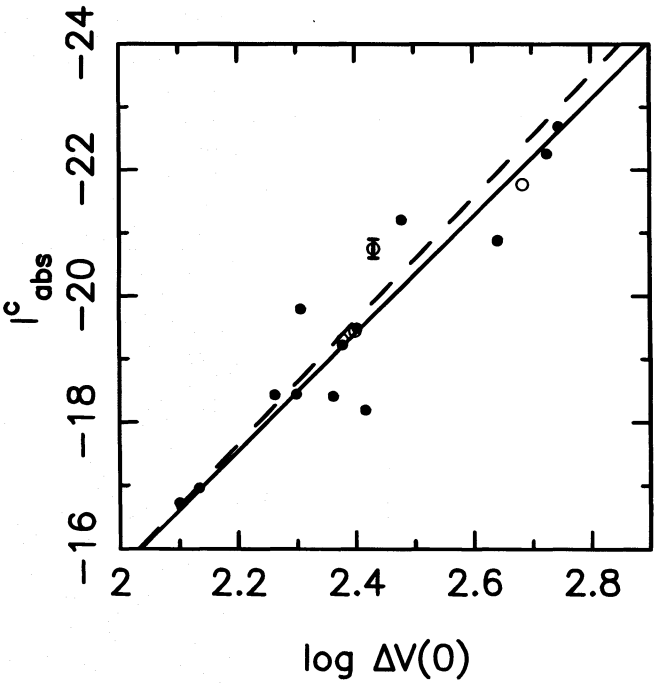

FIG. 10.—Tully-Fisher relation. Thirteen of the local calibrators (*filled circles*) are from Table 1 of Pierce & Tully (1992). Open symbols mark four non–face-on galaxies of the NGC 1023 group. NGC 925 is the open circle with error bars. Solid line is the least-squares fit to all 17 galaxies. Dashed line is equation (3) of Mould et al. (1991), which is a fit to 47 Virgo and Ursa Major galaxies.

TABLE 10

PUBLISHED DISTANCES TO NGC 1023 GALAXY GROUP MEMBERS

Galaxy	Method	Distance (Mpc)	Reference
NGC 891.....	PNLF	29.97 ± 0.16	Ciardullo et al. (1991)
	TF	30.4 ± 0.3	Pierce (1994)
NGC 949.....	TF	29.6 ± 0.3	Pierce (1994)
NGC 1023	PNLF	29.97 ± 0.14	Ciardullo et al. (1991)
	SBF	29.88	Tonry (1996)
NGC 1023 Group.....	TF	29.98 ± 0.24	Aaronson & Mould (1983)
NGC 1003	TF	29.7 ± 0.3	Pierce (1994)
NGC 1058	EP	30.2 ± 0.3	Schmidt, Kirshner, & Eastman (1992)

NOTE.—EP = expanding photosphere of Type II supernovae, PNLF = planetary nebulae luminosity function, SBF = surface brightness fluctuations, TF = Tully-Fisher relation.

TABLE 11

PARAMETERS FOR THE NGC 925 LPVs

ID	Chip	R.A. (2000)	Decl. (2000)	$\langle V \rangle$	$\langle V-I \rangle$
1.....	2	2:27:02.21	33:36:10.6	26.01	3.30
2.....	2	2:27:04.07	33:36:12.5	24.51	2.22
3.....	2	2:27:03.52	33:36:24.9	26.02	2.74
4.....	3	2:27:08.64	33:36:00.2	24.45	2.48
5.....	3	2:27:08.56	33:35:52.4	24.09	2.29
6.....	3	2:27:08.88	33:35:47.4	24.57	2.71
7.....	3	2:27:09.21	33:35:42.5	23.72	1.89
8.....	3	2:27:09.73	33:35:21.6	24.50	2.65
9.....	4	2:27:07.43	33:34:07.2	26.23	2.57

NOTE.—Units of right ascension are in hours, minutes, and seconds, and units of declination are in degrees, arcminutes, and arcseconds.

TABLE 12

POSSIBLE VARIABLES IN NGC 925

ID	chip	RA (2000.0)	Dec	$< V >$	$< I >$	$< V-I >$	Possible Period	Found in ALL?	Found in Do?	Comments
1	1	2:27:05.92	33:34:53.1	25.644	24.682	0.962	15.3	Yes		Possible Cepheid
2	1	2:27:04.94	33:34:55.9	26.190	25.171	1.019	10.7	Yes		Possible Cepheid
3	1	2:27:04.57	33:35:01.4	26.554	25.523	1.032	5.5	Yes		Possible Cepheid
4	1	2:27:05.15	33:34:56.9	25.905	24.820	1.085	14.7	Yes		Possible Cepheid
5	2	2:27:06.51	33:35:13.2	24.053	21.414	2.639	...		Yes	Possible LPV
6	2	2:27:06.82	33:35:21.5	27.207	25.485	1.722	29.0		Yes	Possible Cepheid
7	2	2:27:02.64	33:35:51.1	24.744	23.409	1.335	60.0		Yes	Possible Cepheid
8	2	2:27:06.59	33:35:55.3	27.127	25.322	1.805	...		Yes	Possible LPV
9	2	2:27:03.67	33:36:03.4	26.150	25.141	1.009	42.4	Yes	Yes	Possible Cepheid
10	2	2:27:05.67	33:36:17.8	27.064	25.577	1.487	...		Yes	Possible LPV
11	2	2:27:02.70	33:36:30.0	26.975	25.878	1.079	...		Yes	Possible Cepheid or blue LPV
12	3	2:27:07.15	33:35:14.5	26.042	25.063	0.979	6.2	Yes	Yes	Possible Cepheid
13	3	2:27:07.90	33:35:39.0	24.400	23.025	1.375	10.7		Yes	Possible Cepheid
14	3	2:27:08.49	33:36:10.5	26.117	24.783	1.334	11.1	Yes		Possible Cepheid
15	3	2:27:08.51	33:35:59.8	25.186	24.729	0.457	...		Yes	Possible variable, unknown type
16	3	2:27:08.79	33:35:57.1	25.066	22.196	2.870	...		Yes	Possible LPV
17	3	2:27:08.43	33:35:22.4	25.914	25.149	0.765	15.0	Yes		Possible Cepheid
18	3	2:27:08.41	33:35:10.6	24.219	23.245	0.974	41.7	Yes		Possible Cepheid
19	3	2:27:09.33	33:35:59.1	24.151	23.131	1.021	60.0	Yes		Possible Cepheid
20	3	2:27:08.74	33:35:08.6	25.660	24.762	0.898	14.1	Yes		Possible Cepheid
21	3	2:27:09.53	33:35:46.2	24.496	22.264	2.232	...		Yes	Possible LPV
22	3	2:27:10.18	33:36:12.2	23.936	21.675	2.261	...		Yes	Possible LPV
23	3	2:27:09.41	33:35:27.6	25.311	24.307	1.004	15.9	Yes		Possible Cepheid
24	3	2:27:10.25	33:36:11.1	25.450	22.820	2.630	...		Yes	Possible LPV
25	3	2:27:09.34	33:35:17.4	24.513	24.383	0.130	24.4	Yes		Possible Cepheid but very blue
26	3	2:27:09.73	33:35:25.6	25.520	24.382	1.138	...			Possible Cepheid or LPV
27	3	2:27:09.85	33:35:06.7	25.473	24.573	0.900	12.2		Yes	Possible Cepheid
28	3	2:27:10.32	33:35:27.7	24.488	23.342	1.146	54.8	Yes	Yes	Possible Cepheid
29	3	2:27:10.50	33:35:37.7	26.256	25.453	0.803	60.0		Yes	Possible Cepheid
30	3	2:27:10.09	33:35:11.1	26.023	25.421	0.602	7.6		Yes	Possible Cepheid
31	3	2:27:10.66	33:35:26.7	26.057	25.247	0.810	6.0		Yes	Possible Cepheid
32	3	2:27:11.11	33:35:41.8	26.436	25.384	1.052	...		Yes	Possible LPV
33	3	2:27:10.44	33:34:57.6	25.663	24.370	1.293	32.2		Yes	Possible Cepheid/Close to chip edge
34	3	2:27:11.65	33:35:59.3	25.628	24.464	1.164	...	Yes		Possible Variable, unknown type
35	3	2:27:10.99	33:35:13.8	24.970	24.273	0.697	...		Yes	Possible variable, unknown type
36	3	2:27:12.57	33:35:43.8	25.026	24.574	0.452	...		Yes	Possible variable, unknown type
37	3	2:27:12.66	33:35:44.4	26.065	25.101	0.963	11.0	Yes		Possible Cepheid
38	3	2:27:12.90	33:35:43.9	25.524	24.844	0.680	14.4	Yes		Possible Cepheid
39	4	2:27:11.11	33:34:49.2	25.661	25.243	0.418	5.74		Yes	Possible Cepheid
40	4	2:27:08.03	33:34:51.3	24.926	23.861	1.066	32.6	Yes		Possible Cepheid
41	4	2:27:08.53	33:34:41.7	26.300	25.514	0.787	5.0		Yes	or P=16.4. Possible Cepheid
42	4	2:27:09.36	33:34:38.4	25.484	...	...	14.5		Yes	Possible Cepheid. No DoPHOT *I* data
43	4	2:27:08.95	33:34:35.1	26.471	25.584	0.887	7.1	Yes		Possible Cepheid
44	4	2:27:11.39	33:34:23.7	25.696	24.957	0.739	10.4	Yes		Possible Cepheid
45	4	2:27:08.86	33:34:30.0	27.053	...	...	5.4		Yes	Possible Cepheid. No DoPHOT *I* data
46	4	2:27:07.25	33:34:29.5	25.860	25.119	0.741	10.3		Yes	Possible Cepheid
47	4	2:27:10.26	33:34:16.5	25.175	24.257	0.918	14.4	Yes		Possible Cepheid
48	4	2:27:10.59	33:34:02.1	26.213	25.789	0.424	5.4	Yes		Possible Cepheid
49	4	2:27:10.55	33:33:48.7	25.012	25.393	-0.382	18.3	Yes		or P=7.1d. very blue. eclipsing binary?

first 13 of the "local calibrators" from Table 1 of Pierce & Tully (1992). The magnitudes and velocity widths have been corrected for extinction and inclination following Han (1992), rather than as in Pierce & Tully (1992). Solid symbols denote these calibrators. Open symbols mark four non–face-on galaxies in the NGC 1023 group (Pierce 1994). Pierce has suggested that NGC 925 is a foreground galaxy; however, we note that NGC 925 (*open circle with error bars*) does not lie outside the scatter of the present figure. We caution, however, that there are two sources of scatter in Figure 10. One source of scatter comes from assigning a mean distance to a galaxy cluster. Individual galaxies

TABLE 13

SECONDARY STANDARD PHOTOMETRY FOR CHIP 1

ID	R.A.	Decl.	$\langle V \rangle$	σ	$\langle I \rangle$	σ	$\langle V-I \rangle$
1.....	2:27:06.27	33:35:00.2	23.209	0.078	22.662	0.060	0.547
2.....	2:27:06.04	33:34:50.2	24.700	0.079	22.663	0.038	2.037
3.....	2:27:05.81	33:34:43.9	23.513	0.030	23.257	0.034	0.256
4.....	2:27:06.03	33:35:00.8	23.376	0.038	22.897	0.049	0.479
5.....	2:27:05.62	33:34:40.4	24.332	0.076	21.636	0.071	2.696
6.....	2:27:05.92	33:34:56.7	23.768	0.063	23.484	0.059	0.284
7.....	2:27:05.69	33:34:47.1	22.643	0.033	22.403	0.038	0.241
8.....	2:27:05.92	33:35:04.4	23.676	0.043	23.535	0.043	0.140
9.....	2:27:05.76	33:34:55.9	22.723	0.034	22.393	0.054	0.329
10.....	2:27:05.47	33:34:40.8	24.871	0.069	22.271	0.028	2.601
11.....	2:27:05.79	33:34:58.8	22.903	0.038	22.729	0.031	0.174
12.....	2:27:05.53	33:34:57.1	23.937	0.042	24.001	0.059	−0.064
13.....	2:27:05.61	33:35:04.9	24.749	0.049	22.643	0.042	2.106
14.....	2:27:05.31	33:34:56.6	24.071	0.046	23.471	0.047	0.599
15.....	2:27:05.32	33:35:01.6	23.495	0.070	23.067	0.070	0.428
16.....	2:27:05.16	33:34:55.9	22.826	0.034	22.485	0.040	0.341
17.....	2:27:04.93	33:34:44.6	22.315	0.040	22.217	0.029	0.098
18.....	2:27:05.06	33:34:53.9	23.917	0.069	23.648	0.052	0.269
19.....	2:27:05.06	33:34:54.2	23.983	0.059	23.944	0.075	0.039
20.....	2:27:05.22	33:35:07.2	24.032	0.052	23.776	0.057	0.256
21.....	2:27:05.13	33:35:02.8	23.604	0.039	23.383	0.042	0.221
22.....	2:27:04.96	33:34:56.8	22.327	0.044	21.584	0.052	0.743
23.....	2:27:04.98	33:35:00.9	23.740	0.043	23.128	0.051	0.612
24.....	2:27:04.81	33:34:51.9	22.348	0.026	22.495	0.038	−0.148
25.....	2:27:04.82	33:34:53.0	23.452	0.055	23.335	0.037	0.117
26.....	2:27:05.04	33:35:08.1	24.662	0.073	22.687	0.032	1.975
27.....	2:27:04.78	33:34:56.8	23.858	0.038	23.641	0.046	0.216
28.....	2:27:04.69	33:35:01.8	23.726	0.044	23.564	0.037	0.162
29.....	2:27:04.30	33:34:52.7	24.016	0.052	23.937	0.075	0.079
30.....	2:27:04.51	33:35:04.8	23.994	0.054	23.776	0.065	0.218
31.....	2:27:04.48	33:35:05.3	23.914	0.069	23.643	0.049	0.271
32.....	2:27:04.43	33:35:02.4	23.939	0.050	23.591	0.027	0.348
33.....	2:27:04.42	33:35:03.3	23.792	0.052	23.725	0.043	0.068
34.....	2:27:04.23	33:34:54.2	22.653	0.038	22.334	0.028	0.319
35.....	2:27:04.21	33:34:56.8	23.384	0.054	23.227	0.059	0.157
36.....	2:27:04.17	33:34:55.9	22.628	0.037	22.569	0.048	0.059
37.....	2:27:04.10	33:34:52.1	23.458	0.054	23.279	0.070	0.179
38.....	2:27:04.22	33:35:04.8	24.420	0.054	22.170	0.059	2.249

NOTE.—Units of right ascension are in hours, minutes, and seconds, and units of declination are in degrees, arcminutes, and arcseconds.

within the cluster are not all at exactly that distance, and so they will produce some scatter in the Tully-Fisher diagram when the mean cluster distance is used. The second source of scatter is intrinsic. Either because of observational error or because of the very nature of the Tully-Fisher relation as it is defined, different galaxy clusters may scatter about a mean Tully-Fisher relation. At this time, the true intrinsic scatter of the Tully-Fisher relation remains controversial.

The solid line in Figure 10 is the least-squares fit to all 17 galaxies. The dashed line is equation (3) of Mould et al. (1991), which is a fit to 47 Virgo and Ursa Major galaxies with inclination angles greater than 45°, as observed by Pierce & Tully (1988), rescaled to a distance of 16 Mpc for these clusters (Ferrarese et al. 1996). We note that the field (*solid line*) and cluster (*dashed line*) calibrations are similar. It will be interesting to revisit this result after Cepheid distances are available for all of the ~18 galaxies in the Key Project sample.

The work presented in this paper is based on observations made by the NASA/ESA *Hubble Space Telescope*, obtained by the Space Telescope Science Institute, which is operated by AURA, Inc., under NASA contract 5-26555. We gratefully acknowledge the support of the NASA and STScI support staff, with special thanks to our program coordinator, Doug Van Orsow. Support for this work was provided by NASA through grant GO-2227-87A from STScI. N. A. S. would like to thank J. Hesser, P. Stetson, and the Dominion Astrophysical Observatory for kindly allowing her to visit and use DAO resources. The research described in this paper was partially carried out by the Jet Propulsion Laboratory, California Institute of Technology, under a contract with the National Aeronautics and Space Administration. This research has made use of the NASA/IPAC Extragalactic Database (NED), which is operated by the Jet Propulsion Laboratory, California Institute of Technology, under a contract with the National Aeronautics and Space Administration. This research has made use of the SIMBAD database, operated at CDS, Strasbourg, France.

TABLE 14

SECONDARY STANDARD PHOTOMETRY FOR CHIP 2

ID	R.A.	Decl.	$\langle V \rangle$	σ	$\langle I \rangle$	σ	$\langle V-I \rangle$
1.....	2:27:05.02	33:35:13.6	23.239	0.052	23.222	0.062	0.017
2.....	2:27:03.96	33:35:17.2	23.178	0.031	22.924	0.046	0.254
3.....	2:27:05.71	33:35:14.9	23.150	0.035	22.886	0.047	0.264
4.....	2:27:06.53	33:35:15.6	23.252	0.046	23.153	0.076	0.098
5.....	2:27:05.01	33:35:20.7	22.878	0.032	20.832	0.029	2.046
6.....	2:27:05.68	33:35:19.4	23.968	0.043	22.069	0.040	1.898
7.....	2:27:04.21	33:35:25.4	22.699	0.036	22.596	0.064	0.102
8.....	2:27:05.68	33:35:22.2	23.324	0.043	23.275	0.042	0.049
9.....	2:27:03.95	33:35:28.1	23.233	0.054	22.141	0.036	1.092
10.....	2:27:04.92	33:35:29.2	22.534	0.051	22.337	0.024	0.197
11.....	2:27:05.97	33:35:29.1	22.383	0.045	22.289	0.040	0.094
12.....	2:27:05.96	33:35:29.8	22.699	0.038	21.133	0.029	1.566
13.....	2:27:06.71	33:35:33.2	24.088	0.062	21.908	0.047	2.180
14.....	2:27:04.78	33:35:40.0	23.694	0.041	21.547	0.031	2.147
15.....	2:27:06.78	33:35:35.7	23.207	0.046	23.109	0.051	0.098
16.....	2:27:03.49	33:35:44.6	23.749	0.072	21.523	0.065	2.226
17.....	2:27:03.47	33:35:46.2	23.298	0.036	23.153	0.052	0.146
18.....	2:27:02.75	33:35:49.3	23.876	0.049	21.910	0.027	1.966
19.....	2:27:07.17	33:35:38.3	23.074	0.050	22.660	0.037	0.414
20.....	2:27:03.10	33:35:49.3	24.201	0.059	22.047	0.048	2.154
21.....	2:27:04.23	33:35:47.4	23.297	0.055	23.155	0.028	0.143
22.....	2:27:02.52	33:35:53.3	22.640	0.031	22.393	0.025	0.247
23.....	2:27:06.16	33:35:44.2	21.222	0.046	20.822	0.027	0.400
24.....	2:27:03.47	33:35:53.2	24.609	0.067	21.971	0.051	2.638
25.....	2:27:02.72	33:35:55.4	23.717	0.088	21.556	0.049	2.161
26.....	2:27:03.03	33:35:54.8	22.540	0.036	22.099	0.023	0.440
27.....	2:27:02.26	33:35:59.7	23.235	0.038	22.654	0.031	0.581
28.....	2:27:02.63	33:36:01.1	23.934	0.058	21.823	0.039	2.112
29.....	2:27:02.00	33:36:03.4	22.394	0.051	22.108	0.034	0.286
30.....	2:27:02.71	33:36:05.3	23.832	0.047	23.279	0.059	0.553
31.....	2:27:02.07	33:36:09.8	22.738	0.042	22.338	0.038	0.400
32.....	2:27:02.67	33:36:08.7	21.257	0.032	19.064	0.024	2.193
33.....	2:27:04.31	33:36:05.0	23.478	0.046	21.130	0.016	2.348
34.....	2:27:06.41	33:36:05.0	23.608	0.049	21.518	0.025	2.089
35.....	2:27:03.88	33:36:12.8	23.035	0.049	22.592	0.032	0.444
36.....	2:27:03.40	33:36:25.7	23.966	0.059	22.218	0.089	1.748
37.....	2:27:04.23	33:36:26.0	22.375	0.026	19.809	0.036	2.566

NOTE.—Units of right ascension are in hours, minutes, and seconds, and units at declination are in degrees, arcminutes, and arseconds.

APPENDIX

1. DOPHOT PHOTOMETRY

The DoPHOT reductions followed the procedures described in Saha et al. (1996), Ferrarese et al. (1996), and Hill et al. (1996). In this section, we briefly describe modifications and improvements that were made to the reduction procedures applied here.

The variant of the DoPHOT program, optimized for *HST* reductions, runs in a fixed-position mode, in which coordinates are mapped from a master image to each epoch in order to ensure consistent photometry; thus, accurate coordinate transformations were vital. As mentioned in above, the NGC 925 data were acquired on slightly different field centers and roll angles because of guide star acquisition failures. This required cubic spatial distortion corrections to be applied to the WFPC2 data. The corrections were at the 0.5 pixel level, sufficient to significantly improve the photometry.

The image used to generate the master list of objects was made by combining the 20 CR split F555W images observed at the same roll angle. Four F814W images were combined in a similar fashion. These images were combined using the technique described by Saha et al. (1996) and Hill et al. (1996). The PSF of the combined image was ~ 1.4 pixels FWHM, only slightly degraded from the FWHM on an individual frame. The improvement in signal-to-noise ratio in the combined images more than compensates for the slight degradation in resolution. Transformations from the master image to the individual epochs were made via a three-step process. First, coordinates from each image (including the master image) were transformed from raw CCD coordinates to "undistorted coordinates" using the 20 coefficients of the cubic fit given by Holtzman et al. (1995b). Second, a six coefficient linear transformation was then used to map master coordinates to the individual epochs. Finally, the inverse cubic coefficients were used to transform back to the raw CCD coordinates of each epoch. Typical residuals between the linear fit of the master to each epoch were ± 0.09 PC pixels in the "undistorted coordinate" system

As with any PSF-fitting procedure, an important step involves the conversion of the fitted magnitudes to total aperture magnitudes via an aperture correction. Hill et al. (1996) derived standard DoPHOT PSFs and aperture corrections for the DoPHOT reductions. On the crowded images, there are often only a few bright uncrowded stars suitable for aperture corrections; accordingly, these corrections constitute the most uncertain point in the calibration process. An improved procedure for the aperture corrections was implemented for these reductions. Aperture corrections were estimated in a series

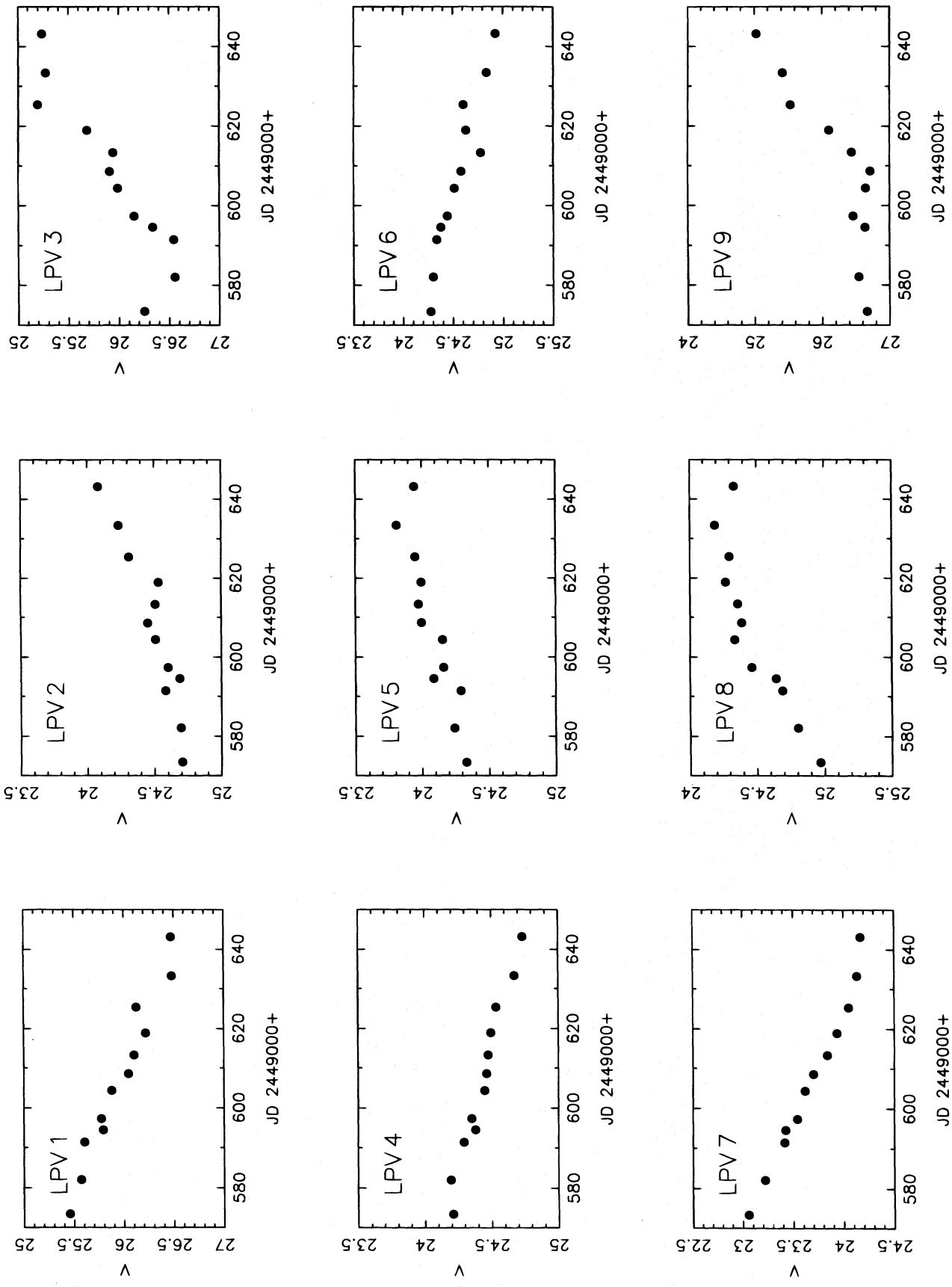

FIG. 11.—Heliocentric Julian Date vs. magnitude for the long-period variables in NGC 925

TABLE 15

SECONDARY STANDARD PHOTOMETRY FOR CHIP 3

ID	R.A.	Decl.	$\langle V \rangle$	σ	$\langle I \rangle$	σ	$\langle V-I \rangle$
1.....	2:27:08.15	33:36:01.5	23.262	0.049	21.028	0.021	2.234
2.....	2:27:07.82	33:35:37.8	23.200	0.031	23.013	0.044	0.187
3.....	2:27:08.09	33:35:49.2	22.461	0.031	22.103	0.038	0.359
4.....	2:27:07.92	33:35:38.0	22.601	0.020	22.405	0.033	0.197
5.....	2:27:08.26	33:35:51.9	23.805	0.074	21.654	0.049	2.151
6.....	2:27:08.37	33:35:50.5	22.704	0.030	22.574	0.042	0.131
7.....	2:27:08.78	33:36:12.0	21.394	0.024	20.782	0.023	0.612
8.....	2:27:08.40	33:35:48.9	23.123	0.046	22.773	0.035	0.350
9.....	2:27:08.47	33:35:50.9	22.886	0.036	22.841	0.070	0.045
10.....	2:27:08.79	33:36:03.9	23.459	0.043	22.884	0.060	0.575
11.....	2:27:08.78	33:36:01.9	22.037	0.037	21.509	0.069	0.528
12.....	2:27:08.36	33:35:37.6	22.709	0.039	22.483	0.045	0.225
13.....	2:27:08.73	33:35:53.7	22.885	0.035	22.017	0.044	0.868
14.....	2:27:08.82	33:35:55.5	22.301	0.028	22.023	0.047	0.278
15.....	2:27:08.54	33:35:37.8	23.094	0.026	22.837	0.063	0.256
16.....	2:27:09.45	33:36:14.3	22.713	0.022	22.307	0.044	0.406
17.....	2:27:09.41	33:36:10.0	23.292	0.035	22.888	0.053	0.404
18.....	2:27:08.46	33:35:14.4	22.050	0.031	21.066	0.066	0.985
19.....	2:27:08.58	33:35:19.5	22.053	0.058	21.226	0.044	0.827
20.....	2:27:09.69	33:36:09.7	23.767	0.060	21.332	0.026	2.435
21.....	2:27:08.75	33:35:06.3	22.028	0.038	21.527	0.031	0.501
22.....	2:27:08.88	33:35:08.3	22.259	0.030	21.904	0.014	0.356
23.....	2:27:09.29	33:35:18.0	22.765	0.042	22.224	0.032	0.541
24.....	2:27:09.48	33:35:27.8	22.790	0.030	22.526	0.038	0.264
25.....	2:27:09.31	33:35:13.7	21.925	0.027	21.259	0.056	0.666
26.....	2:27:09.74	33:35:35.0	22.458	0.045	22.018	0.036	0.440
27.....	2:27:09.90	33:35:40.9	22.268	0.048	22.132	0.040	0.137
28.....	2:27:09.97	33:35:37.1	21.742	0.055	19.175	0.016	2.567
29.....	2:27:10.35	33:35:53.3	20.821	0.055	19.906	0.012	0.915
30.....	2:27:10.30	33:35:12.2	23.278	0.039	22.132	0.020	1.146
31.....	2:27:11.89	33:35:47.2	22.237	0.046	21.899	0.049	0.337
32.....	2:27:12.01	33:35:51.9	22.406	0.035	22.087	0.045	0.319
33.....	2:27:11.87	33:35:33.3	21.254	0.044	20.321	0.044	0.933
34.....	2:27:11.64	33:35:11.6	22.941	0.031	22.493	0.047	0.448

NOTE.—Units of right ascension are in hours, minutes, and seconds, and units of declination are in degrees, arcminutes, and arcseconds.

of eight concentric apertures out to 8 pixels radius. The sky value was then adjusted iteratively in order to flatten the growth curve in the outer three apertures. The value from a radius of 5 pixels was then used as the aperture correction. We tested the reliability of the aperture corrections by determining independent corrections for each epoch. Epoch to epoch variations were typically 1%–2% and were never more than 5%. This suggests that there were no large changes in the PSF over the 70 day window of observations.

2. DOPHOT DISTANCE ANALYSIS

As an end-to-end check on our reduction procedures, the distance to NGC 925 was derived independently using the Cepheid periods and magnitudes derived from the DoPHOT reductions, as well as an alternate fitting procedure.

The PL fitting was performed using the same calibration based on observations of LMC Cepheids, as described in § 5. The fit to the NGC 925 PL relations were fixed in slope to the LMC values, with only the zero-point offset determined. In this case, 68 of the 80 Cepheids in Table 7 were used to estimate the distance. Five stars were rejected because they fell well outside the instability strip in the DoPHOT color-magnitude diagram. Six other Cepheids with periods outside the 10–63 day period range were rejected, and one other Cepheid was rejected because it fell more than 3 σ from the mean PL relation in both V and I.

Two fitting procedures were used. The first simply determined the median fit in log P versus magnitude plane. The discreteness of this procedure was minimized by fitting a line to the difference between the number of Cepheids above and below the PL relation, as a function of distance moduli in the region near the median. The second method minimized the absolute deviations of the Cepheids about the PL relation.

The apparent distance moduli obtained from these two fitting procedures yielded identical apparent distance moduli in V and I of $\mu_V = 30.31 \pm 0.05$ mag and $\mu_I = 30.10 \pm 0.04$ mag. The true distance modulus is then obtained using the same procedure as described in § 5 for the DAOPHOT data, yielding $A_V = 0.54$ mag and true distance modulus $\mu_0 = 29.80 \pm 0.10$ mag.

3. LONG-PERIOD VARIABLES AND CANDIDATE VARIABLES

Several long-period variable (LPV) star candidates were found in NGC 925. Table 11 lists the chip, position, and intensity-averaged mean $\langle V \rangle$ magnitude and $\langle V-I \rangle$ color for each variable. Because the periods of these variables exceed our 70 day observing window, our mean-magnitude estimates are only approximate. Figure 11 shows Heliocentric Julian Date versus V magnitude for the nine LPVs.

TABLE 16

SECONDARY STANDARD PHOTOMETRY FOR CHIP 4

ID	R.A.	Decl.	$\langle V \rangle$	σ	$\langle I \rangle$	σ	$\langle V-I \rangle$
1.....	2:27:09.87	33:34:57.3	24.071	0.042	22.164	0.027	1.908
2.....	2:27:07.58	33:35:00.4	23.187	0.049	22.851	0.044	0.336
3.....	2:27:08.42	33:34:56.4	24.051	0.059	21.785	0.050	2.266
4.....	2:27:09.25	33:34:53.9	23.251	0.040	22.521	0.060	0.730
5.....	2:27:10.27	33:34:47.6	23.187	0.042	23.138	0.040	0.049
6.....	2:27:07.22	33:34:55.8	23.751	0.088	21.287	0.045	2.464
7.....	2:27:08.20	33:34:52.2	23.767	0.078	21.204	0.025	2.563
8.....	2:27:08.87	33:34:49.4	22.787	0.034	21.918	0.021	0.869
9.....	2:27:09.10	33:34:47.9	23.355	0.045	23.066	0.066	0.289
10.....	2:27:08.78	33:34:46.9	23.996	0.036	21.647	0.034	2.349
11.....	2:27:10.48	33:34:39.5	23.682	0.050	23.380	0.060	0.301
12.....	2:27:10.51	33:34:38.7	23.351	0.046	22.913	0.053	0.438
13.....	2:27:10.19	33:34:36.6	22.896	0.035	21.055	0.017	1.841
14.....	2:27:12.07	33:34:27.5	23.771	0.073	21.480	0.041	2.291
15.....	2:27:07.38	33:34:40.4	24.227	0.066	22.153	0.025	2.075
16.....	2:27:06.65	33:34:41.7	23.469	0.044	22.619	0.067	0.850
17.....	2:27:06.42	33:34:41.3	22.768	0.046	22.100	0.070	0.668
18.....	2:27:07.84	33:34:36.4	23.551	0.047	23.241	0.066	0.310
19.....	2:27:10.15	33:34:29.3	22.092	0.030	21.804	0.039	0.288
20.....	2:27:09.84	33:34:30.0	23.646	0.039	23.531	0.052	0.115
21.....	2:27:06.35	33:34:38.3	23.056	0.049	22.188	0.063	0.868
22.....	2:27:10.04	33:34:25.4	22.090	0.070	21.406	0.049	0.684
23.....	2:27:06.61	33:34:32.6	23.856	0.052	21.761	0.026	2.095
24.....	2:27:06.97	33:34:30.7	23.520	0.036	23.615	0.061	−0.095
25.....	2:27:10.52	33:34:18.8	23.625	0.063	23.575	0.067	0.050
26.....	2:27:06.20	33:34:28.9	23.635	0.049	23.517	0.041	0.117
27.....	2:27:08.96	33:34:20.8	22.837	0.046	22.551	0.030	0.287
28.....	2:27:08.15	33:34:20.9	22.966	0.037	22.550	0.030	0.416
29.....	2:27:06.53	33:34:16.4	22.911	0.038	22.887	0.086	0.024
30.....	2:27:07.50	33:34:11.6	23.667	0.049	23.458	0.052	0.209
31.....	2:27:06.94	33:34:10.9	21.584	0.033	21.038	0.021	0.546
32.....	2:27:08.20	33:34:05.1	23.371	0.052	22.487	0.035	0.885
33.....	2:27:07.21	33:34:07.9	21.485	0.028	20.873	0.020	0.612
34.....	2:27:07.37	33:34:07.0	23.518	0.040	22.726	0.036	0.792
35.....	2:27:06.84	33:34:06.5	24.994	0.089	21.589	0.030	3.405
36.....	2:27:07.27	33:34:04.2	23.584	0.039	22.254	0.033	1.330
37.....	2:27:06.15	33:34:04.6	22.667	0.034	22.330	0.032	0.336
38.....	2:27:06.16	33:34:03.8	23.542	0.046	21.560	0.031	1.981
39.....	2:27:06.59	33:34:02.1	23.158	0.031	22.368	0.028	0.790
40.....	2:27:07.35	33:33:59.6	22.147	0.022	21.470	0.019	0.677
41.....	2:27:06.14	33:34:01.7	23.436	0.050	22.174	0.043	1.262
42.....	2:27:06.22	33:33:57.4	23.051	0.069	22.683	0.031	0.368
43.....	2:27:09.79	33:33:46.9	23.362	0.031	23.145	0.064	0.217
44.....	2:27:07.28	33:33:53.6	23.421	0.057	23.045	0.046	0.376
45.....	2:27:09.76	33:33:45.3	23.431	0.074	21.557	0.055	1.874
46.....	2:27:06.44	33:33:54.0	23.080	0.036	22.908	0.057	0.172

NOTE.—Units of right ascension are in hours, minutes, and seconds, and units of declination are in degrees, arcminutes, and arcseconds.

There were many other candidate variables that for one reason or another did not make our final list of Cepheids but which are possible variable stars. Most of these are cases in which a star looks variable using one dataset (i.e., ALLFRAME) but does not appear to be varying in the other dataset. Table 12 lists these candidates. Columns (1)–(4) list the usual information: identification number, the WFPC2 chip where it is found, and the right ascension and declination of the candidate. Columns (5)–(7) list the intensity-weighted average $\langle V \rangle$, $\langle I \rangle$, and $\langle V-I \rangle$ magnitudes of the candidates. Column (8) gives a possible period for the candidate. We do not list periods for the possible long-period variables. Columns (9) and (10) indicate whether the candidate was found to be variable in the ALLFRAME (ALL) or DoPHOT (Do) datasets. The mean magnitude and color information for each candidate comes from the dataset in which it was found. That is, if the star appeared to be varying in the DoPHOT dataset, the mean $\langle V \rangle$, $\langle I \rangle$, and $\langle V-I \rangle$ magnitudes are DoPHOT means, not ALLFRAME means.

4. SECONDARY STANDARDS

Tables 13, 14, 15, and 16 contain standard V and I photometry for a selected number of fairly isolated stars in each chip.

REFERENCES

Aaronson, M., & Mould, J. 1983, ApJ, 265, 1
Baiesi-Pillastrini, G. C., & Palumbo, G. G. C. 1986, A&A, 163, 1
Bottinelli, L., Gouguenheim, L., Paturel, G., & de Vaucouleurs, G. 1985a, A&AS, 59, 43
Bottinelli, L. 1985b
Bottinelli, L., Gouguenheim, L., & Teerikorpi, P. 1988, A&A, 196, 17
Burrows, C. J., et al. 1994, Wide-Field and Planetary Camera 2 Instrument Handbook (Baltimore: STScI)
Cardelli, J. A., Clayton, G. C., & Mathis, J. S. 1989, ApJ, 345, 245
Chiosi, C., Wood, P., & Capitanio, N. 1993, ApJS, 86, 541

Ciardullo, R., Jacoby, G., & Harris, W. 1991, ApJ, 383, 487
de Vaucouleurs, G., et al. 1991, Third Reference Catalogue of Bright Galaxies (New York: Springer)
Ferrarese, L., et al. 1996, ApJ, 464, 568
Freedman, W. L. 1988, ApJ, 326, 691
Freedman, W. L., & Madore, B. F. 1990, ApJ, 365, 186
Freedman, W. L., et al. 1994a, Nature, 371, 757
———. 1994b, ApJ, 427, 628
Guthrie, B. N. G., & Napier, W. M. 1991, MNRAS, 253, 533
Han, M. 1992, ApJ, 391, 617
Hill, R., et al. 1996, ApJ, submitted
Holtzman, J., et al. 1995a, PASP, 107, 1065
———. 1995b, PASP, 107, 156
Hughes, S. M. G., et al. 1994, ApJ, 428, 143
Kelson, D., et al. 1996, ApJ, 463, 26
Kennicutt, R. C., Freedman, W. L, & Mould, J. R. 1995, AJ, 110, 1476
Lafler, J., & Kinman, T. D. 1965, ApJS, 11, 216
Madore, B. F., & Freedman, W. L. 1991, PASP, 103, 933
Mould, J., et al. 1991, ApJ, 383, 467
Pierce, M. J. 1994, ApJ, 430, 53
Pierce, M., & Tully, B. 1988, ApJ, 330, 579
Pierce, M., & Tully, B. 1992, ApJ, 387, 47
Saha, A., et al. 1996, ApJ, 466, 55
Saha, A., & Hoessel, J. G. 1990, AJ, 99, 97
Sandage, A., & Bedke, 1988, Atlas of Galaxies Useful for Measuring the Cosmological Distance Scale (Washington, DC: NASA)
Sandage, A., & Tammann, G. A. 1981, A Revised Shapley-Ames Catalog of Bright Galaxies (Washington, DC: Carnegie Inst. Washington)
Schechter, P. L., Mateo, M., & Saha, A. 1993, PASP, 105, 1342
Schmidt, B., Kirshner, R., & Eastman, 1992, ApJ, 395, 366
Stellingwerf, R. F. 1978, ApJ, 224, 953
Stetson, P. B. 1987, PASP, 99, 191
Stetson, P. B. 1990, PASP, 102, 932
———. 1994, PASP, 106, 250
———. 1996, PASP, in press
Stetson, P. B., et al. 1996, in preparation
Strauss, M. A., et al. 1992, ApJS, 83, 29
Tifft, W. G. 1990, ApJS, 73, 603
Tonry, J. 1996, private communication
Tully, R. B. 1980, ApJ, 237, 390
Welch, D. L., & Stetson, P. B. 1993, AJ, 105, 1813
Zaritsky, D., Kennicutt, R., & Huchra, J. 1994, ApJ, 420, 87